

Determination of the Cabibbo-Kobayashi-Maskawa matrix element $|V_{cb}|$

Giulia Ricciardi

Dipartimento di Fisica E. Pancini, Università di Napoli Federico II and
I.N.F.N. Sezione di Napoli,
Complesso Universitario di Monte Sant'Angelo, Ed. 6, Via Cintia, 80126 Napoli, Italy
E-mail: giulia.ricciardi@na.infn.it

Marcello Rotondo

Laboratori Nazionali dell'INFN di Frascati, Via Enrico Fermi 40, 00040 Frascati
(Roma), Italy
E-mail: marcello.rotondo@lnf.infn.it

Nov 2019

Abstract.

In this review we present and discuss the determination of the magnitude of the Cabibbo-Kobayashi-Maskawa (CKM) matrix parameter V_{cb} . The CKM matrix parametrizes the weak charged current interactions of quarks in the Standard Model (SM), and a precise determination of its elements has always been one of the most important targets of particle physics. The precise knowledge of the $|V_{cb}|$ value plays a pivotal role in testing the flavour sector of the SM and in the analyses of the unitarity of the CKM matrix.

The SM does not predict the values of the CKM matrix elements, which have to be extracted by experimental data. Given the variety of channels that allow the extraction of $|V_{cb}|$, different theoretical and experimental techniques are mustered for the $|V_{cb}|$ determination. The exertion toward precision represents not only a significant test of our theoretical procedures but a stimulus towards better detection performances.

The most precise measurements of $|V_{cb}|$ come from semileptonic decays, that being tree level at the lowest order in the SM are generally considered unaffected by physics beyond the SM. After summarizing the characteristics of the SM that set the frame for the determination of $|V_{cb}|$, we discuss inclusive and exclusive semileptonic B decays. We analyze the $|V_{cb}|$ extraction methods and recent results, detailing both the theoretical and experimental techniques, and, finally, outline future prospects. We also comment on exclusive decays into heavy leptons, on the observables $R(D)$ and $R(D^*)$, on decays to excited D meson states and on baryon decays.

Contents

1	Introduction	5
2	The flavour scenario	6
2.1	The Yukawa terms in the SM Lagrangian	6
2.2	The Cabibbo-Kobayashi-Maskawa matrix	8
2.3	The unitarity triangles	10
3	Semileptonic B meson decays	11
3.1	Inclusive decays	12
3.1.1	Heavy Quark Expansion	14
3.1.2	Mass schemes	15
3.2	Exclusive decays into light leptons	17
3.2.1	Form factors	19
3.2.2	Zero recoil and beyond	21
3.2.3	Unitarity bounds	24
3.2.4	BGL and CLN parameterizations	26
3.3	Decays to excited D -meson states	28
3.4	Decays into heavy leptons	31
3.5	Comparison with baryon decays	33
4	Experimental techniques	34
4.1	B -hadron production	34
4.1.1	B -Factories	34
4.1.2	Hadron Colliders	36
4.2	Semileptonic measurements at B -Factories	38
4.2.1	Soft pion from D^*	40
4.2.2	B tagging	41
4.3	Semileptonic measurements at LHCb	42
4.3.1	Techniques for kinematic reconstruction	44
5	Inclusive V_{cb} determination	45
5.1	Moment measurements	46
5.1.1	Hadron moments	46
5.1.2	Lepton moments	47
5.2	Results	47
6	Exclusive V_{cb} determination	50
6.1	The $B \rightarrow D^* \ell \nu_\ell$ channel	50
6.1.1	Belle untagged measurement	51
6.1.2	BaBar tagged measurement	54
6.1.3	Results	56

<i>CONTENTS</i>	4
6.2 The $B \rightarrow D\ell\nu_\ell$ channel	58
6.2.1 Belle tagged analysis	59
6.2.2 Results	60
6.3 The $B_s \rightarrow D_s^{(*)}\mu\nu_\mu$ channel	62
6.4 Direct measurement of $ V_{ub} / V_{cb} $	64
6.5 The $ V_{cb} $ puzzle	66
7 Future prospects	68
8 Bibliography	71

1. Introduction

Nowadays accuracy in measurements and theoretical calculations of physical observables is indispensable to check the Standard Model (SM) and explore the small region of parameters space left to its extensions, at our energies. The increase in precision demands an accurate knowledge of the parameters of the Cabibbo-Kobayashi-Maskawa (CKM) matrix, which are not predictable within the SM, and must be extracted by data. In the last decades, a large effort has gone towards their determination, mostly driven by increasingly higher statistics at new and improved facilities, accompanied by more complex and sophisticated theoretical computations.

Among the CKM matrix elements, V_{cb} takes central stage. Its role is pivotal in the unitarity analyses of the CKM matrix. The so-called unitarity clock, the circle around the origin in the $\bar{\rho}-\bar{\eta}$ plane, is proportional to the ratio $|V_{ub}/V_{cb}|$, and $|V_{cb}|$ normalizes the whole unitarity triangle. Relations between $|V_{cb}|$ and other observables can be exploited to estimate their values, within or beyond the SM, and an accurate determination of $|V_{cb}|$ is necessary for their correct assessment. One example are B decays originated by flavour changing neutral currents, such as rare radiative $B \rightarrow X_s \gamma$ or semileptonic $B \rightarrow X_s \ell^+ \ell^-$ decays, where X_s are hadronic states with strangeness different from zero. In the SM, the $b \rightarrow s$ quark transitions cannot occur at tree level, but start at one loop, mediated by the so-called penguin diagrams, with an up-type quark running in the loop. Top and charm quark contributions are proportional to $V_{tb}V_{ts}^*$ and $V_{cb}V_{cs}^*$ respectively (unitarity can be used to cancel $V_{ub}V_{us}^*$ in the rate). Other examples are in the kaon sector, where ϵ_K , ϵ'/ϵ and branching ratios of rare kaon decays depend sensitively on values of $|V_{cb}|$ (and $|V_{ub}|$) [1].

The semileptonic decays of beauty hadrons, dominated at the quark level by the weak transition $b \rightarrow c \ell \nu_\ell$, are used to determine with high precision the magnitude of the matrix element V_{cb} . The heavy mass of the B meson allows to exploit simplifications in the limit of infinite quark mass and to better separate perturbative and non-perturbative regimes. Another advantage is that semileptonic decays are mediated at leading order in perturbation theory tree-level processes. The exchange of a new physics (NP) particle is strongly constrained at tree level. A clean determination of CKM parameters from tree level processes is therefore a valuable input for other NP more sensitive estimates. Past, present and future B factories have provided and will provide an unparalleled level of precision in branching ratios and related observables, and LHCb is following suit.

There are two approaches to determine $|V_{cb}|$, which allow almost equally precise measurements: the inclusive and the exclusive approach. In the inclusive approach, the $B \rightarrow X_c \ell \nu_\ell$ decays, where X_c , the hadronic state originated by the charm quark, is not reconstructed in any specific final state. Sufficiently inclusive quantities can be expressed as a double series in α_s and Λ_{QCD}/m_b , in the framework of the Heavy Quark Expansion (HQE). In the exclusive approach, one consider decays where a specific hadronic final state is reconstructed, as $B \rightarrow D \ell \bar{\nu}_\ell$ and $B \rightarrow D^* \ell \bar{\nu}_\ell$ decays. The inclusive and exclusive semileptonic determinations rely on different theoretical calculations and on different

experimental techniques which have, to a large extent, uncorrelated statistical and systematic uncertainties. This independence makes their expected agreement a useful test of our understanding of both experiments and theory. Since at least three decades, there is a tension among the $|V_{cb}|$ values, depending on whether they are extracted using exclusive or inclusive semileptonic channels. In the present general scenario of data in optimal agreement within the SM, this tension is intriguing, and alone motivates, in our view, more and more precise theoretical and experimental investigations.

In this paper we review the theoretical background and the experimental techniques relevant for the $|V_{cb}|$ determination. In section 2 we introduce the flavour sector of the SM Lagrangian and the CKM matrix. In section 3 we discuss exclusive and inclusive semileptonic decays (into light and heavy leptons) and the theoretical tools necessary for their analyses. In section 4 we review the experimental techniques used at the B -Factories and LHCb to study semileptonic decays, pointing out the various sources of systematic uncertainties. Sections 5 and 6 are devoted to inclusive and exclusive $|V_{cb}|$ determinations, respectively. Finally, in section 7, we examine future prospects at Belle-II and LHCb facilities, and future theoretical directions of development.

2. The flavour scenery

2.1. The Yukawa terms in the SM Lagrangian

The SM is a gauge field theory describing the electromagnetic, weak interactions and strong interactions of quarks and leptons. It has supported calculations of physical quantities with unflinching precision for the past 50 years. Although there are challenges that the SM does not address, a complete, coherent framework, in agreement with data, which encompasses and extends the SM, has still to emerge.

The SM Lagrangian is invariant under $SU(2)_L \otimes U(1)_Y \otimes SU(3)_c$ gauge transformations. Fields in the SM Lagrangian are classified according to irreducible representations of this gauge group. Gauge invariance in the SM Lagrangian leads one to expect massless vector bosons, in contrast with the experimental evidence that the weak interactions are short ranged. Such impasse is surmounted by the so-called Higgs mechanism. According to the Higgs mechanism, the vector bosons W^\pm and Z^0 couple through the EW covariant derivative to a complex scalar ϕ , the Higgs (or Brout-Englert-Higgs) field, which behaves as a doublet under the $SU(2)_L$ symmetry and has hypercharge $1/2$. When ϕ gets a vacuum expectation value different from zero (spontaneously symmetry breaking), the SM Lagrangian acquires extra terms which are precisely mass terms for the Higgs and the W^\pm and Z^0 bosons.

In order to give mass to quarks and charged leptons, and additional gauge invariant Lagrangian, the Yukawa Lagrangian \mathcal{L}_Y , is added to the SM Lagrangian

$$\mathcal{L}_Y = - \sum_{i,j=1}^3 \left(Y_{ij}^{(d)} \bar{q}_L^i \phi d_R^j + Y_{ij}^{(u)} \bar{q}_L^i \phi_C u_R^j + Y_{ij}^{(\ell)} \bar{l}_L^i \phi e_R^j + h.c. \right) \quad (1)$$

where $h.c.$ stands for Hermitian conjugate. The fields ϕ and its charge conjugate

$\phi_C \equiv i\tau_2\phi^*$ are Higgs doublets of hypercharge $Y = 1/2$ and $Y = -1/2$, q_L^i and ℓ_L^i are the $SU(2)_L$ left-handed fundamental doublets for three generations, u_R^i , d_R^i and e_R^i are right-handed up-type, down-type quarks and charged leptons, respectively. The gauge symmetry does not constrain the boson-fermion $Y^{(u,d,\ell)}$ couplings, referred as Yukawa couplings, which are complex number completely arbitrary.

After spontaneous symmetry breaking, the Yukawa Lagrangian in the quark sector can be written as

$$\mathcal{L}_{Yq} = -\bar{\hat{d}}_L M^{(d)} \hat{d}_R - \bar{\hat{u}}_L M^{(u)} \hat{u}_R + h.c. \quad (2)$$

where M_{ij} are three by three complex matrices, connected to the Yukawa couplings and equally arbitrary. The up-type quarks have been indicated with $\hat{u} \equiv (u, c, t)$ and the down-type quark with $\hat{d} \equiv (d, s, b)$. These are flavour eigenstates, that is states participating in gauge interactions, but not yet mass eigenstates. Indeed, the $M^{(u)}$ and $M^{(d)}$ matrices are not necessarily Hermitian, nor there is an a priori theoretical reason that they should be diagonal in the generation index. By what is known in mathematics as a singular value decomposition, they can be both made hermitian and diagonal by a bi-unitary transformation

$$U_L^{u\dagger} M^{(u)} U_R^u = M_D^u \quad U_L^{d\dagger} M^{(d)} U_R^d = M_D^d \quad (3)$$

where M_D^u and M_D^d are diagonal with positive eigenvalues and $U_{L(R)}^{u(d)}$ are unitary matrices. It corresponds to the transformations of the quark states

$$\begin{aligned} \hat{u}_L &\rightarrow U_L^u \hat{u}_L & \hat{u}_R &\rightarrow U_R^u \hat{u}_R \\ \hat{d}_L &\rightarrow U_L^d \hat{d}_L & \hat{d}_R &\rightarrow U_R^d \hat{d}_R \end{aligned} \quad (4)$$

The new states are the physical ones, since the mass matrix is diagonal in that basis.

The change from flavour to mass quark eigenstates (4) in the Yukawa sector has to be registered by other sectors of the Lagrangian. One can easily observe that the neutral and electromagnetic currents remain invariant, since they couple separately up-type and down-type quarks. On the contrary, the charged current interactions are affected by this change of basis and the part of the Lagrangian describing the hadronic exchanges of charged bosons W^\pm becomes

$$\mathcal{L}_{CC} = \frac{g}{\sqrt{2}} (W_\mu^+ \bar{\hat{u}}_L \gamma^\mu V \hat{d}_L + W_\mu^- \bar{\hat{d}}_L \gamma^\mu V^\dagger \hat{u}_L) \quad (5)$$

in terms of the quark mass eigenstates. A new unitary matrix, the Cabibbo-Kobayashi-Maskawa (CKM) matrix, defined as

$$V \equiv U_L^{u\dagger} U_L^d \quad (6)$$

has appeared in the SM. It is a unitary matrix, being the product of unitary matrices, and it parameterizes the change of basis (4), but its elements are otherwise completely arbitrary and has to be determined experimentally.

2.2. The Cabibbo-Kobayashi-Maskawa matrix

In the SM, the CKM matrix is a key element in describing the flavour dynamics. As seen above, it is unitary, but this is its only theoretical constraint. The parameters of the CKM, which can be complex, have to be determined experimentally, and there is no a priori theoretical way to determine their values within the SM framework. The CKM matrix V induces flavour-changing transitions inside and between generations in the charged sector at tree level. By contrast, there are no flavour-changing transitions in the neutral sector at tree level. We can write

$$V = \begin{pmatrix} V_{ud} & V_{us} & V_{ub} \\ V_{cd} & V_{cs} & V_{cb} \\ V_{td} & V_{ts} & V_{tb} \end{pmatrix} \quad (7)$$

Due to the unitarity, not all the entries of the CKM matrix are independent. The independent parameters are four in the case of three generations, and can be interpreted as three rotation angles and one phase. There are several equivalent parameterization of the CKM matrix. A common one is

$$V = \begin{pmatrix} c_{12}c_{13} & s_{12}c_{13} & s_{13}e^{-i\delta} \\ -s_{12}c_{23} - c_{12}s_{23}s_{13}e^{i\delta} & c_{12}c_{23} - s_{12}s_{23}s_{13}e^{i\delta} & s_{23}c_{13} \\ s_{12}s_{23} - c_{12}c_{23}s_{13}e^{i\delta} & -c_{12}s_{23} - s_{12}c_{23}s_{13}e^{i\delta} & c_{23}c_{13} \end{pmatrix}, \quad (8)$$

where $c_{ij} = \cos \theta_{ij}$ and $s_{ij} = \sin \theta_{ij}$, with i and j labeling families that are coupled through that angle ($i, j = 1, 2, 3$). This CKM parameterization can be seen as the product of three rotations, with the phase put on the smallest element. The rotation angles may be restricted to lie in the first quadrant, provided one allows the phase δ to be free. As a consequence, c_{ij} and s_{ij} can all be chosen to be positive. The angle θ_{12} is generally called the Cabibbo angle (θ_C), and $\sin \theta_C \simeq 0.22$, corresponding to a value $\theta_C \simeq 13^\circ$. The angle of mixing between the second and the third family is $\theta_{23} \simeq 2^\circ$, and between the first and the third is $\theta_{13} \simeq 0.2^\circ$. The phase δ is constrained by measurements of the CP violation in K decays to be in the range $0 < \delta < \pi$. Its value is approximately $\delta \simeq 1.2$. In this parameterization, the s_{ij} are simply related to directly measurable quantities

$$\begin{aligned} s_{13} &= |V_{ub}| \\ s_{12} &= |V_{us}| / \sqrt{1 - |V_{ub}|^2} \sim |V_{us}| \\ s_{23} &= |V_{cb}| / \sqrt{1 - |V_{ub}|^2} \sim |V_{cb}| \end{aligned} \quad (9)$$

where we have set $|V_{ub}| \ll 1$, as indicated by data.

According to experimental evidence, the CKM matrix has a hierarchical structure. Transitions within the same generation are characterized by matrix elements of order $O(1)$. Transitions between the first and second generations are suppressed by a factor of $O(10^{-1})$, between the second and third generations by a factor of $O(10^{-2})$ and between the first and third generations by a factor of $O(10^{-3})$. This hierarchy has prompted

another useful parameterization, the so-called Wolfenstein parameterization [2], based on a series expansion in the small parameter $\lambda = |V_{us}|$. At order λ^3 we have

$$V = \begin{pmatrix} 1 - \lambda^2/2 & \lambda & A\lambda^3(\rho - i\eta) \\ -\lambda & 1 - \lambda^2/2 & A\lambda^2 \\ A\lambda^3(1 - \rho - i\eta) & -A\lambda^2 & 1 \end{pmatrix} + O(\lambda^4). \quad (10)$$

This parameterization corresponds to a particular choice of phase convention which eliminates as many phases as possible and puts the one remaining complex phase in the matrix elements V_{ub} and V_{td} . In this parameterization the unitarity of the matrix is explicit, up to λ^3 corrections. The real, independent, parameters A , ρ and η are known to be roughly of order unity, while λ , that is essentially the sine of the Cabibbo angle, s_{12} , is a small number, of order 0.2. Relative sizes of amplitudes depending on CKM parameters can be roughly estimated by counting powers of λ in the Wolfenstein parameterization.

It is convenient to express the Wolfenstein parameters through phase convention-independent quantities

$$\begin{aligned} s_{12}^2 &= \lambda^2 = \frac{|V_{us}|^2}{|V_{ud}|^2 + |V_{us}|^2} \\ s_{23}^2 &= A^2\lambda^4 = \frac{|V_{cb}|^2}{|V_{ud}|^2 + |V_{us}|^2} \\ \bar{\rho} + i\bar{\eta} &= -\frac{V_{ud}V_{ub}^*}{V_{cd}V_{cb}^*} \end{aligned} \quad (11)$$

where $\bar{\rho}$ and $\bar{\eta}$ are two new parameters that substitute ρ and η . These relations ensure that the CKM matrix written in terms of λ , A , $\bar{\rho}$, and $\bar{\eta}$ is unitary to all orders in λ [3]. When terms of the $\mathcal{O}(\lambda^6)$ are neglected, we have

$$V_{\text{CKM}} \simeq \begin{pmatrix} 1 - \frac{1}{2}\lambda^2 - \frac{1}{8}\lambda^4 & \lambda & A\lambda^3(\bar{\rho} - i\bar{\eta}) \\ -\lambda + \frac{1}{2}A^2\lambda^5[1 - 2(\bar{\rho} + i\bar{\eta})] & 1 - \frac{1}{2}\lambda^2 - \frac{1}{8}\lambda^4(1 + 4A^2) & A\lambda^2 \\ A\lambda^3[1 - (\bar{\rho} + i\bar{\eta})] & -A\lambda^2 + \frac{1}{2}A\lambda^4[1 - 2(\bar{\rho} + i\bar{\eta})] & 1 - \frac{1}{2}A^2\lambda^4 \end{pmatrix} \quad (12)$$

Since we have defined

$$s_{13}e^{i\delta} = V_{ub}^* = A\lambda^3(\rho - i\eta) \quad (13)$$

the following relation holds

$$\rho + i\eta = \left(1 + \frac{\lambda^2}{2}\right)\bar{\rho} + i\bar{\eta} + O(\lambda^4) \quad (14)$$

Thus one can reproduce the CKM matrix (12) at the same order in ρ and η by the substitutions $\bar{\rho} \rightarrow \rho$ and $\bar{\eta} \rightarrow \eta$ in all entries, except V_{td} where the substitution is $(\bar{\rho} + i\bar{\eta}) \rightarrow (1 - \frac{1}{2}\lambda^2)(\rho + i\eta)$.

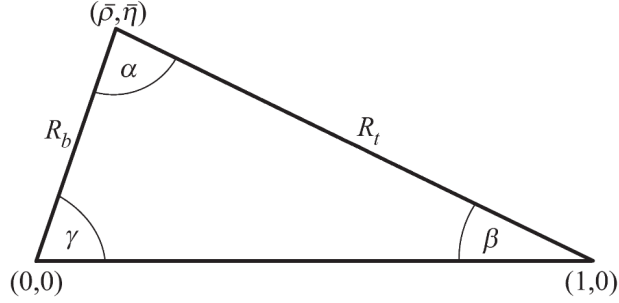


Figure 1. The unitarity triangle in the complex plane.

2.3. The unitarity triangles

The unitarity of the CKM matrix implies

$$\begin{aligned} \sum_{i=1}^3 |V_{ij}|^2 &= 1 \quad j = 1, 2, 3 \\ \sum_{i=1}^3 V_{ji} V_{ki}^* &= \sum_{i=1}^3 V_{ij} V_{ik}^* = 0 \quad j, k = 1, 2, 3 \quad j \neq k \end{aligned} \quad (15)$$

The equalities for the off-diagonal terms are sums of three complex numbers, depending on the four CKM parameters. They are

$$V_{ud} V_{us}^* [\mathcal{O}(\lambda)] + V_{cd} V_{cs}^* [\mathcal{O}(\lambda)] + V_{td} V_{ts}^* [\mathcal{O}(\lambda^5)] = 0 \quad (16)$$

$$V_{ud}^* V_{cd} [\mathcal{O}(\lambda)] + V_{us}^* V_{cs} [\mathcal{O}(\lambda)] + V_{ub}^* V_{cb} [\mathcal{O}(\lambda^5)] = 0 \quad (17)$$

$$V_{us} V_{ub}^* [\mathcal{O}(\lambda^4)] + V_{cs} V_{cb}^* [\mathcal{O}(\lambda^2)] + V_{ts} V_{tb}^* [\mathcal{O}(\lambda^2)] = 0 \quad (18)$$

$$V_{cd}^* V_{td} [\mathcal{O}(\lambda^4)] + V_{cs}^* V_{ts} [\mathcal{O}(\lambda^2)] + V_{cb}^* V_{tb} [\mathcal{O}(\lambda^2)] = 0 \quad (19)$$

$$V_{ud} V_{ub}^* [\mathcal{O}(\lambda^3)] + V_{cd} V_{cb}^* [\mathcal{O}(\lambda^3)] + V_{td} V_{tb}^* [\mathcal{O}(\lambda^3)] = 0 \quad (20)$$

$$V_{ud}^* V_{td} [\mathcal{O}(\lambda^3)] + V_{us}^* V_{ts} [\mathcal{O}(\lambda^3)] + V_{ub}^* V_{tb} [\mathcal{O}(\lambda^3)] = 0 \quad (21)$$

In these relations it is indicated in parenthesis the order of each term in the expansion parameter λ . These equalities give way to a geometric representation in terms of $\bar{\rho}$, $\bar{\eta}$, A and λ , since in the complex plane they can be geometrically represented by triangles, all characterized by the same area [4]. Only the last two of the six triangles corresponding to these equalities have sides of the same order of magnitude, $\mathcal{O}(\lambda^3)$ (i.e., the triangles are not squashed). In particular, the triangle defined by (20), rescaled by a factor $V_{cd} V_{cb}^*$ is commonly referred to as the unitarity triangle (UT) (see figure 1). Because it involves the term $V_{cd} V_{cb}^*$ and $V_{ud} V_{ub}^*$, the UT arises naturally in analyses involving B mesons. With the bases of the UT normalized to unity, the coordinates of the UT apex

are $(\bar{\rho}, \bar{\eta})$. The sides R_b and R_t are given by the magnitudes of

$$\begin{aligned} R_b &= \frac{V_{ud}V_{ub}^*}{V_{cd}V_{cb}^*} = \left(1 - \frac{\lambda^2}{2}\right) \frac{1}{\lambda} \frac{V_{ub}^*}{|V_{cb}|} \\ R_t &= \frac{V_{td}V_{tb}^*}{V_{cd}V_{cb}^*} = \frac{1}{\lambda} \frac{V_{td}}{|V_{cb}|} \end{aligned} \quad (22)$$

As can be seen, a special role is played by $|V_{cb}|$, which normalizes the UT triangle. Due to its economical structure in terms of only four parameters, the CKM matrix can be determined experimentally by exploiting several different flavour changing decays or processes related to neutral-meson mixing. One tries to measure as many observable as possible, in function of the UT triangle parameters, over-constraining the shape of the triangle and testing that it closes. The consistency of the various measurements probes the consequences of unitarity in the three generations SM and discrepancies with the SM expectations signal the possibility of NP in some observable. An extensive program of measurements of the UT parameters has been carried through at different experiments since the nineties. Due to the complexity of non-perturbative strong interactions, it is convenient to analyze processes with a limited number of hadrons in the initial or final state, as semileptonic B decays into one hadron, or observables (typically ratios) for which uncertainties due to such QCD effects reduce or cancel. Besides, since the potential sensitivity to NP is limited for tree-level processes, they are often preferred to fix the CKM parameters. Tree level processes are e.g. the semileptonic B decays into charmed states, mediated by the quark decay $b \rightarrow c\ell\nu_\ell$ at the lowest order in the SM. The results from tree-level processes can be used as input for precise SM predictions of rare, loop-induced processes. Since the start of the analyses on the UT triangle, there has always been an intensive strain to combine all available measurements (global analysis) in order to obtain statistically meaningful constraints on the CKM parameters, in the framework of the SM and some of its extensions \ddagger .

3. Semileptonic B meson decays

Semileptonic B decays are the processes of election when it comes to a precise determination of the magnitude of the CKM matrix element V_{cb} . At the lowest order in the SM, semileptonic B decays are mediated by the a tree level quark decay, the $b \rightarrow c\ell\nu_\ell$ decay, whose amplitude is proportional to V_{cb} , as illustrated in figure 2. The presence of leptons in the final states simplifies the QCD analyses, since hadronic and leptonic currents factorize.

There are two methods for $|V_{cb}|$ determination with semileptonic B decays, taking the name from the hadronic processes involved. In the so-called exclusive method, $|V_{cb}|$ is extracted by studying exclusive decays, in particular $B \rightarrow D^{(*)}\ell\nu_\ell$. Having only one hadron in the final state facilitates the analysis (e.g. no final state rescattering). The inclusive method refers to the investigation of the inclusive semileptonic decay

\ddagger A systematic program in this direction is carried on by the CKMfitter [5] and UTfit collaborations [6].

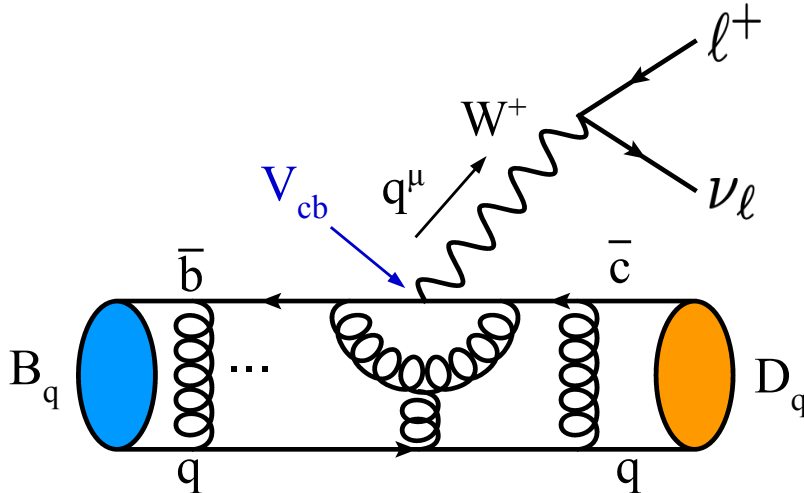


Figure 2. Diagram of the $B_q \rightarrow D_q \ell^+ \nu_\ell$ decay. The amplitude of this process is proportional to V_{cb} . The transfer four-momentum q^μ is given by $q^\mu \equiv p_B^\mu - p_D^\mu = p_\ell^\mu - p_{\nu_\ell}^\mu$. The diagram is at the lowest order in the weak interactions and the gluon configuration depicted is merely indicative.

$B \rightarrow X_c \ell \nu_\ell$ decays, where the final state X_c is a hadronic state originated by the charm quark. The inclusive and exclusive determinations rely on different theoretical calculations and make use of different techniques which, to a large extent, have uncorrelated experimental uncertainties. Comparing the results of these two largely independent approaches represents also a powerful test of our understanding of hadron dynamics. We detail both approaches in the following.

3.1. Inclusive decays

In inclusive $B \rightarrow X_c \ell \nu_\ell$ decays, the final state X_c is a hadronic state originated by the charm quark. Inclusive decays can be interpreted as a sum over all possible hadronic final states; the details of the hadronic final states are lost, and transition amplitudes are expected to be sensitive only to the dynamics of the initial B meson. Quark-hadron duality is generally assumed, which means, loosely speaking, that the inclusive hadronic observables, when integrated over large enough portions of phase space, are described in terms of the underlying parton-level processes, provided all possible sources of corrections stemming from QCD are properly accounted for §.

Both perturbative and non-perturbative QCD interactions affect decay processes in an essential way. A basic tool to disentangle their contributions to the decay amplitude in a systematic fashion is provided by the operator product expansion (OPE). The OPE formalism allows us to express the non-perturbative physics in terms of B meson matrix elements of local, gauge invariant, operators, and the perturbative physics in

§ For reviews on quark-hadron duality see for instance [7,8]

terms of Wilson coefficients, which can be computed as a series in a perturbative QCD coupling α_s . In other terms, the OPE separates the physics associated with soft scales (parametrized by the matrix elements of the local operators) from that associated with hard scales, which determine the Wilson coefficients. Semileptonic B decays have an intrinsic large 'dynamic' scale of energy release of the order of the b -quark mass, while the soft scale is of the order of the hadronic scale Λ_{QCD} . The large hierarchy between these two scales leads naturally to Λ_{QCD}/m_b as an expansion parameter of non-perturbative effects and to a description of the heavy b -quark in the framework of the Heavy Quark Effective Theory (HQET) (for a review see for instance [9]).

Jumping to the conclusions, sufficiently inclusive quantities (typically the total semileptonic width and the moments of the kinematic distributions) can be expressed as a double series in α_s and Λ_{QCD}/m_b . This expansion is referred to as Heavy Quark Expansion (HQE). The expansion for the total semileptonic width takes the form

$$\begin{aligned} \Gamma(B \rightarrow X_c \ell \nu) = & \frac{G_F^2 m_b^5}{192\pi^3} |V_{cb}|^2 [c_3 \langle O_3 \rangle + \\ & + c_5 \frac{\langle O_5 \rangle}{m_b^2} + c_6 \frac{\langle O_6 \rangle}{m_b^3} + O\left(\frac{\Lambda_{QCD}^4}{m_b^4}, \frac{\Lambda_{QCD}^5}{m_b^3 m_c^2}, \dots\right)] \end{aligned} \quad (23)$$

Here c_d ($d = 3, 5, 6 \dots$) are short distance coefficients, calculable in perturbation theory as a series in the strong coupling α_s , and O_d denote local operators of (scale) dimension d . The hadronic expectation values of the operators encode the nonperturbative corrections and can be parametrized in terms of HQE parameters, whose number grows with powers of Λ_{QCD}/m_b . The leading term is given by the free b -quark decay (parton model). A remarkable feature of (23) is the absence of a contribution of order $1/m_b$, due to the absence of an independent gauge invariant operator of dimension four. The power corrections start at $O(\Lambda_{QCD}^2/m_b^2)$, and are comparatively suppressed. The fact that nonperturbative, bound state effects in inclusive decays are strongly suppressed (at least two powers of the heavy quark mass) explains a posteriori the success of parton model in describing such processes. Due to the relative sizes of the b and c quarks, at higher orders in the expansion, terms suppressed by powers of m_c also appear, starting with $O(\Lambda_{QCD}^5/m_b^3 m_c^2)$.

Similar expansions give the moments of distributions of charged-lepton energy, hadronic invariant mass and hadronic energy. As most experiments can detect the leptons only above a certain threshold in energy, the charged-lepton energy moments are defined as

$$\langle E_\ell^n \rangle = \frac{1}{\Gamma_{E_\ell > E_{cut}}} \int_{E_\ell > E_{cut}} E_\ell^n \frac{d\Gamma}{dE_\ell} dE_\ell \quad (24)$$

where E_ℓ is the charged lepton energy in the $B \rightarrow X_c \ell \nu_\ell$ decays, n is the order of the moment, $\Gamma_{E_\ell > E_{cut}}$ is the semileptonic width above the energy threshold E_{cut} and $d\Gamma/dE_\ell$ is the differential semileptonic width as a function of E_ℓ . The hadronic mass moments are

$$\langle m_X^{2n} \rangle = \frac{1}{\Gamma_{E_\ell > E_{cut}}} \int_{E_\ell > E_{cut}} m_X^{2n} \frac{d\Gamma}{dm_X^2} dm_X^2 \quad (25)$$

Other moments (and cuts on other observables) can be defined in a similar way. It is sometimes convenient to employ central moments, computed relative to the averages $\langle E_l \rangle$ and $\langle m_X^2 \rangle$, that is

$$l_n(E_{cut}) \equiv \langle (E_l - \langle E_l \rangle)^n \rangle \quad h_n(E_{cut}) \equiv \langle (m_X^2 - \langle m_X^2 \rangle)^n \rangle \quad (26)$$

Let us stress that the HQE is valid only for sufficiently inclusive measurements and away from perturbative singularities, therefore the relevant quantities to be measured are global shape parameters (moments of various kinematic distributions) and the total rate. While the general structure of the expansion is the same for all the above mentioned observables, the perturbative coefficients are in general different.

Details on HQE will be given in section 3.1.1 and the sensitivity of rates and momenta to the definition of quark masses briefly discussed in section 3.1.2. In section 5 we will draw conclusions on the inclusive $|V_{cb}|$ extraction.

3.1.1. Heavy Quark Expansion In order to discuss the characteristics and the status of the HQE in $B \rightarrow X_c \ell \nu_\ell$ decays, let us go back to the expansion for the total semileptonic width in (23). The hadronic expectation values of the local operators O_d are the (normalized) forward matrix elements, written in the short-hand notation as

$$\langle O_d \rangle \equiv \frac{\langle B | O_d | B \rangle}{2m_B} \quad (27)$$

where m_B is the B meson mass, included in the definition for the normalization and dimensional counting. This set of operators, built with dimensional criteria using HQET b quarks fields, is basically the same set of operators, albeit with different weights, that appears in other B decay rates as well as distributions. While we can easily identify these operators and their dimensions, we cannot compute their hadronic expectation values from first principles, and we have to express them in function of a number of HQET parameters, which increases with powers of $1/m_b$.

The lowest-order terms of HQE are the dimension-three operators. In the HQET formalism, v_μ is the B meson velocity ($v^2 = 1$, $v_0 > 0$) and $b_v(x) = e^{-im_b v \cdot x} b(x)$ is the b field whose space time dependence is determined by the residual momentum $k_\mu = p_\mu - m_b v_\mu$, which is due to binding effects of the heavy quark inside the heavy B meson, and it is of order Λ_{QCD} . Owing to Lorentz invariance and parity there are only two combinations which can appear, namely $O_3 = \bar{b}_v \not{v} b_v$ and $O'_3 = \bar{b}_v b_v$. Since the operators b_v differ from the full QCD operators only by a phase redefinition, the equalities $\bar{b}_v \not{v} b_v = \bar{b} \not{v} b$ and $\bar{b}_v b_v = \bar{b} b$ hold. The matrix element of the former is

$$\langle B | \bar{b} \not{v} b | B \rangle = v^\mu \langle B | \bar{b} \gamma_\mu b | B \rangle = v^\mu (2m_B v_\mu) = 2m_B \quad (28)$$

The penultimate equality follows because $\bar{b} \gamma_\mu b$ is the conserved b quark number current. The hadronic expectation value of the operator $\bar{b}_v b_v$ between the heavy meson states can be expanded in $1/m_b$, finding that it differs from the hadronic expectation value of the operator $\bar{b}_v \not{v} b_v$ by terms of order $1/m_b^2$. Thus the matrix elements of the dimension-three contribution are known; they incorporate the parton model result which dominates asymptotically, i.e. for $m_b \rightarrow \infty$.

At order $1/m_b^0$ in the HQE, that is at the parton level, the perturbative corrections up to order α_s^2 to the width and to the moments of the lepton energy and hadronic mass distributions are known completely [10–16]. The terms of order $\alpha_s^{n+1}\beta_0^n$, where β_0 is the first coefficient of the QCD β function, $\beta_0 = (33 - 2n_f)/3$, have also been computed following the Brodsky-Lepage-Mackenzie (BLM) procedure [13, 17].

By using the equation of motion in HQET, one can check that there are no matrix elements of dimension four operators that occur in the HQE. This means that there are no corrections suppressed by a single power of Λ_{QCD}/m_b .

The next order is Λ_{QCD}^2/m_b^2 , and at this order the HQE includes two operators, called the kinetic energy and the chromomagnetic operator. Their matrix elements, μ_π^2 and μ_G^2 , respectively, are defined as

$$\begin{aligned}\mu_\pi^2 &\equiv \frac{1}{2m_B} \langle B | \bar{b}_v \vec{\pi}^2 b_v | B \rangle \\ \mu_G^2 &\equiv \frac{1}{2m_B} \langle B | \bar{b}_v \frac{i}{2} \sigma_{\mu\nu} G^{\mu\nu} b_v | B \rangle\end{aligned}\tag{29}$$

where $\vec{\pi} = -i\vec{D}$, D^μ is the covariant derivative and $G^{\mu\nu}$ is the gluon field tensor. The matrix element μ_π^2 is naturally associated with the average kinetic energy of the b quark inside the B meson while the matrix element μ_G^2 is connected to the $B^* - B$ hyperfine mass splitting. Both matrix elements generally depend on a cut-off μ chosen to separate soft and hard physics, which can be implemented in different ways, or schemes. Perturbative corrections to the coefficients of the kinetic operator [18, 19] and the chromomagnetic operator [20–22] have been evaluated at order α_s .

Two independent parameters, $\rho_{D,LS}^3$, are also needed to describe matrix elements of operators of dimension six, that is at order $1/m_b^3$. Their coefficients have long been known at tree level, i.e. neglecting perturbative corrections [23]. Very recently an analytical calculation of the α_s corrections for the coefficient ρ_D^3 has been presented [24].

Starting at order Λ_{QCD}^3/m_b^3 , terms with an infrared sensitivity to the charm mass appear, at this order as a $\log m_c$ contribution [25–27]. At higher orders these contributions, sometimes dubbed intrinsic charm contribution, in form of powers of Λ_{QCD}/m_c , have to be considered as well. Indeed, roughly speaking, since $m_c^2 \sim O(m_b \Lambda_{QCD})$ and $\alpha_s(m_c) \sim O(\Lambda_{QCD})$, contributions of order $\Lambda_{QCD}^5/m_b^3 m_c^2$ and $\alpha_s(m_c) \Lambda_{QCD}^4/m_b^2 m_c^2$ are expected comparable in size to contributions of order Λ_{QCD}^4/m_b^4 .

Presently, the matrix elements have been identified and estimated up to the order $1/m_b^4$ and $1/m_b^5$ [28–30]. In HQE the number of independent parameters needed to describe the nonperturbative physics of matrix elements grows with the order in $1/m_b$. At dimension seven and eight, nine and eighteen independent matrix elements appear, respectively, and for higher orders one has an almost factorial increase in the number of independent parameters.

3.1.2. Mass schemes In QED, the location of the divergence in the propagator of the electron can be taken as a physical definition of the electron mass, and it is indicated as on-shell or pole mass. This definition is not naturally extended to quarks, which are

confined and can never be seen as asymptotic states. While not measurable per se due to confinement, one can still define a pole mass for quarks in a formally consistent way within perturbation theory. However, this mass will be plagued by ambiguities related to non-perturbative effects in QCD, the so-called renormalon ambiguities (for a review see for instance [31]), when related to observable quantities. Alternative definitions of mass for a quark can be used, each with its own advantages and disadvantages, but all requiring a careful description of the adopted framework (prescription or scheme).

The HQE nonperturbative parameters depend on the heavy quark mass, although sometimes the infinite mass limit of these parameters is taken. They are affected by the particular theoretical scheme that is used to define the quark masses.

A commonly used definition of the mass of the quark is the minimal subtraction ($\overline{\text{MS}}$) mass, which corresponds to the running renormalized mass in perturbative QCD, when, in dimensional regularization, the finite parts of the relevant counterterms are set to zero. In the $\overline{\text{MS}}$ subtraction scheme, also $\ln(4\pi)$ and γ_E factors are subtracted off. The $\overline{\text{MS}}$ prescription has the advantage of computational simplicity. The mass $m_b^{\overline{\text{MS}}}(\mu)$ depends on a scale μ and it is not affected by renormalon ambiguities. It is sometimes referred as a short-distance mass, since it is well defined in the infrared regime. The $\overline{\text{MS}}$ is quite appropriate for describing heavy flavour production, but not for treating heavy meson decays, where the dynamics is characterized by scales lower than the heavy scale m_b .

Alternative scheme have been proposed, sometimes referred as threshold schemes; we list the most commonly used to describe heavy quarks in heavy mesons. In the kinetic scheme [32–34], the so-called “kinetic mass” $m_b^{\text{kin}}(\mu)$ is the mass entering the non-relativistic expression for the kinetic energy of a heavy quark. It is defined by introducing an explicit factorization scale, and subtracting the physics at scales below this scale from the quark-mass definition. More technically, its definition requires using heavy-quark sum rules for semileptonic $b \rightarrow c$ decays in the small velocity (SV) limit.

Other examples of threshold schemes are the PS (Potential subtracted) scheme [35] and the 1S scheme [36–38]. The PS mass and the kinetic mass are similar, in the sense that they both subtract out the troublesome infrared part by introducing an explicit factorization scale. The PS scheme is based on the properties of nonrelativistic quark-antiquark systems, whose dynamics depends on the total static energy. The contribution to the potential from the region of small momenta, identified as the source of the leading renormalon, is subtracted from the PS mass. The 1S mass is defined as half the energy of the 1S state Υ state calculated in perturbation theory. In the 1S scheme there is a mismatch with the usual perturbation theory, overcome by a working tool, the so-called ‘ Υ expansion’, whose validity has been questioned [39].

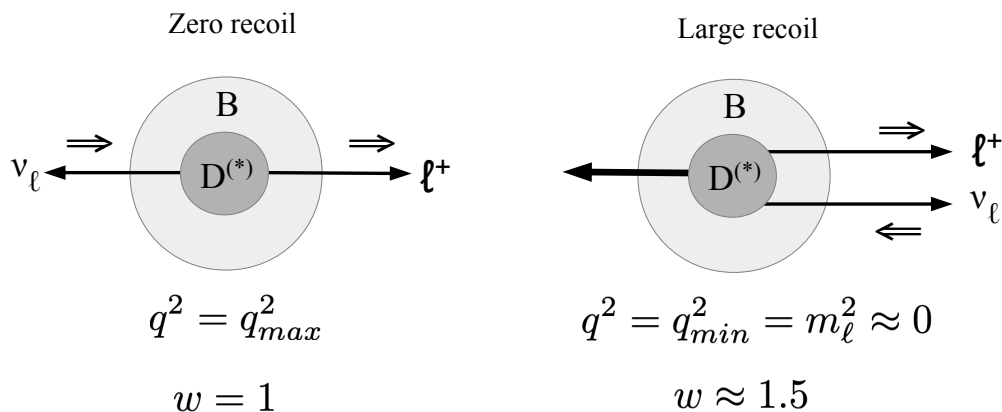


Figure 3. In the "zero recoil" kinematic configuration the hadron is at the rest in the B meson rest frame, so the two leptons are produced back to back. In the "large recoil" limit the leptons are produced parallel and opposite to the hadron that acquires the largest momentum. The spin of the right-handed neutrino and the left-handed positron are also depicted.

3.2. Exclusive decays into light leptons

In this section we discuss the exclusive semileptonic CKM favoured $B \rightarrow D^{(*)} \ell \nu_\ell$ decays, when $\ell = e, \mu$. Neglecting lepton masses, their SM differential ratios can be written as

$$\begin{aligned} \frac{d\Gamma}{dw}(B \rightarrow D^* \ell \nu_\ell) &= \frac{G_F^2}{48\pi^3} (m_B - m_{D^*})^2 m_{D^*}^3 \chi(w) (w^2 - 1)^{\frac{1}{2}} |V_{cb}|^2 |\eta_{EW}|^2 |\mathcal{F}(w)|^2 \\ \frac{d\Gamma}{dw}(B \rightarrow D \ell \nu_\ell) &= \frac{G_F^2}{48\pi^3} (m_B + m_D)^2 m_D^3 (w^2 - 1)^{\frac{3}{2}} |V_{cb}|^2 |\eta_{EW}|^2 |\mathcal{G}(w)|^2 \end{aligned} \quad (30)$$

where m_X is the mass of the X meson, p_X its 4-momentum and w is the recoil parameter, defined as $w = p_B \cdot p_{D^{(*)}} / (m_B m_{D^{(*)}}) = v_B \cdot v_{D^{(*)}}$; v_B and $v_{D^{(*)}}$ are the 4-velocities of the initial and final-state mesons. The recoil parameter is related to the energy transferred to the leptonic pair $q^2 = (p_B - p_{D^{(*)}})^2 = (p_\ell + p_{\nu_\ell})^2$, namely $w = (m_B^2 + m_{D^{(*)}}^2 - q^2) / (2m_B m_{D^{(*)}})$. In the B meson rest frame the expression for w reduces to the Lorentz boost $w = \gamma_{D^{(*)}} = E_{D^{(*)}} / m_{D^{(*)}}$. The values of the recoil parameter are limited by kinematics. The superior limit occurs when $q^2 = q_{min}^2 = m_\ell^2$, that is at $w = (m_B^2 + m_{D^{(*)}}^2) / (2m_B m_{D^{(*)}})$, assuming massless leptons. The inferior limit (the zero recoil point) is at $w = 1$, and corresponds at $q_{max}^2 = (m_B - m_{D^{(*)}})^2 \simeq 11$ GeV². Intuitively an higher q^2 (lower w) corresponds to an higher mass of the virtual W boson, which, at the two-body decay level, implies a lower "kick" to the $D^{(*)}$.

In figure 3, we give an illustration of the kinematics of the decays at low and high q^2 in the B meson rest frame. These simple pictures can be useful to gain some intuition about semileptonic B decays. For example the large *helicity* suppression at zero recoil of $B \rightarrow D \ell \nu_\ell$ decay compared to $B \rightarrow D^* \ell \nu_\ell$ decay, can be easily understood: the lepton and the neutrino are back to back, this means that the component of the total angular

momentum of the leptons along their line of flight is unity and cannot be compensated by the pseudoscalar D meson. At the other extreme, $q^2 \approx 0$, where the hadron recoil velocity is maximum, the lepton and the neutrino are parallel and their combined spin along this direction is null. For the $B \rightarrow D^* \ell \nu_\ell$ decays this means that the D^* is fully polarized having null spin projection along the lepton direction.

As seen in (30), the differential cross sections are proportional to

- the squared modulus of the CKM matrix element: $|V_{cb}|^2$
- a single form factor, $\mathcal{F}(w)$ and $\mathcal{G}(w)$, for $B \rightarrow D^* \ell \nu_\ell$ and $B \rightarrow D \ell \nu_\ell$, respectively
- η_{EW} , a structure-independent correction factor that accounts for electroweak effects [40]. In the literature, a long-distance EM radiation effect (Coulomb correction) is sometimes added to this factor [41]
- a phase space factor, $(w^2 - 1)^{1/2}$ and $(w^2 - 1)^{3/2}$ for $B \rightarrow D^* \ell \nu_\ell$ decays and $B \rightarrow D \ell \nu_\ell$ decays, respectively, that vanish at the zero recoil point. For $B \rightarrow D^* \ell \nu_\ell$ there is an additional phase space factor $\chi(w)$

$$\chi(w) = (w + 1)^2 \left(1 + \frac{4w}{w + 1} \frac{m_B^2 - 2w m_B m_{D^*} + m_{D^*}^2}{(m_B - m_{D^*})^2} \right) \quad (31)$$

The hardship of the extraction of $|V_{cb}|$ is due to the presence of the form factors, which cannot be computed in the framework of perturbation theory. In the heavy quark limit ($m_{b/c} \rightarrow \infty$), that is to lowest order in heavy quark effective theory, heavy quark symmetries predict that both form factors equal a single universal Isgur-Wise function, $\mathcal{F}(w) = \mathcal{G}(w) = \xi(w)$, which is absolutely normalized to unity at zero recoil, that is $\xi(w = 1) = 1$. This property has an intuitive reason. The no-recoil point corresponds to the kinematic situation where the D meson stays at rest in the rest frame of the decaying B ($v = v'$); the decaying b -quark, at rest, is transformed into a c -quark, also at rest. The light hadronic cloud does not notice the flavour change $b \rightarrow c$ and it is transferred from the B to the D meson with probability one. The form factor function is identical for $B \rightarrow D$ and $B \rightarrow D^*$ transitions, because these are related by the heavy-quark spin symmetry. For a realistic analysis, corrections to the heavy-quark limit have to be considered. At zero recoil, the heavy quark symmetries also provide the structure of the symmetry breaking non-perturbative corrections at finite heavy quark mass m , which start at order $1/m^2$ and $1/m$ for the $\mathcal{F}(w = 1)$ and $\mathcal{G}(w = 1)$ form factors, respectively.

In order to extract $|V_{cb}|$, we need not only to compute the form factors, but also to measure experimental decay rates. The advantage in the computation of the form factors provided by the heavy quark symmetries at $w = 1$ has the hindrance that the differential rates in (30) vanish at zero-recoil. Thus one needs to extrapolate the experimental points taken at $w \neq 1$ to the zero recoil point $w = 1$, using a parameterization of the dependence on w of the form factors, which introduces additional uncertainties. In other words, the $|V_{cb}|$ determination may proceed according to the following steps:

- 1) theoretical determination of the form factors \mathcal{F}/\mathcal{G} at zero recoil $w = 1$;
- 2) theoretical parameterization of the w dependence;

- 3) experimental measurements of the exclusive decays rates at non-zero recoil points, yielding the products $|\eta_{EW}|^2 |\mathcal{F}(w)|^2 |V_{cb}|^2$ or $|\eta_{EW}|^2 |\mathcal{G}(w)|^2 |V_{cb}|^2$;
- 4) extrapolation of the experimental points to zero recoil and $|V_{cb}|$ extraction.

Since a few years there is an endeavor to amend this strategy, by calculating form factors directly at non-zero recoil points, with evident advantages on the extraction of $|V_{cb}|$. Some results are already available in the $B \rightarrow D\ell\nu_\ell$ channel.

Several parameterizations for the momentum dependence of the form factors are on the market. Traditionally, the form factors are parameterized with an explicit pole and a sum of effective poles, see e.g. Ball and Zwicky [42, 43] and Becirevic and Kaidalov [44]. Although these parameterizations capture some known properties of form factors, in general they do not allow an easy quantification of systematic uncertainties. Recent determinations adopt a more systematic approach that aims at exploiting the positivity and analyticity properties of two-point functions of vector currents. In these parameterizations w is mapped onto a complex variable z via the conformal transformation $z = (\sqrt{w+1} - \sqrt{2})/(\sqrt{w+1} + \sqrt{2})$. The form factors may be written in form of an expansion in z , which converges rapidly in the kinematic region of heavy hadron decays. The coefficients of the expansions are subject to unitarity bounds based on analyticity [45–48]. To this type belong the CLN (Caprini-Lellouch-Neubert) [49], the BGL (Boyd-Grinstein-Lebed) [50] and the BCL (Bourrely-Caprini-Lellouch) [51] parameterizations. Further details are given in section 3.2.3. The experimental measurements of the form factors are described in sections 6.1 and 6.2 for the $B \rightarrow D^*\ell\nu_\ell$ and $B \rightarrow D\ell\nu_\ell$ decays, respectively.

3.2.1. Form factors From the field theory point of view, it is convenient to define form factors as coefficients of independent Lorentz structures appearing in the hadronic transition matrix elements. In the framework of HQET, the independent Lorentz 4-vectors are the velocities of the two mesons, rather than their momenta. This can be intuitively understood by considering that in the heavy flavour limit, $m_{b,c} \rightarrow \infty$ (m_b/m_c fixed), when the weak current changes the flavour $b \rightarrow c$, the light degrees of freedom inside the meson become aware of the change in the heavy quark velocities, $v_B \rightarrow v_{D^{(*)}}$ ($v_B \equiv p_B/m_B$, $v_{D^{(*)}} \equiv p_{D^{(*)}}/m_{D^{(*)}}$), rather than of the change in momenta. Since the only scalar formed from the velocities ($v_B^2 = v_{D^{(*)}}^2 = 1$ by definition) is $w = v_B \cdot v_{D^{(*)}}$, we can set [9]

$$\begin{aligned}
\frac{\langle D|V^\mu|B\rangle}{\sqrt{m_B m_D}} &= h_+(w)(v_B + v_D)^\mu + h_-(w)(v_B - v_D)^\mu \\
\frac{\langle D^*|V^\mu|B\rangle}{\sqrt{m_B m_{D^*}}} &= h_V(w)\varepsilon^{\mu\nu\rho\sigma}v_{B\nu}v_{D^*\rho}\epsilon^*_{\sigma} \\
\frac{\langle D^*|A^\mu|B\rangle}{\sqrt{m_B m_{D^*}}} &= ih_{A_1}(w)(1+w)\epsilon^{*\mu} - i[h_{A_2}(w)v_B^\mu + h_{A_3}(w)v_{D^*}^\mu]\epsilon^* \cdot v_B \quad (32)
\end{aligned}$$

where $\epsilon^{*\mu}$ is the D^* polarization vector, which respects the equality $\sum_{\alpha=1}^3 \epsilon_\alpha^{*\mu} \epsilon_\alpha^{*\nu} = -g^{\mu\nu} + v_{D^*}^\mu v_{D^*}^\nu$. In the conventional, relativistic normalization of the meson states

$|B(D^{(*)})\rangle$, the factor $1/\sqrt{m_{B(D^{*})}}$ on the left side of Eqs. (32) is omitted; its addition pertains to a mass independent renormalization [9].

In the heavy flavour limit there is only one form factor, the Isgur-Wise function $\xi(w)$ [52, 53]. In that limit, the form factors become

$$h_+(w) = h_V(w) = h_{A_1}(w) = h_{A_3}(w) = \xi(w) \quad h_-(w) = h_{A_2}(w) = 0 \quad (33)$$

The form factor $\mathcal{G}(w)$ in (30) can be expressed as a combination of $h_+(w)$ and $h_-(w)$ [9]

$$\mathcal{G}(w) = h_+(w) - \frac{m_B - m_D}{m_B + m_D} h_-(w) \quad (34)$$

Similarly, the form factor $\mathcal{F}(w)$ can be written as [9]

$$\begin{aligned} \mathcal{F}(w) = & \left\{ 2(1 - 2wr + r^2) \left[h_{A_1}^2 + \left(\frac{w-1}{w+1} \right) h_V^2 \right] + \right. \\ & \left. + [(1-r)h_{A_1} + (w-1)(h_{A_1} - h_{A_3} - rh_{A_2})]^2 \right\} \times \\ & \times \left\{ (1-r)^2 + \frac{4w}{w+1}(1-2wr+r^2) \right\}^{-1} \end{aligned} \quad (35)$$

where $r = m_{D^*}/m_B$. The form factor $\mathcal{F}(w)$ is dominated by the axial vector form factor h_{A_1} as $w \rightarrow 1$. It is sometimes convenient to define two ratios of the form factors

$$R_1 = \frac{h_V}{h_{A_1}} \quad R_2 = \frac{h_{A_3} + rh_{A_2}}{h_{A_1}} \quad (36)$$

In the infinity mass limit, heavy quark spin symmetry implies that $R_1 = R_2 = 1$, independently of the w value.

With respect to comparison with experimental results, the above definition of form factors is not the most convenient, since the combinations of form factors most easily obtained from data are those appearing in a sum of squares in the differential rates, namely, the helicity amplitudes. They are particular linear combinations of the original form factors, and thus simply form a different basis for the description of the matrix elements. In the $B \rightarrow D^* \ell \nu_\ell$ decay, one can use three helicity amplitudes, labeled H_\pm and H_0 , corresponding to the three polarization states of the D^* , two transverse and one longitudinal. The form factor $\mathcal{F}(w)$ can be expressed in terms of the helicity amplitudes as

$$\chi(w) |\mathcal{F}(w)|^2 = \frac{1 - 2wr + r^2}{12m_B m_{D^*} (1-r)^2} \left(H_0^2(w) + H_+^2(w) + H_-^2(w) \right) \quad (37)$$

The helicity amplitudes, in turn, depend on the $h_x(w)$ form factors

$$\begin{aligned} H_0(w) &= \frac{\sqrt{m_B m_{D^*}}}{1 - 2wr + r^2} (w+1) [(w-r)h_{A_1}(w) - (w-1)(rh_{A_2}(w) + h_{A_3}(w))] \\ H_\pm(w) &= \sqrt{m_B m_{D^*}} (w+1) \left[h_{A_1}(w) \pm \sqrt{\frac{w-1}{w+1}} h_V(w) \right] \end{aligned} \quad (38)$$

Other details on the w dependence of form factors and helicity amplitudes is given in section 3.2.4.

3.2.2. Zero recoil and beyond Since more than a decade, the lattice community performs computations of the $B \rightarrow D^{(*)}$ form factors. The difficulties related to heavy fermions on lattice can be naïvely summarized by observing that direct simulation of high mass such $ma \geq 1$, where a represent a lattice spacing, gives discretization errors out of control. As of today $m_b \sim 1/a$ and no direct simulation is possible. The main way out is the usage of effective theories, as HQET [52] and Non-Relativistic QCD (NRQCD) [54]. In broad terms, they eliminate high degrees of freedom, aided by systematic expansions in Λ_{QCD}/m_b . The downside is the introduction of new sources of errors (matching of HQET to QCD, renormalization, control of extrapolation, etc.) to take care of.

Another common approach to non-perturbative calculations of form factors are QCD sum rules. The sum rules are based on the general idea of calculating a relevant quark-current correlation function and relating it to the hadronic parameters of interest via a dispersion relation. They have reached wide application for calculation of exclusive amplitudes and form factors in the form of light cone sum rules (LCSR), employing light-cone OPE of the relevant correlation functions. Uncertainties may originate from the truncation of the expansions, the input parameter uncertainties, and the assumption of quark-hadron duality. Direct sum rules calculations, without extrapolations, hold in the kinematic region of large recoil (small q^2), where the lattice calculation are substantially more difficult, and are in this respect complementary to lattice analyses.

Let us now report recent results in literature, starting from the $B \rightarrow D^* \ell \nu_\ell$ channel, which is less suppressed in the phase space and whose branching fractions are more precise (even twice) in the majority of experimental measurements.

The form factor for the $B \rightarrow D^* \ell \nu$ channel, in the lattice unquenched $N_f = 2 + 1$ approximation has been estimated at zero recoil. The FNAL/MILC collaboration, which used Wilson fermions for both c and b heavy quarks, gives [41]

$$\mathcal{F}(1) = 0.906 \pm 0.004_{stat} \pm 0.012_{sys} \quad (39)$$

The first error is statistical and the second one is the sum in quadrature of all systematic errors. The total uncertainty is around the (1-2)% level. The largest error is the heavy quark discretization error related to the Fermilab action.

A more recent value of the lattice form factor $\mathcal{F}(1)$ at zero recoil has been presented by the HPQCD collaboration, which used the fully relativistic HISQ (Highly improved staggered quarks) action for light, strange and charm quarks and the NRQCD action for the b quark [55]

$$\mathcal{F}(1) = 0.895 \pm 0.010_{stat} \pm 0.024_{sys} \quad (40)$$

The dominant error arises from missing $O(\alpha_s^2)$ matching of NRQCD currents to QCD. Both the results in (39) and (40) are in good agreement. Another recent calculation by HPQCD focuses on $B_s \rightarrow D_s^* \ell \nu_\ell$ [56]. They use the HISQ action for all valence quarks in order to perform the normalizations of all required currents non-perturbatively and avoid a large source of systematic uncertainty. From their result for $\mathcal{F}_s(1)$ they extract $\mathcal{F}(1)$ by using the $\mathcal{F}(1)/\mathcal{F}_s(1)$ ratio computed in their older paper [55], and obtain [56]

$$\mathcal{F}(1) = 0.914 \pm 0.024 \quad (41)$$

in agreement with all previously mentioned determinations. All the above form factor values are reported in Table 1.

The LANL/SWME collaboration is working [57–59] to reduce the charm discretization error, the dominant ($\sim 1\%$) error in [41], to below the percent level [60] by using an improved version of the Fermilab action, the Oktay-Kronfeld action. Their calculation is carried out on the $N_f = 2 + 1 + 1$ MILC HISQ ensembles, at two lattice spacings $a \sim 0.12, 0.09$ fm and pion masses $m_\pi \sim 220, 310$ MeV. Preliminary results for $B \rightarrow D^* \ell \nu_\ell$ decays form factor h_{A_1} at zero recoil are reported. A crucial planned step will be to improve the currents up to order λ^3 , where $\lambda_{b,c} \sim \Lambda_{QCD}/2m_{b,c}$. They also plan to analyze two more data sets measured, to include other physical pion masses and finer lattices and to increase statistics.

At the current level of precision, it would be important to extend form factor unquenched calculations for $B \rightarrow D^*$ semileptonic decays to non-zero recoil, in order to reduce the uncertainty due to the extrapolation to $w = 1$. Indeed, at finite momentum transfer, only old quenched lattice results are available [61]. Stimulated by this objective, theory work on lattice is rapidly progressing.

Nearly final results at non-zero recoil, with $w \in [1, 1.1]$, are already available from the Fermilab/MILC collaboration [62–64]. Their latest analysis includes 15 MILC asqtad (a^2 , tadpole improved) ensembles with $N_f = 2+1$ flavors of sea quarks and lattice spacings ranging from $a \sim 0.15$ fm down to 0.045 fm. The valence light quarks employ the asqtad action, whereas the b and c quarks are treated using the Fermilab action. The analysis shows a larger slope at small recoil than the experimental measurements, and the source of this behavior is currently under investigation.

The work in progress of the JLQCD collaboration is based on Möbius domain-wall quarks, at zero and non-zero recoil, from $N_f = 2 + 1$ QCD [65]. The systematics of the continuum and chiral extrapolation are under investigation. A recent update [66] extends the w range to $w \in [1, 1.1]$ and simulates b quark masses up to $0.7 a^{-1}$ (at lattice cutoffs $a^{-1} \sim 2.4, 3.6$ and 4.5 GeV) to control discretization errors. Their preliminary results for $h_{A_1}(1)$ are in reasonable agreement with the previous estimates by Fermilab/MILC [41] and HPQCD [55].

For the $B \rightarrow D \ell \nu_\ell$ decays, lattice-QCD calculation of the hadronic form factors at non-zero recoil have become available since 2015 ||. In 2015, the FNAL/MILC collaboration has calculated the form factors for a range of recoil momenta and parameterized their dependence on momentum transfer using the BGL z -expansion. Their analysis employs ensembles at four values of the lattice spacing ranging between approximately 0.045 fm and 0.12 fm. The z expansion fit to lattice-only data gives [68]

$$\mathcal{G}(1) = 1.054 \pm 0.004_{stat} \pm 0.008_{sys} \quad (42)$$

Two months later, new results on $B \rightarrow D \ell \nu_\ell$ form factors at non-zero recoil were announced by the HPQCD Collaboration [69]. Their results are based on NRQCD

|| Prior results at non-zero recoil were only available in the quenched approximation [67].

Table 1. Latest lattice form factor estimates at zero recoil

Collaboration	Refs.	$\mathcal{F}(1)$	Refs.	$\mathcal{G}(1)$
FNAL/MILC	[41]	$0.906 \pm 0.004 \pm 0.012$	[68]	$1.054 \pm 0.004 \pm 0.008$
HPQCD	[55]	$0.895 \pm 0.010 \pm 0.024$	[69]	1.035 ± 0.040
HPQCD	[56]	0.914 ± 0.024		
$\mathcal{F}^{B_s \rightarrow D_s^*}(1)$			$\mathcal{G}^{B_s \rightarrow D_s}(1)$	
HPQCD	[56]	$0.9020 \pm 0.0096 \pm 0.0090$	[70]	1.068 ± 0.004
Atoui et al.			[71]	1.052 ± 0.046

action for b quarks and the HISQ action for c quarks, together with $N_f = 2 + 1$ MILC gauge configuration. By using the CLN parameterization they obtain at zero recoil

$$\mathcal{G}(1) = 1.035 \pm 0.040 \quad (43)$$

Both the FNAL/MILC [68] and HPQCD [69] estimates for the form factors at zero recoil are reported in Table 1. They are in good agreement, although the HPQCD one has larger errors coming mainly from discretization effects and the systematic uncertainty associated with the perturbative matching, as in the $B \rightarrow D^*$ case.

Until the very recent LHCb measurement [72], the lattice QCD results for $B_s \rightarrow D_s^{(*)}$ form factors could not be compared with experiment. Now the $B_s \rightarrow D_s^{(*)} \ell \nu_\ell$ decays supply a new method for precisely determining $|V_{cb}|$. These decays are more advantageous from the point of view of lattice, since the larger mass of the valence s quark compared to u or d quarks makes the calculations of the form factors less computationally expensive.

There are two analyses of the $B_s \rightarrow D_s^*$ zero-recoil form factors [55, 56], both from the HPQCD collaboration using $N_f=2+1+1$ MILC HISQ ensembles. These analyses differ in the treatment of the b quark. The calculation of [55] uses an NRQCD b -quark, while [56] uses the relativistic ‘heavy-HISQ’ approach on fine ensembles down to $a \sim 0.45$ fm to avoid the main systematic uncertainty, which comes from the perturbative current matching known to $O(\alpha_s)$. The results are in agreement, and in Table 1 we have reported the more recent value $\mathcal{F}^{B_s \rightarrow D_s^*}(1) = 0.9020 \pm 0.0096_{stat} \pm 0.0090_{sys}$ [56].

Lattice QCD calculations of $B_s \rightarrow D_s$ form factors have already been performed at high q^2 , close to zero recoil, where statistical errors are smaller. The signal/noise degrades exponentially as the spatial momentum of the meson in the final state grows. Systematic errors from missing discretization (and relativistic) corrections also grow away from zero recoil.

A recent published result for the zero-recoil vector form factors $\mathcal{G}^{B_s \rightarrow D_s}(1) = 1.068 \pm 0.004$ was provided by the HPQCD Collaboration [70] and it is reported in Table 1. The dominant source of uncertainty is due to discretization effects, followed by perturbative matching uncertainties. In Table 1 we also report the zero recoil value given by a $N_f = 2$ determination which uses twisted Wilson quarks $\mathcal{G}^{B_s \rightarrow D_s}(1) = 1.052 \pm 0.046$

[71]. The MILC collaboration has determined the ratios between the semileptonic decay $\bar{B}^0 \rightarrow D^+ \ell^- \bar{\nu}_\ell$ and $\bar{B}_s^0 \rightarrow D_s^+ \ell^- \bar{\nu}_\ell$ [73], and, more recently, the ratios of the scalar and vector form factors for the decays $B_s \rightarrow K \ell \nu_\ell$ and $B_s \rightarrow D_s \ell \nu_\ell$ [74]. They have used $N_f = 2 + 1$ asqtad ensembles, and the clover action with Fermilab interpretation for b and c valence quarks. Preliminary results on semileptonic $B_s \rightarrow D_s$ form factors have also been presented by the RBC/UKQCD Collaboration [75–77]. In the valence sector they have used domain wall fermions for u/d , s and c quarks, whereas b quarks have been simulated with the relativistic heavy quark action.

Very recently, the HPQCD Collaboration has presented a lattice QCD determination of the $B_s \rightarrow D_s \ell \nu_\ell$ scalar and vector form factors over the full physical range of momentum transfer [78]. They work with a highly improved quark action and cover a range of values of the lattice spacing that includes very fine lattices and results from lighter than physical b quarks.

In alternative to lattice, form factor estimates are available via zero recoil sum rules, giving [79, 80] $\mathcal{F}(1) = 0.86 \pm 0.02$, in good agreement with the lattice value in (39), but slightly lower in the central value. Recently, information on all form factors parameterizing matrix elements of the basis of dimension-six operators, including those appearing only in connection of new physics effects, has become available in the framework of QCD LCSR [81], and exploited for $|V_{cb}|$ determinations from $B \rightarrow D^{(*)} \ell \nu_\ell$ decays [82].

3.2.3. Unitarity bounds As mentioned above, the extraction of $|V_{cb}|$ involves an extrapolation to the zero-recoil point, for which a parameterization of the form factors in terms of w is needed. In this section we describe briefly parameterizations built on the basis of dispersion relations and unitarity bounds. Since more than 50 years, it has been known that nontrivial constraints on an hadronic form factor can be derived starting from a given inequality on a suitable integral of the square modulus of the form factor, along the unitarity cut. Let $F(t)$ denote a generic form factor, depending on a variable t , which is real analytic in the complex t -plane cut along the positive real axis from the lowest unitarity branch point t_+ to ∞ . The essential inequality just mentioned is expressed as

$$\int_{t_+}^{\infty} dt \rho(t) |F(t)|^2 < I \quad (44)$$

where both the function $\rho(t) \geq 0$ and the quantity I are known. Such integral condition can be provided by an observable or, alternatively, by the dispersion relation satisfied by a suitable correlator. The positive spectral function of the correlator has, by unitarity, a lower bound involving the modulus squared of the relevant form factor. Therefore, the constraints derived in this framework are often referred to as “unitarity bounds”. Through complex analysis, this condition leads to constraints on the values at interior points or on the expansion parameters.

Many applications of this approach to the heavy-to-heavy and heavy-to-light form factors, the light-meson form factors, the electro-magnetic form factor of the pion, the

strangeness changing $K\pi$ form factors, and so on, can be found in literature (for a review see e.g. [83]). Here we sketch the application to $B \rightarrow D^{(*)}$ decays; details and demonstrations can be found elsewhere (e.g. in [48, 84–86] and therein). The two-point QCD function Π^{2P} of a flavor-changing current J is rendered finite by making one or two subtractions, leading to dispersion relations. For one subtraction one can write

$$\chi \equiv \frac{\partial}{\partial q^2} \Pi^L(q^2) = \frac{1}{\pi} \int_0^\infty dt \frac{\text{Im} \Pi^L(t)}{(t - q^2)^2} \quad (45)$$

where $\Pi^{2P}(q^2) = 1/q^2(q^\mu q^\nu - q^2 g^{\mu\nu}) \Pi^T(q^2) + q^\mu q^\nu / q^2 \Pi^L(q^2)$. Similarly for $\Pi^T(q^2)$. The functions χ may be computed reliably in perturbative QCD for values of q^2 far from the kinematic region where the current can produce manifestly nonperturbative effects, like pairs of hadrons. For heavy quarks a reasonable choice is $q^2 = 0 \ll (m_b + m_c)^2$. The spectral functions $\text{Im} \Pi$ are evaluated by unitarity, inserting into the unitarity sum a complete set of states X that couple the current to the vacuum

$$\text{Im} \Pi^L = \frac{1}{2} \sum_X (2\pi)^4 \delta^4(q - p_X) |\langle 0 | J | X \rangle|^2 \quad (46)$$

Since the sum is semi-positive definite, by taking a subset of hadronic states, namely the states with only the two heavy mesons, one can obtain a strict inequality. We recover an upper bound of the form of (44) in the pair-production region, that is

$$\frac{1}{\pi\chi} \int_{t_+}^\infty dt \frac{W(t) |F(t)|^2}{(t - q^2)^2} \leq 1 \quad (47)$$

where $W(t)$ is a computable function, expressed as a product of phase-space factors, and $t_+ = (m_B + m_{D^{(*)}})^2$ is the unitarity threshold. A similar result holds for Π^T . In the case of semileptonic B decays, q^2 ranges from approximately zero to $t_- = (m_B - m_{D^{(*)}})^2$, but the form factors can be continued analytically in the complex plane.

The inequality (47) makes clear how the perturbative calculation constrains the magnitude of the form factor in the pair-production region, but to turn it into a constraint in the semileptonic region requires that the integrand is analytic below the pair-production threshold $t \leq t_+$. The form factor $F(t)$ may have poles arising from the contribution of bound states, the B_c resonances with the appropriate quantum numbers.

Let us consider a conformal variable transformation as

$$z(t; t_0) \equiv \frac{\sqrt{t_+ - t_0} - \sqrt{t_+ - t}}{\sqrt{t_+ - t} + \sqrt{t_+ - t_0}} = \frac{t - t_0}{(\sqrt{t_+ - t} + \sqrt{t_+ - t_0})^2} \quad (48)$$

This transformation maps the complex t -plane, which contains a branch cut extending from t_+ to ∞ , onto the unit disc $|z| < 1$ in the $z(t)$ plane. The branch point t_+ is mapped onto $z = 1$ and the two edges of the unitarity cut $t \geq t_+$ map to the boundary $|z| = 1$. We can see that z is real for $t \leq t_+$ and a pure phase for $t \geq t_+$; t_0 is a free parameter that represents the t -point mapped onto the origin of the z plane. Let us observe that a simple pole in t_0 can be eliminated by multiplying by $z(t; t_0)$. The change of variable (48) simplifies the next step, aimed at isolating factors that encode the nonanalytic behavior of the form factor $F(t)$, so that the inequality (47) becomes

$$\frac{1}{2\pi i} \int_C \frac{dz}{z} |\phi(z) P(z) F(z)|^2 \leq 1 \quad (49)$$

where C is the unit circle in the complex z plane. Here $\phi(z)$ is an outer function, defined in complex analysis as an analytic function lacking zeros in $|z| < 1$, and $P(z)$ is known as a Blaschke factor (or inner function), a products of suitable chosen $z(t; t_0)$ removing singularities due to the resonances below the pair-production threshold. Since $\phi(z)P(z)F(z)$ is analytic on the whole unit disc, we have managed to isolate the analytic structure of the form factor and can write an expansion as

$$F(t) = \frac{1}{\phi(t; t_0)|P(t)|} \sum_{n=0}^{\infty} a_n z^n(t; t_0) \quad (50)$$

with unknown coefficients a_n . These coefficients are different for each form factor, and must be determined by experiment. Inserting (50) back into (49) gives the constraint

$$\sum_{n=0}^{\infty} a_n^2 \leq 1, \quad (51)$$

which is known as the weak unitarity constraint, and holds for each set of form factors sharing parity and spin quantum numbers. All possible functional dependence of the form factor $F(t)$ consistent with the analyticity, unitarity, and explicit QCD information discussed before are now encoded into the coefficients a_n , which are highly constrained by (51). A randomly chosen shape for a form factor would almost inevitably have some $a_n > 1$, disallowing the bond given by (51). In case the allowed kinematic range for z has $|z| \ll 1$, as for semileptonic $B \rightarrow D^{(*)}$ decays, the convergence of the series is geometrically fast, and only the first few a_n coefficients are relevant to the shape of the form factor. In that case the sum in (51) is well approximated by a sum limited by a finite number, depending on the form factor analysed, rather than by ∞ .

One can further constrain the coefficients of the z expansion by considering several decays related by crossing symmetry; these additional constraints are known as the strong unitarity constraints.

We conclude this section by observing that in case of semileptonic $B \rightarrow D^{(*)}$ decay the above formalism is generally expressed in terms of parent and daughter velocity 4-vectors, and the parameter $w = (m_B^2 + m_{D^{(*)}}^2 - t)/2m_B m_{D^{(*)}}$. The latter kinematic variable turns out to be more convenient than the momentum transfer variable $t = (p_B - p_{D^{(*)}})^2$ in the framework of heavy quark symmetries. The conformal transformation $t \rightarrow z$ in (48) becomes $w \rightarrow z$, and we have [84]

$$z(w; \mathcal{N}) \equiv \frac{\sqrt{1+w} - \sqrt{2\mathcal{N}}}{\sqrt{1+w} + \sqrt{2\mathcal{N}}} \quad \mathcal{N} \equiv \frac{t_+ - t_0}{t_+ - t_-} \quad (52)$$

where $z(w; \mathcal{N})$ maps the physical region $1 < w < 1.5$ onto $0 < z < 0.056$ and vanishes at $w = 2\mathcal{N} - 1$. There are several parameterizations of the form factors for semileptonic $B \rightarrow D^{(*)}$ decays based on the approach outlined in this section; we discuss two examples in the next section.

3.2.4. BGL and CLN parameterizations The unitarity and dispersion relations outlined in section 3.2.3 are at the basis of several different parameterization for the exclusive semileptonic $B \rightarrow D^{(*)}$ decays.

Let us consider the $B \rightarrow D^*$ channel. In the so-called Boyd, Grinstein and Lebed (BGL) parameterization [50, 51, 87], it is convenient to set

$$\begin{aligned} H_0(w) &= F_1(w)/\sqrt{q^2} , \\ H_{\pm}(w) &= f(w) \mp m_B m_{D^*} \sqrt{w^2 - 1} g(w) \end{aligned} \quad (53)$$

These equalities define the form factors $F_1(z)$, $f(z)$, and $g(z)$ in terms of the helicity amplitudes; looking at (38), we observe that $F_1(z)$ and $f(z)$ are connected to axial form factors, and $g(z)$ to the vector one. These new form factors can be expressed by series in the variable z , as seen in section 3.2.3

$$\begin{aligned} f(z) &= \frac{1}{P_{1+}(z)\phi_f(z)} \sum_{n=0}^{\infty} a_n^f z^n , \\ F_1(z) &= \frac{1}{P_{1+}(z)\phi_{F_1}(z)} \sum_{n=0}^{\infty} a_n^{F_1} z^n , \\ g(z) &= \frac{1}{P_{1-}(z)\phi_g(z)} \sum_{n=0}^{\infty} a_n^g z^n \end{aligned} \quad (54)$$

The ϕ functions are the outer functions [84]. The $P_{1\pm}$ factors are the Blaschke factors, which take into account the sub-threshold B_c resonances with the same quantum numbers as the current involved in the definition of the form factor, and depend on the masses of such resonances. Recent determinations can be found in Refs. [88, 89]. The coefficients a_n are the parameters that need to be fitted on data, subject to unitary constraints

$$\sum_{n=0}^{n_g} (a_n^g)^2 < 1, \quad \sum_{n=0}^{n_f} (a_n^f)^2 + \sum_{n=0}^{n_{F_1}} (a_n^{F_1})^2 < 1 \quad (55)$$

They ensure the convergence of the series over the whole physical region $0 < z < 0.056$ [89]. The series are truncated at different n_i . A similar analysis can be done for the $B \rightarrow D$ channel.

Another common parameterization is the so-called Caprini, Lellouch and Neubert (CLN) parameterization [49]. This parameterization is based on the same unitarity bounds as the BGL parameterization, but it employs strong unitarity constraints to reduce the number of parameters of the more general expansion. It makes use of the relations among the form factors due to heavy quark symmetries (HQs), in particular of the connection, at the leading order in the $1/m_b$ expansion, of all the form factors to the single Isgur-Wise function $\xi(w)$. In the heavy-quark limit, all form factors become identical and equal to $\xi(w)$ (see (33)). In order to incorporate corrections to that limit, one form factor, $F_{ref}(w)$, is chosen a reference form factor and expanded around $w = 1$. Its derivatives are bounded by unitarity relations of the kind of (51). The first derivative, the slope, is defined as

$$\rho^2 = - \left. \frac{\partial F_{ref}(w)}{\partial w} \right|_{w=1} \quad (56)$$

The ratio of all other form factors with the reference one are obtained by including the leading short-distance and $1/m_b$ corrections, and expressed in terms of the reference parameters as ρ . Roughly speaking we have, for each form factor $F(w)$

$$F(w) = \left(\frac{F}{F_{ref}} \right)_{HQE} F_{ref}(w) \quad (57)$$

For $B \rightarrow D^* \ell \nu$ decays, in the CLN parameterization, the more convenient variables are the leading form factor $h_{A_1}(w)$ and the ratios of form factors $R_1(w)$, and $R_2(w)$ defined in Eqs. (36). The form factor $h_{A_1}(w)$ up to symmetry-breaking corrections coincides with the Isgur-Wise function, while the two form-factor ratios are equal to 1 in the heavy flavour limit, independently of w . The reference form factor is taken to be the axial vector form factor, see formula (35) in [49]. These parameters are expanded for $w \rightarrow 1$, fixing the series coefficients using dispersive bounds. They are given by [49]

$$\begin{aligned} h_{A_1}(w) &= h_{A_1}(1)[1 - 8\rho^2 z + (53\rho^2 - 15)z^2 - (231\rho^2 - 91)z^3] , \\ R_1(w) &= R_1(1) - 0.12(w - 1) + 0.05(w - 1)^2 , \\ R_2(w) &= R_2(1) + 0.11(w - 1) - 0.06(w - 1)^2 \end{aligned} \quad (58)$$

where $z = (\sqrt{w+1} - \sqrt{2})/(\sqrt{w+1} + \sqrt{2})$. In the $B \rightarrow D \ell \nu$ decays, the reference function is taken to be $\mathcal{G}(w)$, yielding, in the z variable [49]

$$\mathcal{G}(z) = \mathcal{G}(1)[1 - 8\rho_D^2 z + (51\rho_D^2 - 10)z^2 - (252\rho_D^2 - 84)z^3]. \quad (59)$$

In this section, we have restricted our discussion to BGL and CLN parameterizations, whose comparison has excited lively discussions since a couple of years. Indeed, in 2017 the reliability of the CLN approach has been questioned in both $B \rightarrow D \ell \nu_\ell$ [90] and $B \rightarrow D^* \ell \nu_\ell$ channels [91, 92]. Details and updates on the current situation are given in section 6.2.2.

3.3. Decays to excited D -meson states

The interest in semileptonic B decays to excited states of the charm meson spectrum derives mostly by the fact that they contribute as a background to the direct decay $B \rightarrow D^{(*)} \ell \nu_\ell$ at the B factories, and, as a consequence, as a source of systematic error in the $|V_{cb}|$ measurements. Precise knowledge of the properties of the excited D meson states is important to reduce uncertainties in the measurements of semileptonic decays.

The spectrum of mesons consisting of a charm and a \bar{u} or \bar{d} (open charm mesons) is poorly known. A QCD framework for their analysis can be set up by using HQET. In the limit of infinite heavy quark mass, the spin of the heavy quark \vec{s}_h is conserved and decouples from the total angular momentum of the light degrees of freedom \vec{j}_l , which becomes a conserved quantity as well. The separate conservation in strong interaction processes of \vec{s}_h and \vec{j}_l permits a classification of heavy mesons of given radial (principal) quantum number according to the value of \vec{j}_l . Mesons can be collected in doublets: the two states in each doublet (spin partners) have total angular momentum $\vec{J} = \vec{j}_l + 1/2 \hat{s}_h$ and parity $P = (-1)^{L+1}$, since $\vec{j}_l \equiv \vec{L} + \vec{s}_l$, where \vec{L} is the orbital angular momentum

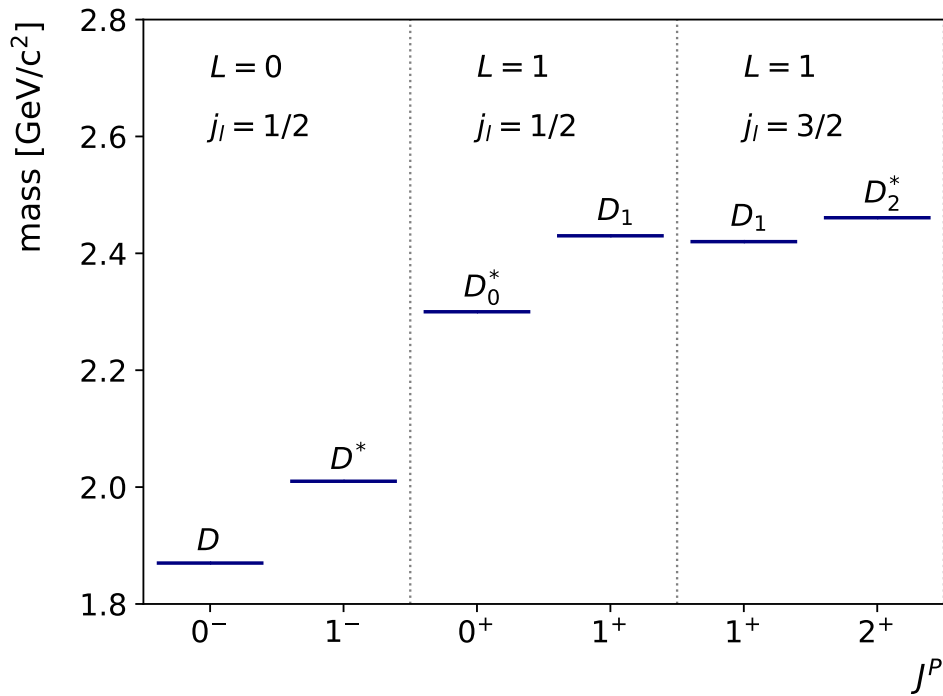


Figure 4. Low-mass D -meson spectrum. For the interpretation of the states see the text.

and \vec{s}_l the spin of the light degrees of freedom. Within each doublet the two states are degenerate in the limit of infinite heavy quark mass.

The low-mass spectrum includes the ground states, with principal (radial) quantum number $n = 1$ and $L = 0$ ($1S$, in the spectroscopic notation), which implies $j_l^P = \frac{1}{2}^-$. The ground state doublet consists of two states with $J^P = (0^-, 1^-)$, that is D and D^* mesons ¶.

When $L = 1$, there are four states ($1P$ states), which are generically referred to as D^{**+} . The doublet having $j_l^P = \frac{1}{2}^+$ is named (D_0^*, D_1) and corresponds to $J^P = (0^+, 1^+)$. These states are identified with $D_0^*(2300)$ (it was $D_0^*(2400)$, see [93]) and $D_1(2430)$. The doublet having $j_l^P = \frac{3}{2}^+$ is named (D_1, D_2^*) and corresponds to $J^P = (1^+, 2^+)$. These states are identified with $D_1(2420)$ and $D_2^*(2460)$. For the states with $j_l = \frac{3}{2}$, the two-body decay $D^{**} \rightarrow D^{(*)}\pi$ must be in the D-wave to conserve j_l . Therefore, the width should be narrow and relatively easy to observe. $D_1(2420)$ and $D_2^*(2460)$ have relatively narrow widths, about 30 MeV, and have been observed and studied by a number of experiments since the nineties. In contrast, for the state with

¶ The naming convention followed is to use $D^*(mass)$ to denote the states having $P = (-1)^J$, that is $J^P = 0^+, 1^-, 2^+, \dots$ (natural spin-parity) and with $D(mass)$ all the others (unnatural spin-parity).

+ Sometimes in literature this term is extended to include all particles in the low-mass spectrum except the ground states.

$j_l = \frac{1}{2}$ the same two-body decay should proceed in S-wave, and widths should be wide. Therefore, $D_0^*(2300)$ and $D_1(2430)$ are more difficult to detect due to the large width, about 200-400 MeV, and were not observed prior to the B -Factory era. The state $D_0^*(2300)$ has been studied by Belle, BaBar and LHCb collaborations in exclusive B decays [94–98], while the state $D_1(2430)$ has been observed by Belle collaboration [94], but its production in semileptonic B decays, studied by BaBar [99] and Belle [100] gives contradictory results. We have reported the above mentioned states in Fig. 4.

When a new state is observed, the concept of a heavy quark spin doublet is the guiding principle to understand the nature of the observed state. However, the spectroscopic identification for heavier states is not very clear. In 2010 BaBar has observed, for the first time, candidates for the radial excitation (2S) of the D^0 , D^{*0} and D^{*+} , as well as the $L = 2$ excited states of the D^0 and D^+ [101]. Resonances in the 2.4-2.8 GeV/ c^2 region of hadronic masses have also been identified at LHCb [96–98,102].

Limits in the experimental scenario concerning B decays into excited states are mirrored by theoretical ambiguities. The analyses from Belle [100] and BaBar [103], which combined one additional pion to the ground and first excited states, revealed a couple of interesting anomalies.

The first is the fact the $B \rightarrow D^{**} \rightarrow D^{(*)}\pi l \nu_l$ branching fraction is composed of approximately equal contributions from the $j_l = 1/2$ and $j_l = 3/2$ states. This is unexpected as most theoretical calculations, using sum rules [104,105], quark models [106–109] (but not constituent quark models, see e.g. [110]), OPE [111,112], indicate that the narrow width states dominate over the broad D^{**} states (the “1/2 vs 3/2” puzzle).

The other puzzle is that the sum of the measured semileptonic exclusive rates having $D^{(*)}$ in the final state is less than the inclusive one (“gap” problem) [100,103]. Indeed, decays into $D^{(*)}$ make up $\sim 70\%$ of the total inclusive $B \rightarrow X_c l \bar{\nu}$ rate and decays into $D^{(*)}\pi$ make up another $\sim 15\%$, leaving a gap of about 15%. This is in contrast to the situation with the tauonic channels, where the branching fractions of the $B \rightarrow D^{(*)}\tau \nu_\tau$ saturate the inclusive $B \rightarrow X_c \tau \nu_\tau$ rate measured at LEP [93]. BaBar used the full dataset to improve the precision on decays involving $D^{(*)}\pi l \nu$ and to search for $D^{(*)}\pi \pi l \nu$ decays [113]. These results have assigned about 0.7% to the $D^{(*)}\pi \pi l \nu$ branching ratio, reducing the significance of the gap from 7σ to 3σ .

One possible weakness common to most theoretical approaches is that they are derived in the heavy quark limit and corrections might be large. For instance, it is expected that $1/m_c$ corrections induce a significant mixing between the two D_1 states, which could soften the 1/2-3/2 puzzle [114]. The possibility of a larger than expected contribution of the first radial excitation of the D^* to the B semileptonic decay into charmed mesons has also been advanced [115,116]. However, no firm conclusion can be drawn until more high quality data on the masses and the widths of the orbitally excited D meson states become available.

3.4. Decays into heavy leptons

Exclusive B decays into τ leptons were first observed by the Belle Collaboration in 2007 [117]. Subsequent measurements by BaBar and Belle reported branching fractions above-yet consistent with-the SM predictions until 2012, when a significant excess over the SM expectation was reported by BaBar [118]. The discrepancy with the SM persists today, triggering a relevant amount of theoretical analyses. No extraction of $|V_{cb}|$ performed so far makes use of semitauonic B meson decays.

Measurements and predictions are usually quoted as branching fraction ratio

$$R(D^{(*)}) \equiv \frac{\mathcal{B}(B \rightarrow D^{(*)}\tau\nu_\tau)}{\mathcal{B}(B \rightarrow D^{(*)}\ell\nu_\ell)} \quad (60)$$

where the denominator is the average for $\ell \in \{e, \mu\}$. This ratio is typically used instead of the absolute branching fraction of $B \rightarrow D^{(*)}\tau\nu_\tau$ decays, in order to cancel uncertainties common to the numerator and the denominator. These include $|V_{cb}|$ and several theoretical uncertainties on hadronic form factors and experimental reconstruction effects. The ratio (60) tests the couplings of the charged gauge bosons to the different lepton families. A discrepancy with the SM predictions challenges the universality of the SM couplings, and indicates physics beyond the SM. Although this ratio cannot be used to determine $|V_{cb}|$ directly, its knowledge is still useful, indirectly, since possible new physics couplings would affect high precision semileptonic analyses aimed at $|V_{cb}|$ extraction, which motivates us to briefly outline the current experimental situation.

In 2012-2013 the BaBar collaboration measured $R(D^{(*)})$ by using its full data sample [118, 119], and reported a significant excess over the SM expectation. In 2015 the Belle collaboration reported a measurement of $R(D)$ and $R(D^*)$ [120], using the hadronic B -tagging in an analysis similar to the BaBar one. In the same year, LHCb collaboration reported the first measurement of $R(D^*)$ in pp collisions [121]. Both these measurements were above the SM expectations. Since then other measurements have been performed; here we report the full list:

- (i) $R(D)$ and $R(D^*)$ with τ reconstructed in the $\tau \rightarrow \ell$ mode ($\ell \in \{e, \mu\}$), and using the hadronic B -tagging approach: BaBar 2012 [118, 119], Belle 2015 [120];
- (ii) $R(D^*)$ with the τ reconstructed in $\tau \rightarrow \mu$ mode: LHCb 2015 [121];
- (iii) $R(D^*)$ with $\tau \rightarrow \ell$, using the semileptonic B -tagging: Belle [122] (this measurement has been superseded by the more recent combined $R(D)$ and $R(D^*)$ measurement [123] using the same tagging approach);
- (iv) $R(D^*)$ and τ polarization with the τ reconstructed in hadronic $\tau \rightarrow \pi(\pi^0)\nu_\tau$ decay mode, and using the hadronic B -tagging: Belle 2016 [124];
- (v) $R(D^*)$ with τ reconstructed in the hadronic $\tau \rightarrow 3\pi(\pi^0)\nu_\tau$ mode: LHCb 2017 [125];
- (vi) $R(D)$ and $R(D^*)$ with $\tau \rightarrow \ell$, using the semileptonic B -tagging: Belle 2019 [123].

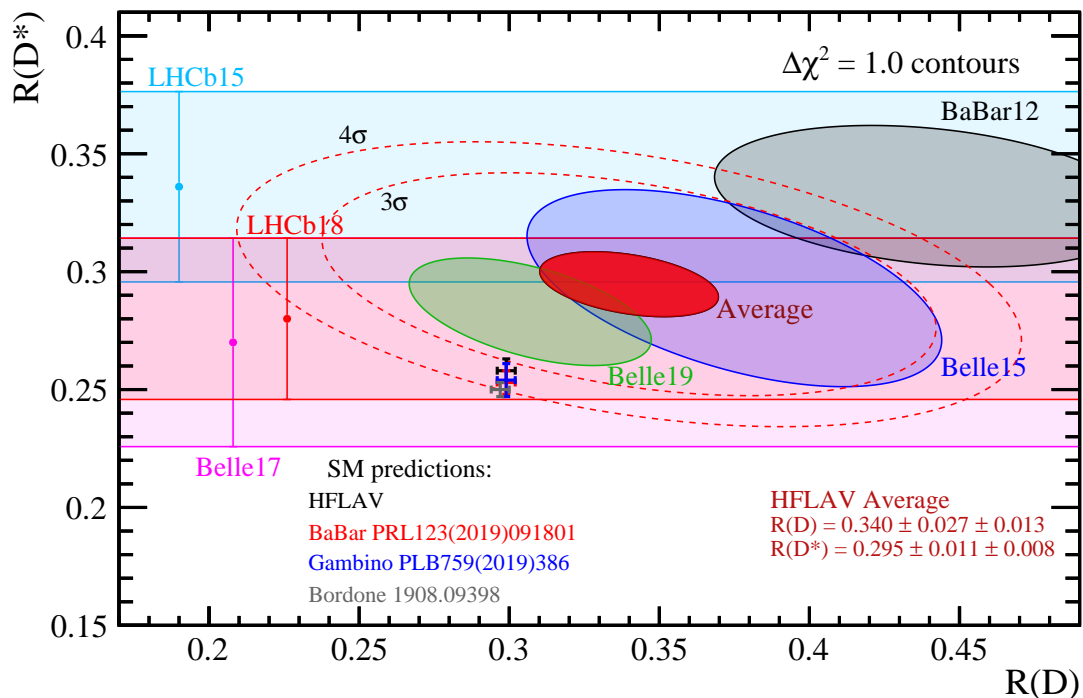


Figure 5. Measurements of $R(D)$ and $R(D^*)$ and their two-dimensional HFLAV average [126]. Contours correspond to $\Delta\chi^2 = 1$, i.e., 68% CL for the bands and 39% CL for the ellipses. The black point with errors is the average of the SM predictions used by HFLAV and obtained from [88, 90, 127, 128]. This prediction and the experimental average, deviate from each other by 3.1σ . The dashed ellipses correspond to a 3σ (99.73%) and 4σ contours. Also very recent predictions are reported.

By averaging the measurements [118, 120, 121, 123–125], the HFLAV Collaboration has found [126]

$$\begin{aligned} R(D^*) &= 0.295 \pm 0.011 \pm 0.008 \\ R(D) &= 0.340 \pm 0.027 \pm 0.013 \end{aligned} \quad (61)$$

where the first uncertainty is statistical and the second one is systematic. The average and the individual measurements included are shown in figure 5.

Several theoretical predictions for $R(D^*)$ in the SM have been performed, starting from 2012 [129]. Some of them use the data presented by the Belle collaboration in 2017 [130] and the BGL parameterization * [88, 127, 128]. Their results are generally consistent with the older predictions, and their arithmetic average, as given by the HFLAV collaboration [126], is

$$R(D^*) = 0.258 \pm 0.005 \quad (62)$$

In the case of $R(D)$, lattice SM predictions by FNAL/MILC [68] and HPQCD [69] collaborations have been averaged by the FLAG collaboration, yielding $R(D) =$

* They were prompted by the debate on the different parameterizations outlined in section 6.1.3.

0.300 ± 0.008 [131]. Like for $R(D^*)$, there are more recent calculations [90, 127, 128] that have performed analyses combining experimental data on $B \rightarrow D\ell\nu_\ell$ decays from Belle and BaBar, and theory calculation; their arithmetic HFLAV average is [126]

$$R(D) = 0.299 \pm 0.003 \quad (63)$$

The HFLAV predictions (62) and (63) are reported in figure 5. The averages for $R(D)$ and $R(D^*)$ in (61) exceed the SM values by about 1.4σ and 2.5σ , respectively. If one considers both deviations, the tension rises to about 3.1σ .

More recent SM predictions [82, 89, 132], while compatible with the previous calculations, are slightly on the lower side, resulting in discrepancies with the HFLAV average between 3.3 and 3.9σ . We show in figure 5 also these more recent predictions.

3.5. Comparison with baryon decays

A significant sample of Λ_b^0 baryons is available at the LHCb experiment, opening the possibility to study their semileptonic decays and to an interesting comparison with semileptonic B meson decays. A Λ -type baryon consists of a heavy quark, and of a spin and isospin zero light di-quark. As in the B meson case, it can be viewed as a state containing a single heavy quark Q , dressed by light degrees of freedom to make up a color singlet hadron, and its decay can be discussed in the framework of the HQET. The eigenstates of the Lagrangian in HQET differ from those of the full theory in the baryon sector in the same way as in the meson sector. For the spin-1/2 Λ_Q baryon the situation is in fact simpler, because the light degrees of freedom carry no angular momentum and hence there is no spin symmetry violating mass splitting.

Let us consider the semileptonic decay of a spin-1/2 baryon Λ_Q to a spin-1/2 baryon $\Lambda_{Q'}$. This transition is governed by the hadronic matrix elements of the flavor changing vector and axial vector currents. They are conventionally parameterized in terms of six form factors F_i and G_i , defined by

$$\begin{aligned} \langle \Lambda_{Q'}(v', s') | \bar{Q}' \gamma_\mu Q | \Lambda_Q(v, s) \rangle &= \bar{u}_{\Lambda'}(v', s') \left[F_1 \gamma_\mu + F_2 v_\mu + F_3 v'_\mu \right] u_\Lambda(v, s) \\ \langle \Lambda_{Q'}(v', s') | \bar{Q}' \gamma_\mu \gamma_5 Q | \Lambda_Q(v, s) \rangle &= \bar{u}_{\Lambda'}(v', s') \left[G_1 \gamma_\mu + G_2 v_\mu + G_3 v'_\mu \right] \gamma_5 u_\Lambda(v, s) \end{aligned} \quad (64)$$

where v and v' are the velocities of the initial and final baryon. The form factors depend on $w = v \cdot v' = (m_Q^2 + m_{Q'}^2 - q^2)/2m_Q m_{Q'}$, where m_Q and $m_{Q'}$ are the masses of the initial and final baryon, and q^2 is the squared invariant mass of the lepton pair. In the infinite quark mass limit, $F_1 = G_1 = \zeta(w)$, a universal Isgur-Wise function, and $F_2 = F_3 = G_2 = G_3 = 0$. An alternate, helicity-based, definition of the form factors was introduced in [133].

The leading power corrections to the decay rate at zero recoil are of order $1/m_Q^2$. The semileptonic decay $\Lambda_b \rightarrow \Lambda_c \ell \nu_\ell$ is particularly simple to analyze near the zero recoil point $w = 1$, where q^2 takes on its maximum value $q_{max}^2 = (m_{\Lambda_b} - m_{\Lambda_c})^2$. In the limit of vanishing lepton mass, angular momentum conservation requires that the weak matrix element $\langle \Lambda_c(v, s') | V_\mu - A_\mu | \Lambda_b(v, s) \rangle$ depends only on the function $G_1(1)$. In semileptonic decay $\Lambda_b \rightarrow \Lambda_c \ell \nu_\ell$ a partial cancellation of $1/m_Q^2$ corrections at zero recoil was found,

with the conclusion that large deviations from the infinite quark mass limit are unlikely, and the heavy quark expansion is well under control [134].

Form factors for the baryon decays $\Lambda_b^0 \rightarrow \Lambda_c^+ \mu \bar{\nu}_\mu$ and $\Lambda_b^0 \rightarrow p \mu^- \bar{\nu}_\mu$ are already available in lattice QCD. They have been computed using RBC/UKQCD $N_f = 2 + 1$ flavors of dynamical domain-wall fermions, six different pion masses and two different lattice spacings [135]. The importance of this computation is that, combined to a recent measurement by LHCb [136], allows for an independent exclusive determination of the ratio $|V_{ub}|/|V_{cb}|$, as we will discuss in section 6.4.

Due to the possibility of new physics in the ratio $R(D^{(*)})$, discussed in section 3.4, an analogous ratio for baryon decays, $R(\Lambda_c) = \mathcal{B}(\Lambda_b \rightarrow \Lambda_c \tau \bar{\nu})/\mathcal{B}(\Lambda_b \rightarrow \Lambda_c \mu \bar{\nu})$, has been identified and analyzed [137].

4. Experimental techniques

4.1. *B-hadron production*

The *b*-hadrons can be produced in different experimental environments: from e^+e^- annihilation, collisions of protons or proton-antiproton collisions. The most recent results on *b*-hadron semileptonic decays come from e^+e^- experiments operating at the energy of the $\Upsilon(4S)$ and from *pp* collisions at LHC.

Understanding the features of the *b*-hadron production in various environments is crucial to understand the experimental setup and analysis techniques developed to study semileptonic decays. In the following we focus on the *b*-hadron production mechanism at the *B*-Factories and *pp* colliders.

4.1.1. B-Factories Studies of *B* meson decays have been performed at e^+e^- colliders working at the center-of-mass energy of $\sqrt{s} = 10.58$ GeV, which corresponds to the mass of the $\Upsilon(4S)$ resonance. The first two experiments working at this resonance were ARGUS (at DORIS accelerator, DESY, Germany) and CLEO (at CESR, USA).

The next generations of e^+e^- colliders have been the modern *B*-Factories, BaBar and Belle, designed to collect data produced in the collisions at PEP-II (at SLAC, USA) and KEKB (at KEK, Japan), respectively. A detailed description of both BaBar and Belle, their performances and their analysis methods can be found in [138].

The main characteristic of the *B*-Factories was the very high luminosity (2 order of magnitude higher than older e^+e^- colliders) achieved by the machines PEP-II and KEKB. The BaBar and Belle experiments stopped their operations in 2008 and 2010, respectively. Nowadays, a decade later, many analyses are still ongoing to exploit the full dataset collected by these two experiments. The present measurements of $|V_{cb}|$ are dominated by the *B*-Factories.

At *B*-Factories, the *B* mesons are produced through the decay of the $\Upsilon(4S)$. An illustration of the process involved is shown in figure 6. The $\Upsilon(4S)$ is the lightest $b\bar{b}$

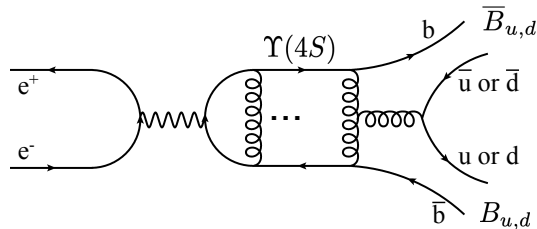


Figure 6. B mesons at B -Factories are produced from the decays of the $\Upsilon(4S)$.

resonance with mass above the $B\bar{B}$ pair production threshold \ddagger . This resonance decays almost exclusively in a couple of B meson pairs. The probabilities to produce $B^0\bar{B}^0$ and B^+B^- from $\Upsilon(4S)$ decays are about the same. The ratio of the branching fraction decays f_{+-}/f_{00} differs slightly from unity because of the small difference due to Coulomb effect, which increase the rate when oppositely charged states are present in the final state. The current average value is $f_{+-}/f_{00} = 1.058 \pm 0.024$ [93].

Because of the small mass difference between the $\Upsilon(4S)$ state and $B\bar{B}$ pairs, the B mesons are produced with very small momentum in the $\Upsilon(4S)$ center of mass. In particular the B meson momentum is $|\vec{p}_B| \simeq 320 \text{ MeV}$. For this reason the decay products of the two B 's are produced almost isotropically in the $\Upsilon(4S)$ rest frame. Evens like these are usually called *spherical*.

The integrated luminosity collected at $\Upsilon(4S)$ energy was 426 fb^{-1} and 711 fb^{-1} at BaBar and Belle, respectively. The integrated luminosity collected by ARGUS and CLEO was only 0.2 fb^{-1} and 16 fb^{-1} , respectively. The high luminosity has been paramount to study CP violation in B mesons decay, because it allows the study of rare processes, with branching ratios of the order of $10^{-4} \div 10^{-6}$. The need to measure time-dependent properties of the B meson decays has driven the design of the B -Factories. A unique characteristic of the B -Factories was the asymmetric energies of the colliding beams, so the $\Upsilon(4S)$ was produced boosted. The boost allowed a better spatial separation of the two B meson decay vertices. For example, in BaBar the boost was $\beta\gamma \approx 0.55$, resulting in an average distance between the two B meson decay vertex of $250 \text{ }\mu\text{m}$, which was in the capability of the vertex detector. To maximize the acceptance of the decay products of the boosted $\Upsilon(4S)$, BaBar and Belle detectors were offset from the interaction point by about 30 cm to keep high the acceptance in the direction of the higher energy beam, resulting in slightly asymmetric detectors.

At the energy \sqrt{s} corresponding to the $\Upsilon(4S)$ mass, the cross section of $e^+e^- \rightarrow \Upsilon(4S)$ is about 1.06 nb , resulting in about $1.1 \times 10^6/\text{fb}^{-1}$ $B\bar{B}$ pairs. But at this energy, only about one forth of all the hadronic events produced are $\Upsilon(4S)$, the rest being non- $B\bar{B}$ events. The cross sections for some important processes at $\sqrt{s} = 10.58 \text{ GeV}$

\ddagger The $\Upsilon(4S)$ mass is above the $B\bar{B}$ pair mass, so the decays proceed through strong decays which dominate over radiative or weak decays. The $\Upsilon(4S)$ is accessible at e^+e^- colliders because the process $e^+e^- \rightarrow \gamma^* \rightarrow b\bar{b}$ allows only states with $J^{PC} = 1^{--}$ quantum numbers.

Table 2. The cross section for some relevant processes at different colliders. The collected integrated luminosity for some of the experiments is reported in parenthesis.

Collider	Process	cross section	experiments
$e^+e^- \rightarrow \Upsilon(4S)$	$b\bar{b}$	1.06 nb	BaBar (426 fb ⁻¹)
	$c\bar{c}$	1.30 nb	Belle (711 fb ⁻¹)
	$d\bar{d}, u\bar{u}, s\bar{s}$	2.09 nb	
$e^+e^- \rightarrow Z$	$b\bar{b}$	6.6 nb	ALEPH, DELPHI (0.14 fb ⁻¹), OPAL, L3
pp 7, 8 TeV	$b\bar{b} \ 2 < \eta < 5$	72 μb	LHCb (3 fb ⁻¹)
	$b\bar{b}$ total	295 μb	CMS, ATLAS (25 fb ⁻¹ each)
pp 13 TeV	$b\bar{b} \ 2 < \eta < 5$	144 μb	LHCb (6 fb ⁻¹)
	$b\bar{b}$ total	600 μb	CMS, ATLAS (150 fb ⁻¹ each)
$p\bar{p}$ 1.96 TeV	$b\bar{b} \ \eta < 1$	30 μb	CDF, D0 (10 fb ⁻¹ each)

are reported in table 2. These events are a background to the study of B meson decays, called *continuum background*. In general they are rejected exploiting the differences between decays of the $\Upsilon(4S)$ and the decays of the $e^+e^- \rightarrow q\bar{q}$. As said before, the B mesons are produced almost at rest in the $\Upsilon(4S)$ frame, so the decay products have a spherical topology, while in $e^+e^- \rightarrow q\bar{q}$ processes the tracks coming from the fragmentation of the two quarks produce a topology with two opposite jets. Furthermore, the average number of particles produced in the quark hadronization in $e^+e^- \rightarrow q\bar{q}$ processes is smaller than in $\Upsilon(4S) \rightarrow B\bar{B}$ processes. The suppression of the continuum background is thus performed requiring a minimum number of tracks, usually three or four, and applying global event shape criteria that allow to separate jet-like events from more spherical events.

Even with these requirements, the continuum, mainly the contribution from $e^+e^- \rightarrow c\bar{c}$, remains an important background in many semileptonic analyses. Therefore part of the data (about one tenth) are taken at a center of mass about 50 MeV below the $\Upsilon(4S)$ mass, in order to have pure continuum events, needed for the study of the background. The study of these continuum events, corrected for the luminosity and for the small energy difference, can be used to predict both the absolute scale and the correct kinematics of the continuum background events.

As we will see in section 4.2.2, many semileptonic analyses gain a lot by an approach called *B-tagging* where the signal B meson is reconstructed together with the second B meson present in the event. The *B-tagging* is very effective in suppressing the continuum background, and more generally, to clean the event reconstruction.

4.1.2. Hadron Colliders At LHC the production mechanism of b -quarks are the quark annihilation $q\bar{q} \rightarrow b\bar{b}$ and gluon fusion processes $q\bar{q}, gg \rightarrow b\bar{b}$, with the latter ones largely dominating [139]. At leading order in perturbation theory $\mathcal{O}(\alpha_s)$, we can draw the tree

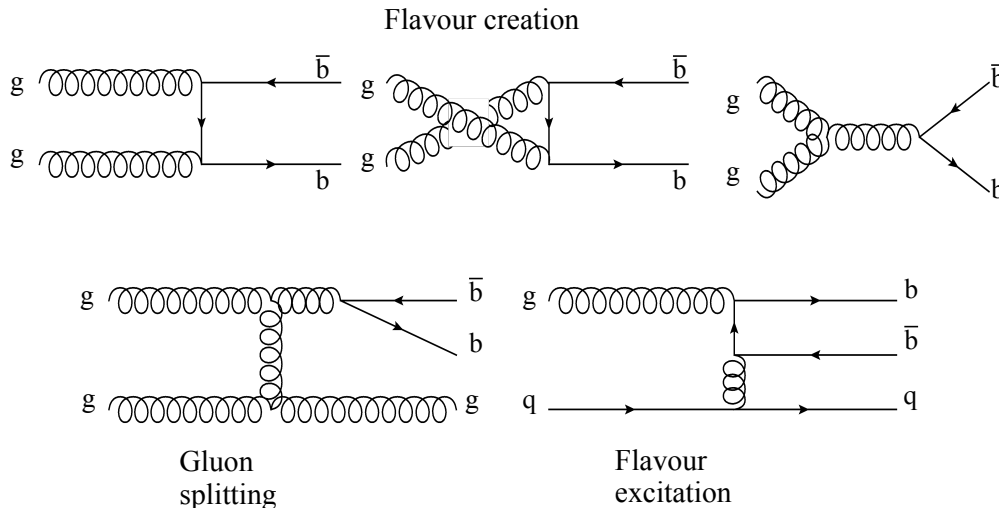


Figure 7. The leading order heavy flavour production processes dominant at LHC.

diagram corresponding to the quark-antiquark annihilation and the flavour creation diagrams shown in figure 7, that is the gluon fusion diagrams in the t -, u - and s -channel (from left to right). The $q\bar{q} \rightarrow b\bar{b}g$ parton process and the processes described by the gluon splitting and the flavour excitation diagrams depicted in figure 7 are order $O(g_s\alpha_s)$ in perturbation theory.

The different processes have different final state kinematics: the flavour creation yields $b\bar{b}$ pairs that are almost back to back and with symmetric transverse momentum p_T ; the flavour excitation produces $b\bar{b}$ pairs with highly asymmetric p_T ; the gluon splitting produces $b\bar{b}$ pairs with small opening angle and small p_T . In the forward (and backward) direction the gluon splitting is the dominant process. The LHCb detector is designed to take advantage of this feature [140].

The particle acceptance region covered by the LHCb experiment is the very forward one with pseudorapidity η in the range $2 < \eta < 5$. The pseudorapidity η of a particle is defined as $\eta = -\ln(\tan\theta/2)$, where θ is the angle of the particle three-momentum \vec{p} relative to the positive direction of the beam axis. The acceptance region at LHCb corresponds only to 4% of the full solid angle, but the collected $pp \rightarrow b\bar{b}$ events represent about 25% of the total cross section. The visible b -hadron cross section in the pseudorapidity range $2 < \eta < 5$ has been measured to be $72 \mu\text{b}$ at 7 TeV and almost double at 13 TeV, being about $144 \mu\text{b}$ [141].

The general purpose experiments CMS and ATLAS have an acceptance limited to the more central region $|\eta| < 2.2$, which corresponds to an efficiency of about 40% for the $pp \rightarrow b\bar{b}$ processes. Semileptonic B meson decays have not yet been studied at these experiments.

Various important result on B meson semileptonic decays have instead been provided by CDF and D0 experiments, that took data provided by $p\bar{p}$ collisions at 1.96 TeV at Tevatron. In table 2 we report a list of relevant cross sections, at different

facilities.

The produced b -quark can hadronize, with different probabilities, called *production fractions*, into a full spectrum of b -hadrons, mainly B^0 , B^+ , B_s , Λ_b . The measured fraction of B^0 and B^+ , in the LHCb acceptance region, is about 36% [126], while the ratio between the B_s and the $B^0 + B^+$ mesons production rate, $f_s/(f_d + f_u)$, is about 0.12 and it has been observed to be slightly dependent on the B_s transverse momentum itself [142]. The Λ_b production fraction, compared to $B^0 + B^+$ production, has been measured and it is $f_{\Lambda_b}/(f_u + f_d) \approx 0.26$. A strong dependence of the f_{Λ_b} on the transverse momentum of Λ_b has been observed [142]. In the LHCb acceptance range, the production rates $B^0 : B^+ : B_s : \Lambda_b$ are approximately in the ratio 0.36 : 0.36 : 0.09 : 0.19, with small fractions (10^{-3}) of B_c and other b -baryons (10^{-2}).

The production fractions are crucial to determine the branching ratios of different hadron B decays. For instance, the number of events $N(H_b)$ (produced in the LHCb acceptance) of a semileptonic process like $H_b \rightarrow H_c \ell \nu_\ell$, is given by

$$N(H_b) = 2 L \sigma(b\bar{b}) \epsilon_{LHCb} f_{H_b} \mathcal{B}(H_b \rightarrow H_c \ell \nu_\ell) \mathcal{B}(H_c) \quad (65)$$

where L is the integrated luminosity, $\sigma(b\bar{b})$ the total $b\bar{b}$ cross section, ϵ_{LHCb} the detector acceptance, f_{H_b} the production fraction of the H_b hadron species, $\mathcal{B}(H_b \rightarrow H_c \ell \nu_\ell)$ is the branching fraction of the process we are considering, and $\mathcal{B}(H_c)$ is the branching fraction of the c -hadron decay channel used to reconstruct H_c .

The precise absolute branching fraction measurements at hadron colliders using equation (65) would be affected by the large uncertainty in the $\sigma(b\bar{b})$ and the knowledge of the detector acceptance for the decay analysed. In general, the branching fraction of a decay channel is measured relatively to a channel with a similar decay topology, which is often a decay of a neutral or charged B meson, whose absolute branching ratio is well known from B -Factories. Measuring ratios of branching fractions, most systematic uncertainties cancel, and the remaining uncertainties come from the knowledge of the ratio of production fraction $f(H_b)/(f_u + f_d)$ and the branching fraction of the normalization channel.

4.2. Semileptonic measurements at B -Factories

Generally speaking, the reconstruction of the decays driven by the partonic decay $b \rightarrow c \ell \nu_\ell$ requires an efficient and reliable reconstruction of the lepton ℓ , where the lepton can be an electron or a muon. In the case of the exclusive reconstruction of the final hadronic state, an high efficiency reconstruction and identification of its decay products is also required. Some analyses also require the reconstruction of the other particles of the events, for example to infer the kinematics of the missing neutrino or reduce the combinatorial background in the signal reconstruction.

For the study of semileptonic B decays at B -Factories the acceptance of the detectors is an important feature. The B -Factories detector geometry is solenoidal around the interaction point, and asymmetric along the beam line. The geometric acceptance is slightly reduced compared to a symmetric detector like CLEO, which

had a geometric acceptance close to 95%. To overcome this limitation, it is crucial to keep the detector performances very high and to exploit the high statistics as much as possible. Detailed descriptions of the B -Factories and of their detectors can be found in [143, 144] and [145]. Here we just briefly describe the most important subdetectors for the study of B meson semileptonic decays:

- (i) a multilayer silicon detector allows the reconstruction of the tracks very close to the interaction point. This is crucial for the decay vertex reconstruction and for the tracking of very low momentum tracks;
- (ii) a low-mass drift chamber used for charged track reconstruction. The drift chamber allows a precise measurement of the momenta and the identification, through the measurement of the energy loss (dE/dx), of the charged particles;
- (iii) a specialized system to identify the nature of the charged particles based on the Cherenkov effect;
- (iv) a calorimeter for the measurement of the electromagnetic showers produced by photons and electrons;
- (v) an instrumented magnetic flux return used for the identification of muons and the detection of K_L mesons.

Despite the relatively long lifetime of the B mesons, their mean flight length transverse to the beam directions is only 30 μm , and about 250 μm in the beam direction. So the B mesons decay in the beam pipe and only the decay products reach the various sub-detectors.

The semileptonic decays are reconstructed starting from the identification of an high-momentum lepton. Typically the minimum lepton momentum is required to be few hundreds of MeV. For some analyses this momentum can be pushed down, but there is a minimum momentum under which the identification is not reliable. For example an electron has to reach the calorimeter to be clearly identified from the measurement of $E/|\vec{p}|$, the ratio between the measured energy released in the calorimeter and the measured momentum of the associated track. A muon needs to reach the muon detector to be identified. Its identification relies on the calorimeter energy measurement, that needs to be compatible with the energy released by a minimum ionizing particle, and the number of the detecting plane traversed in the iron. A muon traverses more planes and releases less hits per plane than a pion. For both electrons and muons, the most relevant source of wrongly identified leptons are the pions. Pions that interact strongly in the calorimeter can mimic the energy released by an electron. The distribution of the energy released in the calorimeter is exploited to separate electrons from pions.

Pions can mimic a muons because there is a finite probability that they go through the iron absorber without interacting (punch through). Moreover pions can decay in flight and generate a muon which is identified in the main detector. Because of the small mass difference between pions and muons, the kink resulting from the pion decay in flight is too small to be detected in most of the cases. At small energy the background

from pion decay in flight is dominant and prevents the reliability of the identified low momentum muons.

The performances of the lepton identification is done by using control samples of electrons and muons. The cleanest sources of electrons and muons are

- (i) Bhabha and di-muon processes, $e^+e^- \rightarrow e^+e^-(\gamma)$ and $e^+e^- \rightarrow \mu^+\mu^-(\gamma)$;
- (ii) decays of the J/ψ into e^+e^- and $\mu^+\mu^-$.

*4.2.1. Soft pion from D^** The study of the exclusive $B \rightarrow D^*\ell\nu$ decays requires the reconstruction of the D^{*+} or D^{*0} . These mesons are reconstructed usually through the decay chains $D^{*+} \rightarrow D^0\pi^+$ and $D^{*0} \rightarrow D^0\pi^0$. Because of the little phase space available in $D^* \rightarrow D\pi$ decays, the emitted π has a slow momentum in the D^* rest frame. As a consequence the momentum of the π is correlated with the variable w , and any inefficiency in reconstructing these pions in the low transverse momentum region affects the signal reconstruction in the zero-recoil phase space region.

A low momentum π^+ does not cross the full tracking device, so its tracking efficiency is strongly dependent on the momentum. For transverse momenta of magnitude p_T around 100 MeV, the tracking relies entirely on the inner silicon trackers. Below 60 MeV, the reconstruction is not possible because the track does not traverse enough layers. A good knowledge of the soft π^+ efficiency is required for precise measurements. At B-Factories the low p_T track reconstruction efficiency is based on an approach used for the first time by the CLEO collaboration and described in detail in [146]. This approach exploits the distribution of the π^+ helicity angle θ^* as a function of the D^{*+} momentum. The helicity angle θ^* is defined as the angle between the slow π^+ momentum in the D^* rest frame and the D^* direction in the laboratory frame. The distribution of θ^* is expected to be symmetrical and can be described by $dN/d\cos\theta^* \propto (1 + \alpha\cos^2\theta^*)$. The angle θ^* is connected with the slow π^+ momentum in the laboratory frame by $p_\pi = \gamma(p_\pi^* \cos\theta^* - \beta E_\pi^*)$ where β and γ are the D^* boost parameters. From the last relation, any asymmetry in the θ^* distribution can be related to the reconstruction efficiency in a region of the slow π^+ momenta.

Some analyses used also the reconstruction of $D^{*0} \rightarrow D^0\pi^0$ decays, where π^0 is reconstructed in $\gamma\gamma$ decays mode. At the B-Factories the photons can be reconstructed with high efficiency down to the energy of about 30-40 MeV, resulting in an efficiency almost uniform in the π^0 momentum and thus on w . One of the limitation on the usage of the soft π^0 is the difficulty to have a reliable control of the absolute efficiency to reconstruct the low momentum π^0 . The approach used in Ref. [147] exploits the $e^+e^- \rightarrow \tau^+\tau^-$ events. In the reconstruction of these events, one τ is reconstructed either in one track and two clusters (sample dominated by $\tau \rightarrow \rho(\pi\pi^0)\nu$) or in one track and no cluster (sample dominated by $\tau \rightarrow \pi\nu, \mu\nu\bar{\nu}$). The other τ is reconstructed in the electron decay mode and used only to tag the τ -pairs. From the comparison of these two samples, it is possible to measure the absolute efficiency to reconstruct a π^0 of momentum greater than 350 MeV. The efficiencies at lower momentum are obtained

from the detailed simulation of the detector. The impact of the higher multiplicity of tracks and clusters present in $B\bar{B}$ events, compared to $\tau^+\tau^-$ events, is evaluated by comparing the rates of the reconstructed D^0 in $K^-\pi^+$ and $K^-\pi^+\pi^0$. The systematic uncertainties on the soft π^0 reconstruction are typically larger than the corresponding uncertainty for charged pions.

4.2.2. B tagging At the B -Factories the decay products of the two B mesons originated from the decays of the $\Upsilon(4S)$ overlap and it can happen than one or more particles can be assigned to the wrong B meson. This source of background can be relevant and the way to evaluate and eventually suppress its contributions depends strongly on the analysis.

In the $\Upsilon(4S) \rightarrow B\bar{B}$ decay, there are only two B mesons in the final state. By reconstructing one of them in exclusive decay modes it is possible to reduce the combinatorial background and also the continuum. This technique, called *B tagging*, has been widely and successfully used at B -Factories. In addition to the background reduction, the information on the direction of the tagged B (B_{tag}) can be used to constrain the kinematics of the full event and improve the resolutions in the study of the signal B meson (B_{sig}) decay. The main disadvantage of the B tagging approach is the small efficiency for the reconstruction of B_{tag} , usually well below 1%. This is because there are many B decay modes, all with small branching fractions and with high multiplicity in the final state, resulting in an overall small detection efficiency.

The B tagging approach can be classified according to two main categories:

- (i) **hadronic tagging:** the B_{tag} is fully reconstructed in a mixture of many different hadronic decay modes. The reconstruction of the B_{tag} starts reconstructing a set of charm mesons (called *seeds*), like D^0 , D^+ , D^{*+} , D^{*0} , D_s , D_s^* or J/ψ from their decay modes. Usually many decay modes of these seeds are added up together to increase efficiency. A seed is then combined with additional charmless mesons (π^\pm , K^\pm , π^0 and K_s) to form a possible B candidates. The two variables used to test the compatibility with a B meson are
 - (a) $\Delta E = E_B^* - E_{beam}^*$, the difference between the energy of the B candidate in $\Upsilon(4S)$ and the expected B candidate energy fixed by the energy of the beams;
 - (b) the energy substituted mass, $m_{ES} = \sqrt{E_{beam}^{*2} - |\vec{p}_B^*|^2}$, where \vec{p}_B^* is the momentum of the B candidate.

A correctly identified B meson gives $\Delta E \approx 0$ and $m_{ES} \approx m_B$. The quantity m_{ES} exploits the feature that the energy of the B mesons is precisely determined by the beam energy, which is known with a resolution better than 2 MeV. The tagging efficiency depends on the multiplicity and the kind of particles present in the analyzed final state. The purity, defined as the probability that a specific decay chain is correctly reconstructed, varies considerably according to the decay mode considered. In case of more B_{tag} candidates, the one with the highest purity is in general chosen. To gain in efficiency, usually more than a thousand possible

decay modes are considered. The hadronic B -tagging approach has been improved over time by both BaBar and Belle. In BaBar, more decay modes and wider mass windows have been implemented according to the specific mode considered. Belle instead has made use of an algorithm described in [148]. This algorithm uses a set of different neural-networks, properly trained, to estimate the probability that a seed has been correctly reconstructed. The output of the final neural network is used to rank the various B_{tag} candidates. At the end, the average overall efficiency is about 0.3 – 0.5% for the tagging B^+ and about 0.3% for the B^0 , with purity of about 10 – 30%. The reconstruction of the four-momentum of the B_{tag} allows to determine clearly the four-momentum of the signal B_{st} , even in B_{sg} with missing particles, using:

$$p_{B_{sig}} = p_{\Upsilon(4S)} - p_{B_{tag}}, \quad (66)$$

where $p_{\Upsilon(4S)} = p_{e^+} + p_{e^-}$ is the four-momentum of the initial $\Upsilon(4S)$, determined by the energy of the initial electron and positron beams. The charge and the flavour of the reconstructed B_{tag} are also exploited to clean the sample and reduce the backgrounds.

- (ii) **semileptonic tagging:** the B_{tag} is reconstructed using both $B \rightarrow D^* \ell \nu_\ell$ and $B \rightarrow D \ell \nu_\ell$ decays. The branching fractions of these decays are among the highest in B decays. Moreover, the efficiency to reconstruct semileptonic decays is higher than the one to reconstruct fully hadronic B decays. The final efficiency of the semileptonic B tagging runs between 0.5 – 1.0%. The final efficiency is higher than the hadronic B tagging, but the background is also higher. Another disadvantage of the semileptonic tagging is that it does not allow tight kinematic constraints for the presence of neutrino in the tag side.

4.3. Semileptonic measurements at LHCb

LHCb is a dedicated experiment that exploits the fact that the $b\bar{b}$ production rate is larger in the forward direction, as described in section 4.1.2. Because the $c\bar{c}$ production has similar production mechanism, and has a cross section about twenty times higher than the $b\bar{b}$, also a huge amount of c -hadrons are produced in the forward direction. The fact that all species of heavy hadrons are produced makes LHCb a unique facility for heavy flavour physics.

The LHCb detector [140, 149] is a single-arm forward spectrometer that covers the pseudorapidity range $2 < \eta < 5$. It consists of the following subdetectors:

- (i) a precise vertex detector for the identification of the vertex (primary vertex, PV) where the inelastic pp collision occurs, and the reconstruction of the decay vertex of the B hadrons;
- (ii) two detectors specialized for the identification of protons, pions and kaons;
- (iii) an electromagnetic calorimeter for electrons and photon identification and energy measurement, and an hadronic calorimeter for the identification of high p_T hadrons;

(iv) a detector for muon identification.

At LHCb, an experimental challenge in the study of semileptonic B decays is represented by the presence of the un-reconstructable neutrino. The momentum of the B hadrons in production is not known. The identification of semileptonic events exploits the very good identification of the B flight direction. The situation is complementary to that of the B -Factories, where, in untagged measurements, the magnitude of the B momenta is known but not their direction. The reconstruction of the kinematics for semileptonic B decays is described in section 4.3.1.

In the forward direction, the B hadrons are highly boosted so they have a mean flight length of about 1 cm. This property, associated with the great vertex resolution, is crucial for a clean reconstruction of the signal event. In particular, the large separation between the B decay vertex and the PV reduces the combinatorial background. Moreover, the decay products of the second B hadron, produced usually within the LHCb acceptance, are in general well separated in η , so the mis-assignment of tracks from B hadrons is in general negligible.

The majority, more than 99%, of inelastic pp collisions does not produce b -quarks and are a relevant source of backgrounds, so the triggering of the events is crucial: it has to be efficient for B -hadrons, and has to have a high reject rate for backgrounds. The trigger in LHCb exploits the fact that the B hadrons are long lived, and that, having a relatively large mass, give decay products with an average p_T larger than the typical particle produced in a pp collisions. The trigger consists in a combination of an hardware trigger stage (L0) and a software one. The L0 trigger relies mainly on the muon detector and the calorimeters response.

For the study of semileptonic decays in LHCb, the presence of a muon is very well suited because the L0 trigger line for muons is very efficient. The L0 muon trigger requires the presence of muons of p_T greater than about 1.7 GeV. This low threshold ensures a large efficiency for B semileptonic decays. For comparison, at CMS and ATLAS this threshold is more than 5 GeV. The trigger for electrons is not as efficient because its identification has to rely on the electromagnetic calorimeter where the trigger threshold has to be increased to avoid large backgrounds. Moreover, electrons are affected by bremsstrahlung that deteriorates their momentum reconstruction. For these reasons, usually only semileptonic decays into muons are exploited in LHCb.

At the luminosity of LHC, a large number of multiple pp collision occurs in the same bunch crossing. On average about 40 inelastic pp collisions (called *pile-up*) are produced. The study of the B -hadron properties requires the detection of the decay vertex and the production vertex, and large pile-up can pollute the clear identification of the PV, and increase the occupancy in the various subdetectors, worsening the B reconstruction. At LHCb, this problem is overcome decreasing locally the luminosity by about a factor 20. That reduces the average number of visible collision per bunch crossing to about 1.8.

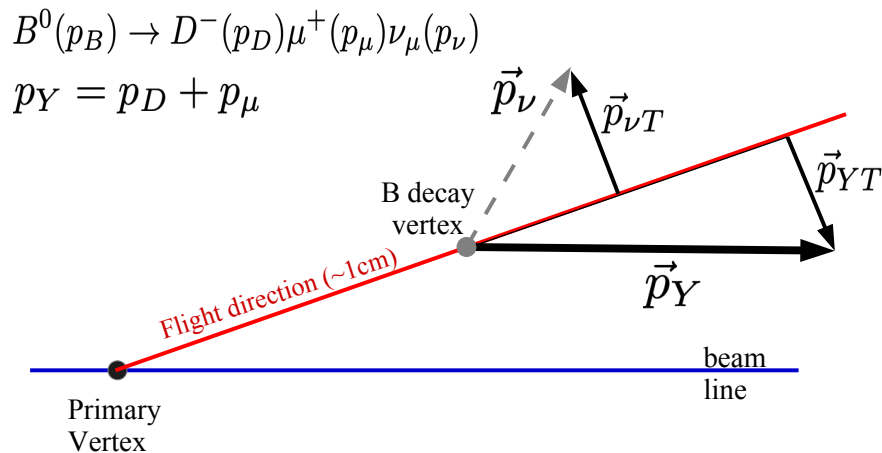


Figure 8. In LHCb the average flight length of the B hadrons is about 1 cm. The good resolution in the vertex reconstruction allows to determine the flight direction.

4.3.1. Techniques for kinematic reconstruction As mentioned above, the precise determination of the flight direction, from the identification of the PV and the decay B vertex, can be used to constrain the decay kinematics of semileptonic decays [150]. In the hypothesis of a single missing particle with known mass, the unknowns are the components of the 3-momentum of the missing particle. Two constraints are obtained by the momentum conservation in the plane transverse to the decay flight, and the third is determined by the assumed mass of decaying B hadron. Because this last constrain is quadratic, there are two possible solutions.

In figure 8 we illustrate the ingredients exploited to constrain the kinematics. Lets consider the decay $B(p_B) \rightarrow D(p_D)\mu(p_\mu)\nu_\mu(p_\nu)$, where the four-momentum of the various particles are given in parenthesis. The visible system $Y \equiv D\mu$ has a four-momentum given by $p_Y = p_D + p_\mu$. It is useful to decompose p_Y in the longitudinal (p_{YL}) and transverse (p_{YT}) components along the B flight direction. If there is only a missing particle, like a neutrino, its transverse component is known just balancing the visible transverse component, $\vec{p}_{\nu T} = -\vec{p}_{YT}$. The only unknown is the magnitude of the longitudinal component $|\vec{p}_{\nu L}|$, or, equivalently, the momentum $|\vec{p}_B|$ of the decaying B meson. The B four-momentum is given by $p_B = p_Y + p_\nu$, so we can write

$$p_\nu = p_B - p_Y \implies m_\nu^2 = m_B^2 + m_Y^2 - 2(E_Y E_B - |\vec{p}_B| |\vec{p}_Y| \cos \theta_{BY}) \quad (67)$$

where θ_{BY} is the angle of Y respect to the flight direction. After setting the mass of the B to its value, substituting $E_B = \sqrt{m_B^2 + |\vec{p}_B|^2}$ in (67), squaring and solving for $|\vec{p}_B|$, we arrive to a simple second degree equation

$$(|\vec{p}_Y|^2 \cos^2 \theta_{BY} - E_Y^2) |\vec{p}_B|^2 + (2M |\vec{p}_Y| \cos \theta_{BY}) |\vec{p}_B| + (M^2 - m_B^2 E_Y^2) = 0 \quad (68)$$

where $M = [(m_B^2 + m_Y^2) - m_\nu^2]/2$. The equation (68) yields two solutions for the B momentum, thus all the kinematic quantities we determine for the decay are affected by this ambiguity; for instance, in the example above, there are two possible $q^2 = (p_B - p_D)^2$

values. Furthermore, the limited vertex resolution gives a fraction of decays with non-physical solution, which are usually excluded in the analyses. The fraction of these events depends by the decay considered but it is usually between 20 and 30%.

Without applying any requirement on the signal, the two solutions are equally probable and cannot be distinguished. However, after the signal selection requirements are applied, the one that gives the systematically smaller $|\vec{p}_B|$ usually has an higher chance to be the correct solution. Thus in practice, resolutions on q^2 of the order of 10-20% can be achieved by selecting only this solution.

Other approaches to improve the kinematic resolution have been used. In [151] it has been proposed a regression algorithm that uses the information of the flight decay length and the production angles to increase the chance to select the right solution. Another possibility is to consider B decays that come from decays of narrow excited B hadron states. The constraint that comes from the mass difference between the excited state and the B meson removes the ambiguity. This approach has been described in [152] and it has been exploited for the first time in the analysis [153], where the $B^+ \rightarrow D/D^*/D^{**}\mu\nu_\mu$ relative fraction have been measured by tagging the B^+ mesons from the $B_{s2}^{*0} \rightarrow B^+K^-$ decay. The price is a reduced signal efficiency due to the low rate of production of the excited B_{s2}^{*0} state, and the low detection efficiency of the soft K^- accompanying the B^+ meson.

5. Inclusive $|V_{cb}|$ determination

In section 3.1 we have introduced the inclusive $B \rightarrow X_c\ell\nu$ decays. The total semileptonic rate for $B \rightarrow X_c\ell\nu$ decays is expressed in the framework of the HQE (see section 3.1.1), which allows to disentangle coefficients and corrections calculable in QCD perturbation theory from genuinely non perturbative parameters. The same holds for the moments of distributions of charged-lepton energy and hadronic invariant mass, defined in (24) and (25), respectively. As underlined in section 3.1.2, the inclusive analysis requires a suitable definition of the quark mass in a coherent framework, or scheme.

The shapes of the kinematic distributions in the $B \rightarrow X_c\ell\nu$ decays are sensitive to the masses of the b and c quarks, and the non-perturbative HQE parameters, thus their knowledge is needed to extract $|V_{cb}|$ from data. Non perturbative parameters can be extracted together with $|V_{cb}|$ in a simultaneous fit (global fit) based on experimentally measured distributions and momenta. Global fit analyses differ by the data sets they are based onto, the theoretical scheme employed, the order of truncation of the HQE expansion. Challenges are experimental selections applied to the data as well as to properly account for correlations.

In the following we describe the measurements of the moments of the charged lepton energy spectrum and the hadronic invariant mass distribution, which, together with the total rate, are the ingredients to extract $|V_{cb}|$ in global fits.

5.1. Moment measurements

The moments of the observables in $B \rightarrow X_c \ell \nu$ inclusive decays have been measured by various experiments. A list of the inputs included in the extraction of $|V_{cb}|$ performed by HFLAV [126] is reported in table 3.

Table 3. Experimental measurements used in the global analysis of $\bar{B} \rightarrow X_c \ell^- \bar{\nu}_\ell$. n is the order of the moment, c is the threshold value of the lepton momentum in GeV.

Exp.	Hadron moments $\langle m_X^{2n} \rangle$	Lepton moments $\langle E_\ell^n \rangle$	Remarks
BaBar [154] [155]	$n = 1, c = 0.9, 1.1, 1.3, 1.5$ $n = 2, c = 0.8, 1.0, 1.2, 1.4$ $n = 3, c = 0.9, 1.3$	$n = 0, c = 0.6, 1.2, 1.5$ $n = 1,$ $c = 0.6, 0.8, 1.0, 1.2, 1.5$ $n = 2, c = 0.6, 1.0, 1.5$ $n = 3, c = 0.8, 1.2$	Lepton momentum spectrum is obtained with an inclusive measurements. The hadronic moments are determined in hadronic tagged B meson sample.
Belle [156] [157]	$n = 1, c = 0.7, 1.1, 1.3, 1.5$ $n = 2, c = 0.7, 0.9, 1.3$	$n = 0, c = 0.6, 1.4$ $n = 1, c = 1.0, 1.4$ $n = 2, c = 0.6, 1.4,$ $n = 3, c = 0.8, 1.2$	Both lepton and hadronic moments measured using the hadronic B tagged events.
CDF [158]	$n = 1, c = 0.7$ $n = 2, c = 0.7$		Hadronic mass measurement obtained from the $D^* \pi$ mass distribution in $B \rightarrow D^{(*)} \pi \ell \nu$ decays, combined with the known $B \rightarrow D^{(*)} \ell \nu$ rates.
CLEO [159]	$n = 1, c = 1.0, 1.5$ $n = 2, c = 1.0, 1.5$		The kinematics of the hadronic part is inferred from the measurement of the neutrino momentum inclusively from the global event missing momentum.
DELPHI [160]	$n = 1, c = 0.0$ $n = 2, c = 0.0$ $n = 3, c = 0.0$	$n = 1, c = 0.0$ $n = 2, c = 0.0$ $n = 3, c = 0.0$	Exploiting the large boost of the B meson produced, the moments are measured without cuts on the lepton energy.

We have already introduced experimental techniques used for the study of semileptonic decays in section 4.2. In the following we provide additional experimental details on some of the measurements performed at the B -Factories.

5.1.1. Hadron moments The BaBar analysis [154] uses the hadronic B tagging technique. After the reconstruction of the B_{tag} , an identified lepton (electron or muon) is required in the event. The momentum of the lepton is required to be greater than 0.8 GeV in the rest frame of the signal B meson. All the tracks and clusters not associated with the B_{tag} and the lepton are combined to reconstruct the four-momentum of the hadronic system X_c . The resolution on the resulting hadronic mass m_X is

improved using a kinematic fit of the full event, considering the conservation of the four-momentum and setting the missing mass to zero. The hadronic moments $\langle m_X^{2n} \rangle$ are reconstructed from the measured m_X spectrum, for different cuts on the minimum lepton energy. The distribution of the mass spectrum for two minimum value of the lepton moments, are reported in figure 9 (left). The different exclusive contributions to the $B \rightarrow X_c \ell \nu$ decay are not disentangled, because of the limited resolution, due mainly to lost or misidentified particles. The reconstructed m_X distribution has to be corrected for the detector efficiency and resolution effects. The true values for the hadronic moments are obtained using a *per-event* corrections to the reconstructed moments, which are determined from simulations. The corrections depend on the lepton energy, the X_c multiplicity and the missing mass in the event.

The Belle analysis [156] also uses the hadronic B tagging method. Belle sets the minimum lepton momentum at 0.7 GeV. The true value of the hadronic moments, is extracted using an unfolding procedure based on the SVD algorithm [161]. This approach requires the knowledge of the migration matrix that connects the reconstructed and the true values of m_X , which is obtained using simulations.

5.1.2. Lepton moments In general the lepton energy momentum $\langle E_\ell^n \rangle$ can be measured with higher precision than the hadronic mass moments. The BaBar analysis [155] uses an inclusive approach where the $B\bar{B}$ candidates are selected requiring two leptons in the event. In this analysis, to reduce the background due to the hadron misidentification for low energy leptons, only electrons are used. A tagging electron is required to have a momentum in the 1.4 – 2.3 GeV range. The second electron in the event, the signal, is studied from momentum greater than 0.6 GeV. The background from the continuum is reduced with the global shape variables. The main source of background is due to lepton from secondary decay of charm mesons. This is reduced by requiring the charge correlation between signal and tagging lepton, and exploiting the kinematic properties of the two leptons. In general the moments have to be computed in the B meson rest frame so in this inclusive analysis further corrections are needed to account for the small motion of the B in the $\Upsilon(4S)$ rest frame.

The Belle analysis of the lepton moments [157] also is limited to electrons, and uses the hadronic B tagging method. One advantage of the tagging approach, is that the four-momentum of the B_{sig} is known from the fully reconstructed B_{tag} so the moments are directly computed in the B rest frame. The moments are extracted from the minimum lepton momentum cut of $p - e^* > 0.4$ GeV, computed in the B rest frame. The distribution of the lepton momentum, for the B^+ sample, is reported in figure 9 (right).

5.2. Results

A recent global analysis of the inclusive $B \rightarrow X_c \ell \nu$ has been done by HFLAV [126]. In this fit the hadronic mass moments $\langle m_X^{2n} \rangle$ of orders $n = 1, 2, 3$ and the lepton energy

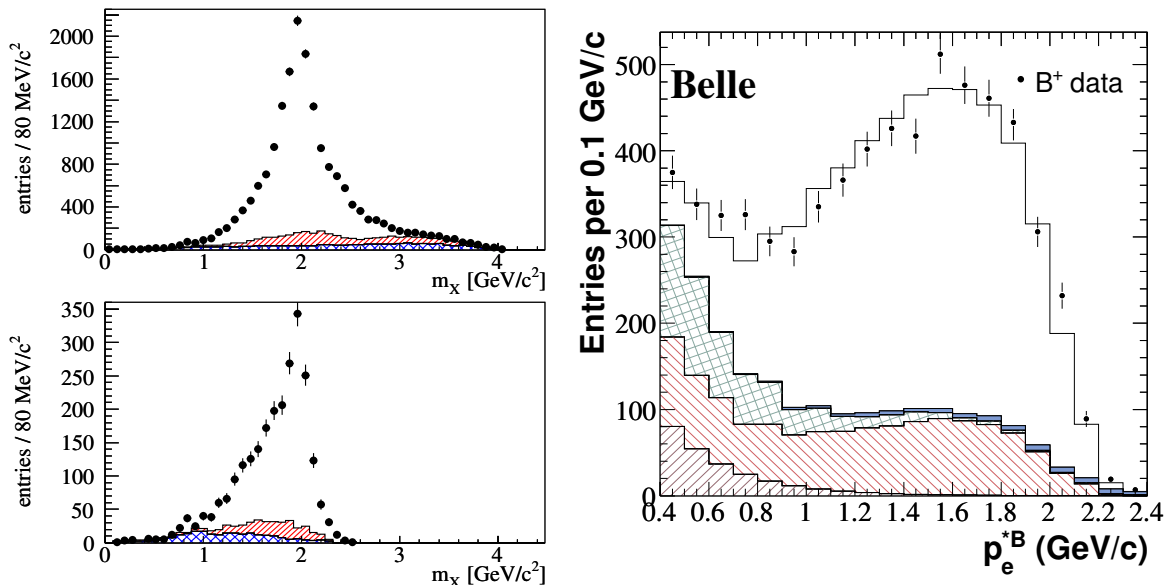


Figure 9. Left: Mass spectra for a lepton momentum cut of $p_\ell^* > 0.6$ GeV (top) and $p_\ell^* > 1.4$ GeV (bottom) obtained by BaBar prior the background subtraction. Plot from [154]. Right: lepton momentum from Belle in the B^+ decays. Plot from [157].

moments $\langle E_\ell^n \rangle$ of order $n = 0, 1, 2, 3$ are used. The lepton energy moments of order $n = 0$ are just the partial branching fractions. The moments are determined with different lower values of the lepton energy (E_{cut}). Because the moments of the same order and with different E_{cut} are strongly correlated, only a sub-sample of the measured moments are used in the global analysis. The list of the moments used is reported in table 3.

The moments of the $B \rightarrow X_c \ell \nu$ decay allow to determine a linear combination of the b and c quark masses. Additional inputs can be used for a precise determination of m_b . The additional information can come from the moments of the photon energy in $B \rightarrow X_s \gamma$ decay, or from an external determination of the c quark mass.

In the framework of kinetic scheme, $|V_{cb}|$ is extracted together with the b and c quark masses and 4 non-perturbative parameters (namely μ_π^2 , μ_G^2 , ρ_D^3 and ρ_{LS}^3). The subset of measurements used and the general approach follow the ones described in [162]. The fit is based on theoretical calculations described in [11, 163]. In this analysis the c quark mass is constrained to the value obtained in [164], which is $m_c^{\overline{\text{MS}}}(3 \text{ GeV}) = 0.989 \pm 0.013 \text{ GeV}$. The result of the fit, projected on some of the lepton energy and hadronic mass moments, is shown in figure 10. Let us report also the resulting values for $|V_{cb}|$ and m_b^{kin}

$$\begin{aligned} |V_{cb}| &= (42.19 \pm 0.78) \times 10^{-3} \\ m_b^{kin} &= 4.554 \pm 0.018 \text{ GeV} \end{aligned} \quad (69)$$

where the quoted uncertainties include both the experimental and the theoretical uncertainties. It is worth to mention that the theoretical uncertainties are dominating. The excellent fit quality points toward the validity of the HQE fit, but the small χ^2 per degree of freedoms of $\chi^2/ndf = 0.32$, could be a signal of some overestimated theoretical

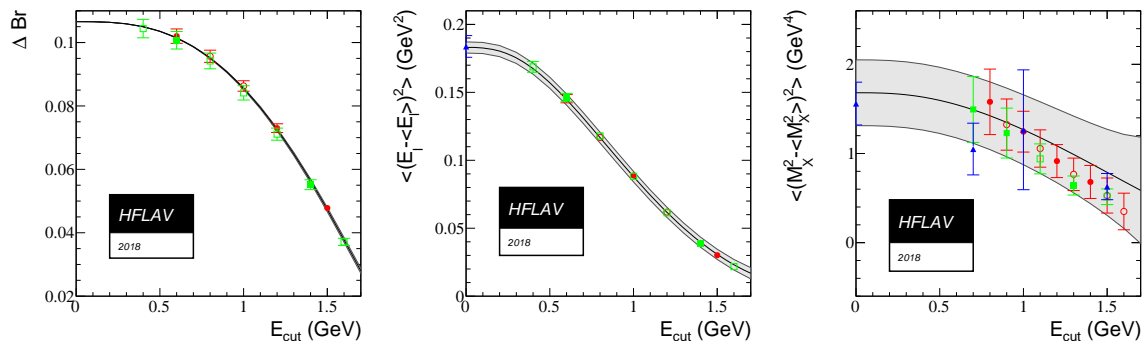


Figure 10. Distributions of the partial semileptonic branching fraction (left), one central lepton momentum (middle) and one hadronic mass central moment (right), with the result of the global fit in the kinetic mass scheme superimposed. The gray band is the theory prediction, fixing the HQE parameters at the fitted value, with the theory uncertainty. BaBar data are shown by circles (red), Belle by squares (green) and other experiments (DELPHI, CDF and CLEO) by triangles (blue). Open symbols (no internal color) are measurements not included in the fit.

uncertainties, or overestimated correlations between the various moments. These points have been discussed extensively for previous version of the global fit in [162].

An analysis performed in the framework of the 1S scheme, and based on the calculation of the lepton and hadron moments described in [165], gives, for $|V_{cb}|$ and the b quark 1S mass

$$\begin{aligned} |V_{cb}| &= (41.98 \pm 0.45) \times 10^{-3} \\ m_b^{1S} &= 4.691 \pm 0.037 \text{ GeV}. \end{aligned} \quad (70)$$

This analysis uses the same list of lepton and hadron moments reported in table 3 and in addition the moments of the photon spectrum in $B \rightarrow X_s \gamma$ decays as further constraints. The central values of $|V_{cb}|$ in (69) and (70) are in good agreement, but the uncertainties are different. The uncertainty on $|V_{cb}|$ from the global fits is 1.8% in the kinetic scheme and only 1.1% in the 1S scheme. However, a direct comparison between these two results is not significant, since the two schemes are not equivalent, as underlined in section 3.1.2. The 1S result [165] is at a disadvantage compared to the one in the kinetic scheme, since it does not include all contributions of order $O(\alpha_s \Lambda_{QCD}^2 / m_b^2)$.

All the analyses considered above include only the minimal set of four matrix elements which appear until order $O(1/m_b^3)$. At higher order, the large increase of HQE parameters complicates a great deal the extraction from data. A model approach that estimates the effects of orders $O(1/m_b^4)$ and $O(1/m_b^5)$, in the so-called Lowest Lying State Approximation, was employed in a recent global fit [166]. Their results indicate that such higher-order terms induce a sub-percent reduction in $|V_{cb}|$, which is not appreciable at the current level of precision. Another recent suggestion is to use a symmetry within the HQE, the reparameterization invariance, to achieve a reduction of independent parameters in some specific observables, that could be measured at e^+e^- colliders and used to extract $|V_{cb}|$ at order $O(1/m_b^4)$ [167].

6. Exclusive $|V_{cb}|$ determination

As discussed in section 3.2, the $|V_{cb}|$ exclusive determination requires the theoretical knowledge of the decay form factors, together with the measurements of the experimental decay rates. In the $B \rightarrow D^* \ell \nu_\ell$ channel, the form factors computed with the aid of heavy quark symmetries are currently available only at the zero recoil point $w = 1$, where the differential rates in (30) vanish. Therefore, a necessary step becomes to extrapolate the experimental measurements of the exclusive decays rates, yielding the products $|\eta_{EW}|^2 |\mathcal{F}(w)|^2 |V_{cb}|^2$ or $|\eta_{EW}|^2 |\mathcal{G}(w)|^2 |V_{cb}|^2$ at non-zero recoil points, to $w = 1$, by using a parameterization of the dependence on w of the form factors. As outlined in sections 3.2.3 and 3.2.4, the use of parameterizations introduces additional uncertainties, which could become significant at the current level of precision.

In the $B \rightarrow D \ell \nu_\ell$ channel, where form factors calculated directly at non-zero recoil points are already available, the role of parameterization becomes less relevant, because the extrapolation to $w = 1$ reduces to an interpolation between experimental results and different theory points.

In section 6.1 we discuss the exclusive determinations of $|V_{cb}|$ in the $B \rightarrow D^* \ell \nu_\ell$ channel, presenting the results in section 6.1.3. Two recent analyses by Belle [168] in 2018 and by BaBar [132] in 2019, using both CLN and BGL parameterizations, are detailed in section 6.1.1 and 6.1.2, respectively. In section 6.2 we discuss the $B \rightarrow D \ell \nu_\ell$ decays, detailing the most precise measurement (Belle [169]) in section 6.2.1 and drawing the conclusions in section 6.2.2. Section 6.3 is devoted to a novel and promising method to determine $|V_{cb}|$, using the $B_s \rightarrow D_s^{(*)} \mu \nu_\mu$ decays.

The B meson decays analyses can be complemented by analyses of bottom baryons. The measurement of the ratio of the branching fractions $\Lambda_b^0 \rightarrow p \mu^- \bar{\nu}_\mu$ and $\Lambda_b^0 \rightarrow \Lambda_c^+ \mu \bar{\nu}_\mu$ by the LHCb Collaboration [136] allows a direct measurement of the ratio $|V_{ub}|/|V_{cb}|$, that we discuss in section 6.4.

6.1. The $B \rightarrow D^* \ell \nu_\ell$ channel

The $B \rightarrow D^* \ell \nu_\ell$ channel, with a branching fraction of about 5%, is the most abundant semileptonic decays of the B mesons. The D^* is reconstructed in the $D^* \rightarrow D\pi$ or $D^* \rightarrow D\gamma$ decay modes, so the $B \rightarrow D^* \ell \nu_\ell$ decay can be seen as a four-body decay. A full description of this decay requires four independent kinematic variables. A customary choice of variables are w , the helicity angle of the D meson (θ_V), the helicity angle of the charged lepton ℓ (θ_ℓ), and the angle χ between the hadronic and leptonic two-body decay planes. These angles are shown in figure 11. Here the set $\cos \theta_V$, $\cos \theta_\ell$ and χ will be collectively called Ω .

The determination of $|V_{cb}|$ using the $B \rightarrow D^* \ell \nu_\ell$ decays has been performed by many experiments in various environments: CLEO, ALEPH, DELPHI, OPAL, and modern B -Factories, BaBar and Belle. The measurements performed by CLEO and LEP experiments, and also the first ones at the B -Factories, extracted $\eta_{EW}|V_{cb}|$ and some parameters of the form factor $\mathcal{F}(w)$ in (30), by measuring only the differential

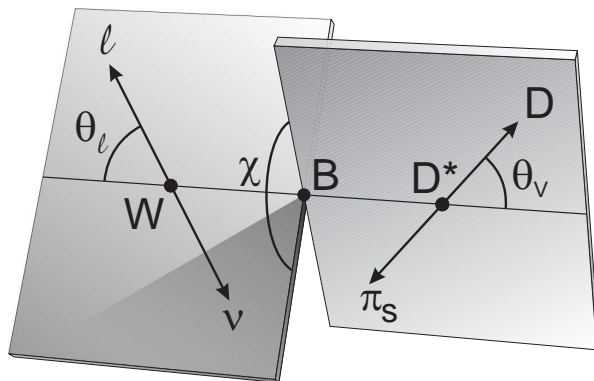


Figure 11. The helicity angles θ_V , θ_ℓ and χ in the $B \rightarrow D^* \ell \nu_\ell$ with the subsequent $D^* \rightarrow D\pi$ decay.

decay rate $d\Gamma$ as a function of w only. Since the fully differential rate in w and Ω depends on the three helicity amplitudes, in these measurements further assumptions are needed. For example, using the CLN parameterization, one relies on external determinations of the $R_1(1)$ and $R_2(1)$ ratios.

The first measurement that extracted information on all the form factors was done by CLEO [170]. In this pioneering measurement, the joint distribution of w and Ω was fit using an unbinned maximum likelihood method. By assuming a linear dependence on w of $h_{A_1}(w)$, and $R_1(w)$ and $R_2(w)$ independent of w , the following values were measured: $R_1 = 1.18 \pm 0.30 \pm 0.12$, $R_2 = 0.71 \pm 0.22 \pm 0.07$ and $\rho^2 = 0.81 \pm 0.15 \pm 0.06$, where the first uncertainty is statistical and the second is systematic. The parameters R_1 and R_2 were found consistent with the heavy quark symmetry limit of $R_1 = R_2 = 1$. The measurement was limited by the statistics available, based only on 2 fb^{-1} only, but it was the first observation that the corrections to the heavy-quark symmetry limit are quite small.

BaBar and Belle have measured these form factors and $|V_{cb}|$ with significant improved precision thanks to the larger statistics, the improved analysis techniques and the better knowledge of the background from the decay into excited D^{**} final states. At B -Factories the $B \rightarrow D^* \ell \nu_\ell$ decay has been studied using both the untagged approach and the hadronic B -tagging technique. In the following we describe in more details the two most recent measurements, one by Belle [168], using the untagged approach, and one from BaBar [132], based on the hadronic B -tagging.

6.1.1. Belle untagged measurement The Belle experiment has measured the shape of the form factors and $|V_{cb}|$ from $B^0 \rightarrow D^{*-} \ell^+ \nu_\ell$ using both the CLN and the BGL parameterizations [168]. This analysis, based on the full dataset of 711 fb^{-1} , extracts the parameters of interests from one-dimensional projections on w and the angles Ω .

A positron or an anti-muon with momentum in the range $0.3\text{-}2.4 \text{ GeV}$ or $0.6\text{-}2.4 \text{ GeV}$ in the laboratory frame, is combined with a D^{*-} candidate. The D^{*-} is

reconstructed from a \bar{D}^0 and slow pion π^- . The invariant mass difference between the $\bar{D}^0\pi^-$ combination and the \bar{D}^0 candidates, $\Delta m = m(\bar{D}^0\pi^-) - m(\bar{D}^0)$, is required to be less than 165 MeV. To reduce the combinatorial background, the \bar{D}^0 is reconstructed only in the $K^+\pi^-$ decay mode, which has a branching fraction of about 3.8% and it is the experimentally cleanest mode.

The most relevant backgrounds leftover, after the selection requirements, are

- Continuum background: $e^+e^- \rightarrow c\bar{c}$, where \bar{c} gives a D^{*-} ;
- Combinatorial background: fake D^{*-} candidates;
- D^{**} : resonant $B \rightarrow D^{**}\ell\nu_\ell$ decays, where D^{**} decays to a D^* , and non-resonant $B \rightarrow D^{(*)}\pi\ell\nu_\ell$ decays;
- Misidentified lepton: D^{*-} candidate is combined with an hadron identified incorrectly as electron or muon;
- Correlated background: when the D^{*-} and the lepton come from the same B , like $B \rightarrow D^*\tau\nu_\tau$, $\tau \rightarrow \ell\nu\nu$; $B \rightarrow D^*X_c$ where $X_c \rightarrow \ell Y$;
- Uncorrelated background: when the D^{*-} and the lepton come from different B 's.

The signal and the background yields for the various sources are extracted performing a binned maximum likelihood fit of the $D^*\ell$ candidates in the variables Δm , $\cos\theta_{BY}$ and p_ℓ . The momentum of the lepton p_ℓ is sensitive to the form factors themselves, thus, to avoid biasing the measurement, it is divided only in two regions, below and above 0.6 GeV. This choice has been useful to constrain the residual lepton misidentification background that affects mainly the low lepton momentum region. The invariant mass difference Δm is sensitive to the combinatorial background. The most powerful variable that allows to separate signal from the D^{**} and the correlated background, is $\cos\theta_{BY}$. In the assumption that the decay is $B \rightarrow D^*\ell\nu$, in the $\Upsilon(4S)$ rest frame, the B direction can be constrained in a cone around the axis given by the $Y \equiv D^*\ell$ direction

$$\cos\theta_{BY} = \frac{2E_B^*E_Y^* - m_B^2 - m_Y^2}{2|\vec{p}_B^*||\vec{p}_Y^*|} \quad (71)$$

where E_B^* and $|\vec{p}_B^*|$ are given by the beam energy and all the other quantities are determined only by the visible system Y . In (71) all the kinematic quantities are computed in the $\Upsilon(4S)$ rest frame. For the signal, $\cos\theta_{BY}$ is constrained in the physical region $(-1.0 \div 1.0)$, instead for the $B \rightarrow D^{**}\ell\nu$ and $B \rightarrow D^*\pi\ell\nu$, where one or more further particles are emitted, it is easy to show that $\cos\theta_{BY}$ is only constrained to be less than +1.0. Thus for D^{**} background $\cos\theta_{BY}$ has a long tail below the -1.0 value. The uncorrelated background is also constrained from $\cos\theta_{BY}$ because its shape extends to the region with $\cos\theta_{BY} > 1.0$. The distribution of $\cos\theta_{BY}$ for the most important physical backgrounds is shown in figure 12 (left).

Because of the bremsstrahlung that affects the electrons, and the finite resolution in the momentum reconstruction of the visible energy, $\cos\theta_{BY}$ for the signal also extends over the physical range. An important source of uncertainty in the computation of

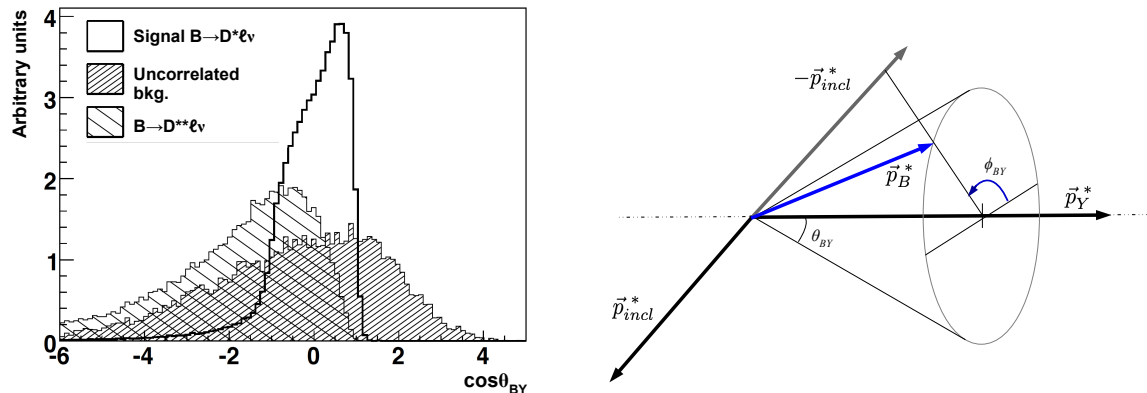


Figure 12. Left: the $\cos\theta_{BY}$ distribution for the signal $B \rightarrow D^* \ell \nu$, the D^{**} and the uncorrelated background. The differences in shapes show the discriminating power of this variable. Because of the bremsstrahlung the tail extend in the $\cos\theta_{BY} < -1$ region. Right: illustration on how the direction of the B meson is determined. The quantity \vec{p}_{incl}^* is given by summing the three-momentum of the particles not associated to the signal. The direction of the signal B , \vec{p}_B^* , is the one that minimizes the distance with the $-\vec{p}_{incl}^*$ vector.

$\cos\theta_{BY}$ is due to the beam energy spread of few MeV that affects the computation of p_B^* and E_B^* hence smearing the $\cos\theta_{BY}$ variable.

The signal yields extraction, from a simultaneous fit to Δm , $\cos\theta_{BY}$ and p_ℓ , is performed for each bin of the kinematic variables considered (w and the angles Ω). After the background subtraction, a total number of 180×10^3 candidates is obtained.

Because of the presence of the neutrino, the B -direction is not known, so these kinematic quantities cannot be calculated directly. From the value of $\cos\theta_{BY}$ per event, it is known only that the B must lie on a cone around the direction of the Y system. Various approaches have been used in different analyses to constrain the B direction on the cone. In this analysis Belle exploits the rest of the events to built a rough estimation of the direction of the other B inclusively. The B direction is chosen as the one on the cone closest to opposite of the other B meson direction. In figure 12(right) is illustrated how the technique works. With this algorithm the resolutions of the kinematic variables are 0.020 for w , 0.038 for $\cos\theta_\ell$, 0.044 for $\cos\theta_V$ and 0.210 for χ . The data are divided in 10 equidistant bins for each of four variables. The distributions of these variables, after the fit, are shown in figure 13. The signal yields in the four one-dimensional projections are simultaneously fitted to extract the shape of the form factors. Because the same events enter into the four projections, the correlation between all the various bins has to be carefully evaluated for both signal and backgrounds.

The measured yields are normalized to the total number of B^0 in the sample analyzed, which is given by $N_{B^0} = 2 \cdot f_{00} \cdot N_{BB}$, where N_{BB} is the total number of BB pairs collected by Belle, known with a precision of 1.4%, and f_{00} is the branching ratio of $\Upsilon(4S) \rightarrow B^0 \bar{B}^0$ determined to be $f_{00} = 0.486 \pm 0.006$ [93].

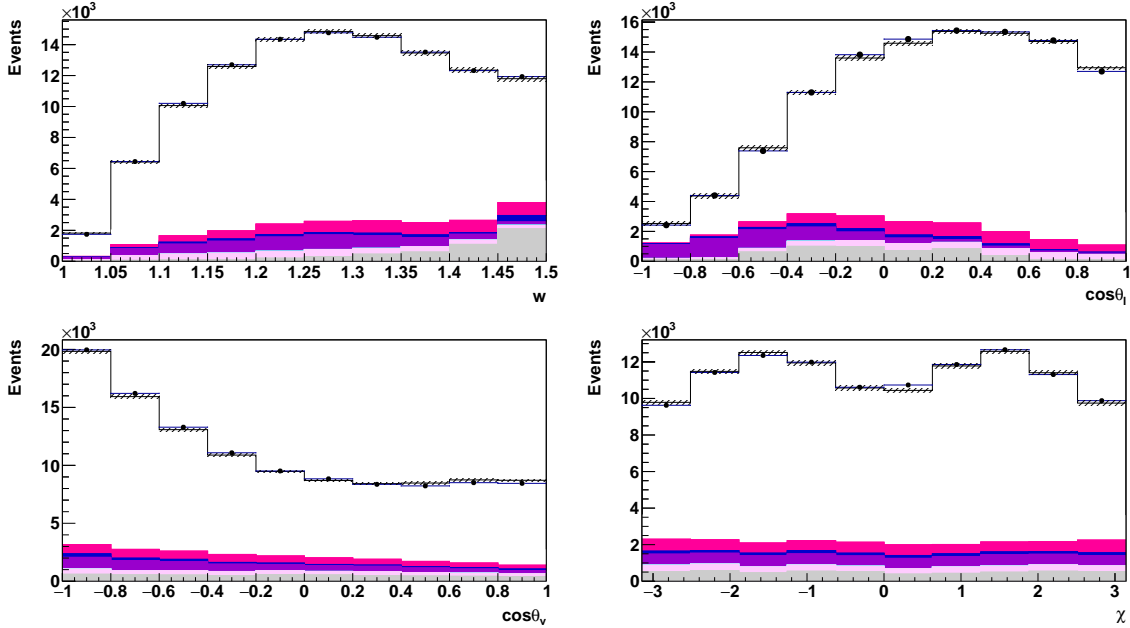


Figure 13. Distribution of the variables w , the cosine of the angles θ_V , θ_ℓ , and the angle χ for the Belle analysis of $B \rightarrow D^* \ell \nu_\ell$. The fit results using the CLN parameterization is superimposed. From [168].

The results of the fit on $\eta_{EW} \mathcal{F}(1) |V_{cb}|$ with the CLN parameterization are given in table 5, together with the results from other measurements obtained with the same parameterization. This result, consistent with the other measurements, is the most precise and dominates the HFLAV average. It is dominated by the systematic uncertainties which give a contribution of 1.6%, while the statistic uncertainty is only 0.4%. The dominant source of systematics is the tracking efficiency, mainly the soft pion one, the lepton identification and the uncertainty on the total number of $\Upsilon(4S)$ candidates. Also the external parameters, $\mathcal{B}(D \rightarrow K\pi)$ and f_{+-}/f_{00} , give significant contributions.

The results of the fit with the BGL parameterization is reported in table 4. The series in the expansion of the form factors are truncated at $n = 1$ for $f(z)$ and $g(z)$, instead $\mathcal{F}_1(z)$ is truncated at $n = 2$. Following the notation used in [89], this BGL configuration is called $\text{BGL}^{(121)}$ and has five free parameters, one more than the CLN one. This parameterization describes the data very well and the data are not sensitive to higher orders coefficients. The unitarity constraints have not been applied. The result on $|V_{cb}|$ obtained with the BGL parameterization is compatible with the CLN one, but has a larger statistical uncertainty. The χ^2/ndf of the fit to Belle data, in both CLN and BGL cases, are acceptable, so the available data are not sensitive to the different parameterizations.

6.1.2. BaBar tagged measurement BaBar has measured the shape of the form factors of $B^0 \rightarrow D^{*-} \ell^+ \nu_\ell$ decays using both CLN and BGL parameterizations [132]. This

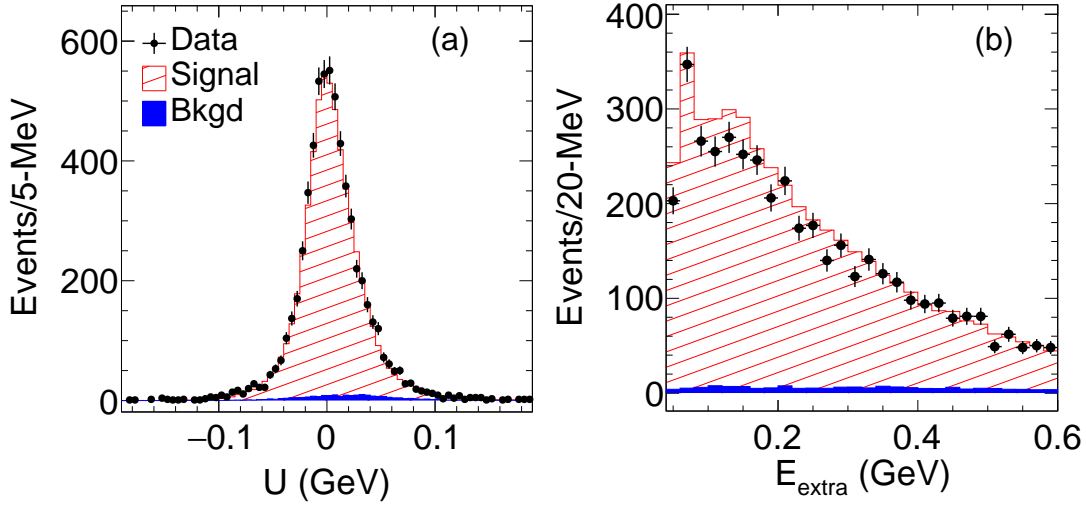


Figure 14. Comparison between data and simulation in the variables U (a) and E_{extra} (b). From [132].

analysis is based on the full dataset of 450 fb^{-1} , and exploits a sample where one of the B is fully reconstructed. The hadronic B -tagging is described in section 4.2. The knowledge of the kinematic of the B_{tag} event by event, and the beam properties, allows to determine the four-momentum of the neutrino from the missing four-momentum $p_{miss} = p_{e^+} + p_{e^-} - p_{B_{tag}} - p_{D^* \ell}$.

In this analysis two decay chains are considered: $B^0 \rightarrow D^{*-} \ell^+ \nu_\ell$ with $D^{*-} \rightarrow \bar{D}^0 \pi^-$, and $B^+ \rightarrow D^{*0} \ell^+ \nu_\ell$ with $D^{*0} \rightarrow \bar{D}^0 \pi^0$. The \bar{D}^0 is reconstructed in the three cleanest modes $K^+ \pi^-$, $K^+ \pi^- \pi^0$, $K^+ \pi^- \pi^+ \pi^-$. As usual the D^* is selected requiring Δm to be consistent with the expectations. The lepton is required to have momentum in the laboratory frame greater than 0.2 GeV or 0.3 GeV , if it is an electron or a muon, respectively. Besides the B_{tag} , the D^* and the lepton, no additional tracks are allowed in the event. The full decay chain $e^+ e^- \rightarrow \Upsilon(4S) \rightarrow B_{tag} B_{sig} (\rightarrow D^* \ell \nu_\ell)$ is considered in a kinematic fit that includes constraints on the beam spot, the secondary vertices, the masses of B_{tag} , B_{sig} , D^* and the missing neutrino. The probability of the χ^2 of this constrained fit is the main discriminating variable against the backgrounds. The sample is further cleaned rejecting candidates with large values for E_{extra} , which is defined as the sum of the energy of the photons not associated with the signal. The overall background level is only 2% and it is due to $B\bar{B}$ events decaying generically. The agreement between the signal and simulations for the E_{extra} and the variable $U = E_{miss} - |\vec{p}_{miss}|$ is very good, as can be seen in figure 14. After all the selection requirements, a total of about 5900 signal candidates is obtained.

The shape of the form factors is extracted using an unbinned maximum likelihood fit where the signal events are described by the four dimensional decay rate $d\Gamma/dwd\Omega$. All events in the signal region, defined by $|U| < 90 \text{ MeV}$, are considered in the likelihood as signal, and the small residual background is subtracted using information from large sample of $B\bar{B}$ simulated events.

The extraction of $|V_{cb}|$ is performed indirectly by adding to the likelihood the constraint that the semileptonic decay width Γ is given by $\Gamma = \mathcal{B}/\tau_B$, where \mathcal{B} is the $B \rightarrow D^*\ell\nu$ branching fraction and τ_B is the B meson lifetime. The values of these external inputs are taken from HFLAV [126].

The result with the BGL parameterization is reported in table 4 and with the CLN one in table 5. They are perfectly compatible and also compatible with the HFLAV average. Because of the limited signal statistics, The form factors are truncated at $n = 1$, $\text{BGL}^{(111)}$, to avoid the violation of the unitarity constraints due to poorly determined parameters. Higher order terms in BGL are checked and found to have a negligible effect on the shape of the form factors.

The dominant source of systematic uncertainty on the measurement of $|V_{cb}|$ is due to the remnant background that contaminates the angular distributions. The resolution on the kinematic variables is about a factor five better than the one possible with the untagged measurement. The impact of the finite resolution is evaluated using the simulation and turns out to be negligible.

Table 4. Fit results with the BGL parameterization of some recent analyses. The notation is $\text{BGL}^{n_f, n_{F1}, n_g}$ where n_f , n_{F1} and n_g are the order of the z -expansions for the $f(z)$, $F_1(z)$ and $g(z)$ respectively. The parameters cannot be compared directly because different constants are used, in particular the B_c^* masses value in the Blasckhe factor. Furthermore BaBar assumes $t_0 = t_+ - \sqrt{t_+(t_+ - t_-)}$, while the other fits assume $t_0 = t_-$.

BGL	Bigi et al. [91] BGL ²²²	Belle [168] BGL ¹²⁰	BaBar [132] BGL ¹¹¹	Gambino et al. [89] BGL ²²²
$ V_{cb} \times 10^{-3}$	$41.7^{+2.0}_{-2.1}$	38.3 ± 0.97	38.36 ± 0.90	$39.6^{+1.1}_{-1.0}$
a_0^f	0.01223 ± 0.00018	0.0131 ± 0.0002	0.0129 ± 0.0003	0.01221 ± 0.00016
a_1^f	$-0.054^{+0.058}_{-0.043}$	0.0169 ± 0.0050	0.0163 ± 0.0010	$0.006^{+0.032}_{-0.045}$
a_2^f	$0.20^{+0.7}_{-1.2}$	-	-	$-0.2^{+1.2}_{-0.8}$
$a_1^{F_1}$	$-0.0100^{+0.0061}_{-0.0056}$	0.0070 ± 0.0018	0.0003 ± 0.0011	0.0042 ± 0.0022
$a_2^{F_1}$	0.012 ± 0.010	0.085 ± 0.034	-	$-0.069^{+0.041}_{-0.037}$
a_0^g	$0.012^{+0.011}_{-0.008}$	-0.0241 ± 0.0058	0.0274 ± 0.0011	$0.024^{+0.021}_{-0.009}$
a_1^g	$0.7^{+0.3}_{-0.4}$	-	0.0833 ± 0.0667	$0.05^{+0.39}_{-0.72}$
a_2^g	$0.8^{+0.2}_{-1.7}$	-	-	$1.0^{+0.0}_{-2.0}$

6.1.3. Results Table 5 reports a summary of the measurements of $\eta_{EW}\mathcal{F}(1)|V_{cb}|$ obtained with the CLN parameterization, together with the HFLAV average. Using the FLAG 2019 value for the normalization of the form factor $\eta_{EW}\mathcal{F}(1) = 0.910 \pm 0.013$, the HFLAV average for $|V_{cb}|$ is

$$|V_{cb}| = (38.76 \pm 0.42 \pm 0.55) \times 10^{-3} \tag{72}$$

where the first error is experimental and the second is due to the form factor normalization. The results obtained with CLN and BGL parameterizations are consistent.

In the 2017 the Belle collaboration released an analysis, not published, of $B \rightarrow D^* \ell \nu$ using the hadronic B -tagging [130]. The form factors and $|V_{cb}|$ were extracted from the projections on w and the angles Ω with a fit similar to the one described before for the

Table 5. Results of $B \rightarrow D^* \ell \nu_\ell$ measurements with the CLN parameterization and the current HFLAV average [126]. Only $\eta_{EW} \mathcal{F}(1) |V_{cb}| (\times 10^3)$ and ρ^2 are reported.

	$\eta_{EW} \mathcal{F}(1) V_{cb} (\times 10^3)$	ρ^2	Remarks
BaBar [171]	$33.77 \pm 0.29 \pm 0.98$	$1.184 \pm 0.048 \pm 0.029$	Untagged measurement of the $B^0 \rightarrow D^{*-} \ell^+ \nu_\ell$ decay. Fit to the four projections: w and the three helicity angles. Data fitted with the CLN. Extracted also $R_1(1)$ and $R_2(1)$, together with ρ^2 . The form factors are further constrained to a dedicated measurement performed by BaBar which uses only clean $B^0 \rightarrow D^{*-} e^+ \nu_e$ data samples [172].
BaBar [147]	$34.81 \pm 0.58 \pm 1.06$	$1.125 \pm 0.058 \pm 0.053$	Untagged measurement of $B^+ \rightarrow D^{*0} \ell^+ \nu_\ell$ with D^{*0} reconstructed in $\bar{D}^0 \pi^0$ decay mode. One-dimensional fit of w using only CLN. Parameters $R_1(1)$ and $R_2(1)$ taken from external inputs.
BaBar [173]	$35.75 \pm 0.20 \pm 1.09$	$1.180 \pm 0.020 \pm 0.061$	Global analysis of $B \rightarrow D^* \ell \nu_\ell$ and $B \rightarrow D \ell \nu_\ell$ using inclusive samples of $B \rightarrow D^- \ell \nu_\ell X$ and $B \rightarrow \bar{D}^0 \ell \nu_\ell X$ decays. The fit is performed multidimensional on p_ℓ^* , p_D^* and $\cos \theta_{BY}$ variables. Only the CLN parameterization was used.
Belle [168]	$35.07 \pm 0.15 \pm 0.56$	$1.106 \pm 0.031 \pm 0.008$	Untagged measurement of $B^0 \rightarrow D^{*-} \ell^+ \nu_\ell$. Fit to the four projections. Data fitted with the CLN. Extracted also $R_1(1)$ and $R_2(1)$, together with ρ^2 . Results also using the BGL. Published also the background subtracted spectra of the four projections with all the information, like efficiencies and migration matrix, needed for subsequent refitting.
HFLAV [126]	$35.27 \pm 0.11 \pm 0.36$	$1.122 \pm 0.015 \pm 0.019$	The average includes also older measurements from CLEO and LEP experiments: DELPHI, ATLAS and OPAL. The average Confidence Level is only 0.8%.
Belle [130]	$34.93 \pm 0.23 \pm 0.59$		Tagged measurement of $B^0 \rightarrow D^{*-} \ell^+ \nu_\ell$, not published. For the first time the spectrum of the projections on q^2 and the angular variables was released. The spectrum unfolded and corrected for the efficiency was also released.
BaBar [132]	34.94 ± 0.50	0.96 ± 0.08	Tagged measurement of $B^+ \rightarrow D^{*0} \ell^+ \nu_\ell$ and $B^0 \rightarrow D^{*-} \ell^+ \nu_\ell$ decays. Not included yet in the HFLAV average. The uncertainties include both the statistical and systematics. Fit is unbinned to q^2 and the angular variables. Data fitted using both CLN and BGL. This measurement is not normalized, so $ V_{cb} $ is extracted from the measured $B^0 \rightarrow D^{*-} \ell^+ \nu_\ell$ branching fractions [126].

untagged analysis. The result of the fit, performed using the CLN parameterization, was consistent with previous measurements. The Belle collaboration released also the spectra of the projections on the four kinematic variable, unfolded for the resolution and corrected for the efficiencies. Some groups took this opportunity to fit the Belle data using not only the CLN parameterization but also the BGL one [91, 92, 128, 174]. They observed that the central value of $|V_{cb}|$ using the BGL parameterization was systematically higher than the value obtained with the CLN one, and that, depending on the choice of constraints and inputs of the analysis, could be lifted up to 6 – 7%. For illustration, we report in table 4 the BGL results of [91]. The fact that the BGL result became compatible with the inclusive determination of $|V_{cb}|$ disclosed the possibility that a suitable choice of the parameterization could be enough to solve the $|V_{cb}|$ puzzle. However, some inconsistencies were observed in the fits exploiting the BGL approach; for example it was shown in [174] that the form factor ratio $R_1(w)$ determined from the results of the fits strongly contradicts the HQS predictions.

More data were eagerly needed. They have been provided in 2018 by Belle [168] and in 2019 by BaBar [132]. These analyses, detailed in section 6.1.1 and 6.1.2, respectively, show no sign of discrepancy on $|V_{cb}|$ between the BGL and CLN parameterizations, within the uncertainties. Belle also in this case released the data in a format that allows them to be fitted by outside groups, prompting a new analysis by some among the authors of the 2017 fits [89]. The new fits, which include also the previous Belle analysis, have been performed with both CLN and BGL parameterizations, in different configurations, and the results found to be consistent. Also the BGL discrepancy with HQS mentioned before seems to be overcome. The BGL value is reported in table 4, for comparison with the results of Belle and BaBar.

Nevertheless the initial discrepancies have been useful to revisit the assumptions under the widely used CLN parameterization. The possible systematics due to the parameterization itself had never been considered in the $|V_{cb}|$ extraction. Theoretical analyses have investigated constraints and subtleties of the different approaches, including the studies on the optimal number of parameters of the BGL fit, and the risk of overfitting [89, 175]. Moreover, with only few exceptions, most of the experimental analyses were using only the CLN parameterization. With the increasing precision, it is crucial to describe the shape of the form factors in a model independent way. It is worth to mention now that, when calculation of the form factor at $w > 1$ will be available, the role of parameterizations will become less relevant, because the extrapolation to $w = 1$ will reduce to an interpolation between experimental results and different theory points.

6.2. The $B \rightarrow D\ell\nu_\ell$ channel

The analysis of $B \rightarrow D\ell\nu_\ell$ decays is difficult because of the large background from $B \rightarrow D^*\ell\nu_\ell$ where the D^* decays in $D\pi$ or $D\gamma$, with the soft pion or gamma lost or not detected. This kind of background is usually called *feed-down* in the literature. In the past, untagged approaches have been used, similar to the one described above for the

$B \rightarrow D^* \ell \nu_\ell$, by the CLEO [176] and Belle [177] collaborations. CLEO has used both $B^+ \rightarrow \bar{D}^0 \ell^+ \nu_\ell$ and $B^0 \rightarrow D^- \ell^+ \nu_\ell$ decays. In general, the signal selection relies mostly on the selection of a good D meson candidate, so the combinatorial background is large. The consequence is that only few, low multiplicity D decay modes can be exploited. CLEO in fact uses the $\bar{D}^0 \rightarrow K^+ \pi^-$ and $D^- \rightarrow K^+ \pi^- \pi^-$ decay modes, which are the cleanest. The $B^+ \rightarrow \bar{D}^0 \ell^+ \nu_\ell$ decays with the untagged approach is the most difficult because of the large feed-down: the \bar{D}^0 can come from both $B^+ \rightarrow D^{*0} \ell^+ \nu_\ell$, with D^{*0} decaying in \bar{D}^0 almost all the time, and $B^0 \rightarrow D^{*-} \ell^+ \nu_\ell$ with $D^{*-} \rightarrow \bar{D}^0 \pi^-$, which has a branching fraction of 68%. The $B^0 \rightarrow D^- \ell^+ \nu_\ell$ instead is easier because the D^- comes only from $B^0 \rightarrow D^{*-} \ell^+ \nu_\ell$ with $D^{*-} \rightarrow D^- \pi^0$, which has a branching fraction of only 31%. For this reason Belle analyzed only the $B^0 \rightarrow D^- \ell^+ \nu_\ell$. The larger phase space suppression in the region close to $w \rightarrow 1$ for the $B \rightarrow D$ decays, compared with the $B \rightarrow D^*$, implies a large background in the region crucial for the $|V_{cb}|$ extraction.

The hadronic B -tagging is particularly suitable for the $B \rightarrow D \ell \nu_\ell$, as shown in the BaBar analysis [178], where both $B^0 \rightarrow D^- \ell^+ \nu_\ell$ and $B^+ \rightarrow \bar{D}^0 \ell^+ \nu_\ell$ are studied. The hadronic tagging allows to reduce the combinatorial background in the \bar{D}^0 and D^- reconstruction, and also the feed-down from D^* and D^{**} decays, because the tagging allows to separate clearly $\Upsilon(4S) \rightarrow B^+ B^-$ from $\Upsilon(4S) \rightarrow B^0 \bar{B}^0$ decay modes.

6.2.1. Belle tagged analysis The most precise measurement has been done by Belle [169] and uses an improved hadronic b -tagging approach. The tracks and the clusters of the event, remaining after the identification of the B_{tag} , are used to identify the $B \rightarrow D \ell \nu_\ell$ signal decay. The lepton is required to have a momentum greater than 0.3 GeV for the electron case, and 0.6 GeV for the muon case. The low signal efficiency, due to the reconstruction of the hadronic tag, is partially compensated by the possibility to reconstruct D mesons in many different decays modes, also including π^0 and K_s particles. In particular, the D^- meson is reconstructed in 10 possible final states, covering about 29% of the total rate, and the \bar{D}^0 is reconstructed in 13 final states, corresponding to more than 40% of the total rate.

The discriminating variable used to separate the signal $B \rightarrow D \ell \nu_\ell$ from background is the missing mass squared M_{miss}^2 . The distribution of M_{miss}^2 for a bin in w is reported in figure 15 separately for B^0 and B^+ decays. The signal extraction is performed separately in ten bins in w , in the range from 1 to 1.6, with the Barlow and Beeston algorithm [179], that accounts for statistical uncertainties in both data and simulation. The shapes of the backgrounds and the signal are determined from simulations and fixed in the fit. The fit to extract the signal yields is simultaneous in the four samples: $B^0 \rightarrow D^- e^+ \nu_e$, $B^+ \rightarrow \bar{D}^0 e^+ \nu_e$, $B^0 \rightarrow D^- \mu^+ \nu_\mu$, $B^+ \rightarrow \bar{D}^0 \mu^+ \nu_\mu$. The largest source of systematic uncertainty is due to the calibration of the hadronic B -tagging sample. This calibration is required because the composition and the efficiency of the various hadronic B decay modes used in the B -tagging definition have to be adapted to the data. The other relevant sources of uncertainties are the knowledge of the branching ratios of D^- and \bar{D}^0 mesons, and of the tracking efficiency.

The distribution of the measured differential decay width $d\Gamma/dw$, is shown in figure 16 (left) with the result of the fit using the BGL parameterization, superimposed. The fit also exploits the available lattice calculations from FNAL/MILC [68] and HPQCD [69] for the values of $w \in (1, 1.08, 1.16)$. The lattice calculations are obtained for both $f_+(z)$ and $f_0(z)$, while the experimental $d\Gamma/dw$ depends only on $f_+(z)$. Nevertheless, exploiting the kinematic constraint between f_+ and f_0 at maximum recoil, $f_0(q_{min}^2) = f_+(q_{min}^2)$, the lattice data on $f_0(z)$ help to reduce the uncertainties on $|V_{cb}|$. The fit result depends on the truncation order n of the $f_{+,0}(z)$ series. The default result is obtained with $n = 3$ because the fit stabilizes for $n \geq 3$. The result is $|V_{cb}| = (40.83 \pm 1.13) \times 10^{-3}$. By fitting $d\Gamma/dw$ with the CLN parameterization, and taking $\mathcal{G}(1) = 1.0541 \pm 0.0083$ [41], the results is $|V_{cb}| = (39.86 \pm 1.33) \times 10^{-3}$. The result with the CLN parameterization is less precise than BGL one because in the latter additional lattice point are used.

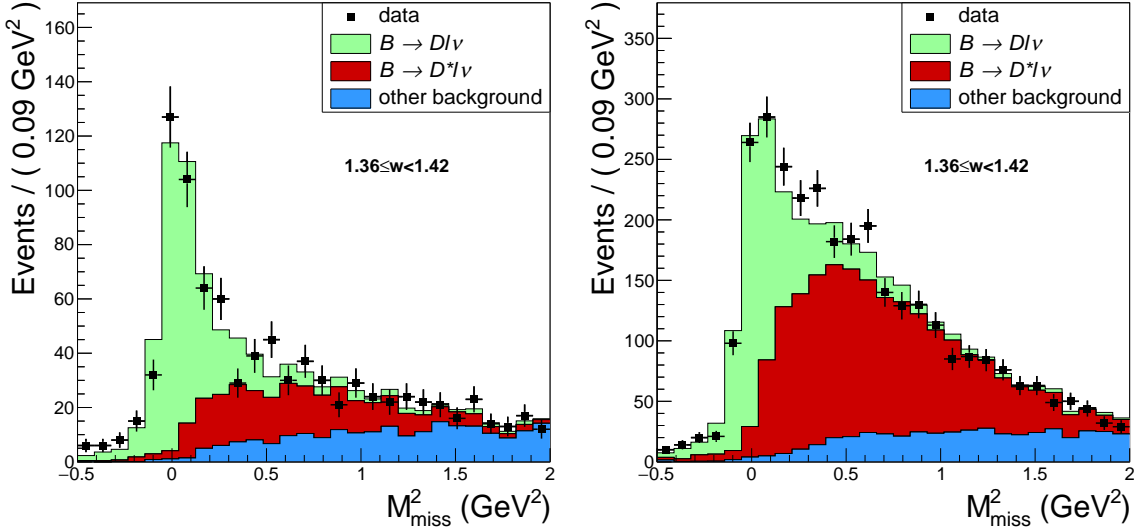


Figure 15. Distribution of M_{miss}^2 from the Belle tagged analysis [169]. The distribution corresponds to the bin with $1.36 < w < 1.42$ separately for $B^0 \rightarrow D^- e^+ \nu_e$ decays (left) and $B^+ \rightarrow \bar{D}^0 e^+ \nu_e$ decays (right). The larger feed-down due to D^* background present in the B^+ sample is clearly visible.

6.2.2. Results A summary of the measurements of $\eta_{EW} \mathcal{G}(1) |V_{cb}|$ obtained with the CLN parameterization is reported in table 6, together with the HFLAV average. Using the $\mathcal{G}(1)$ from [41], the HFLAV average is

$$|V_{cb}| = (39.58 \pm 0.94 \pm 0.37) \times 10^{-3} \quad (73)$$

where the first error is experimental and the second is due to the form factor normalization. This result is compatible with the result from $B \rightarrow D^* \ell \nu_\ell$ given in section 72. A fit of both BaBar and Belle data, combined with lattice calculation and performed using both BGL and CLN parameterizations, gives consistent results, even

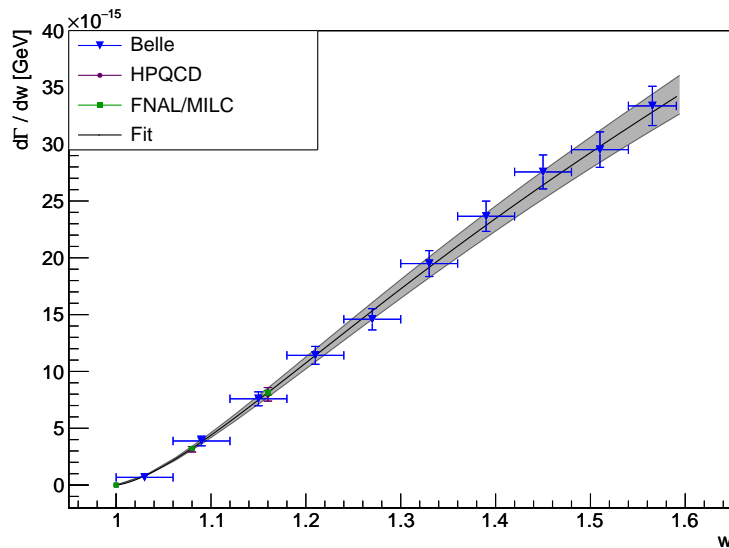


Figure 16. Differential decay width of $B \rightarrow D\ell\nu_\ell$ decay obtained by Belle [169], and results of the combined fit between data and lattice calculations from FNAL/MILC and HPQCD.

Table 6. Results of $B \rightarrow D\ell\nu_\ell$ measurements with the CLN parameterization and the current HFLAV average [126]. Both $\eta_{EW}\mathcal{G}(1)|V_{cb}|$ and ρ^2 are reported.

	$\eta_{EW}\mathcal{G}(1) V_{cb} $ ρ^2	Remarks
BaBar [173]	$42.76 \pm 1.71 \pm 1.26$ $1.200 \pm 0.088 \pm 0.043$	Global analysis of $B \rightarrow D^*\ell\nu_\ell$ and $B \rightarrow D\ell\nu_\ell$ using inclusive samples of $B \rightarrow D^-\ell\nu_\ell X$ and $B \rightarrow \bar{D}^0\ell\nu_\ell X$ decays. The fit is multidimensional on p_ℓ^* , p_D^* and $\cos\theta_{BY}$ variables. Only the CLN parameterization was used.
BaBar [178]	$43.84 \pm 0.76 \pm 2.19$ $1.215 \pm 0.035 \pm 0.062$	Tagged measurement using both B^0 and B^+ . The sample is normalized to the inclusive $B \rightarrow X\ell\nu$ which is known with an uncertainty of only 1%. The fit is based on CLN.
Belle [169]	$42.22 \pm 0.60 \pm 1.21$ $1.090 \pm 0.036 \pm 0.019$	Tagged measurement using both B^0 and B^+ . Both fits use CLN and BGL, as well as the lattice data points at non-zero recoil from FNAL/MILC [68] and HPQCD [69]. This analysis published also the unfolded w spectrum corrected for the efficiency.
HFLAV [126]	$42.00 \pm 0.45 \pm 0.89$ $1.131 \pm 0.024 \pm 0.023$	The average includes also an older measurement from CLEO.

if the BGL value, $|V_{cb}| = (40.49 \pm 0.97) \times 10^{-3}$, is slightly higher than the one obtained with CLN [90].

6.3. The $B_s \rightarrow D_s^{(*)}\mu\nu_\mu$ channel

LHCb has recently extracted V_{cb} from semileptonic B_s^0 decays for the first time [72]. The measurement uses both $B_s^0 \rightarrow D_s^- \mu^+ \nu_\mu$ and $B_s^0 \rightarrow D_s^{*-} \mu^+ \nu_\mu$ decays using 3 fb^{-1} collected in 2011 and 2012. The value of $|V_{cb}|$ is determined from the observed yields of B_s^0 decays normalized to those of B^0 decays after correcting for the relative reconstruction and selection efficiencies. The normalization channels are $B^0 \rightarrow D^- \mu^+ \nu_\mu$ and $B^0 \rightarrow D^{*-} \mu^+ \nu_\mu$ with the D^- reconstructed with the same decay mode of the D_s ($D_{(s)}^- \rightarrow [K^+ K^-]_\phi \pi^-$). With this choice the signal and the reference channels have the same particles in the final state and similar kinematics, minimizing in this way the systematic uncertainties.

The shape of the form factors are extracted as well, exploiting the kinematic variable $p_\perp(D_s)$, which is the component of the D_s^- momentum perpendicular to the B_s^0 flight direction. This variable is highly correlated with q^2 and also slightly correlated with the helicity angles in the $B_s^0 \rightarrow D_s^{*-} \mu^+ \nu_\mu$ decay.

The D_s^* is not explicitly reconstructed, but its contribution is disentangled from the D_s using the corrected mass m_{corr} , which is defined as $m_{corr} = \sqrt{m_Y^2 + |p_\perp(Y)|^2 + |p_\perp(Y)|}$, where $p_\perp(Y)$ is the transverse momentum (to the flight direction) of the visible system $Y \equiv D_s^- \mu^+$ and m_Y is its invariant mass. The variable m_{corr} is useful to discriminate D_s , D_s^* and the feed-down background categories: it peaks at the mass of the B_s when there is a single massless particle missing, and peaks at lower values when there are other missing particles associated with the signal candidate, like in $B_s \rightarrow D_s \mu \nu_\mu X$ decays. ††.

Analogously to the $B \rightarrow D \ell \nu_\ell$ and $B \rightarrow D^* \ell \nu_\ell$ decays described before, one of the most relevant backgrounds to $B_s^0 \rightarrow D_s^- \mu \nu_\mu$ signal decays is due to the semileptonic B_s^0 decays into excited strange charmed states with $L = 1$, which in turn decay into D_s and D_s^* with the emission of pions and photons. There are no experimental measurements of the semileptonic B_s decays into these excited states. Of the four $L = 1$ excited states D_s^{**} , only the states with $j_l = 1/2$, namely $D_{s0}(2317)$ and $D_{s1}(2460)$, are known to decay into D_s in the final state because they have a mass below the kinematic threshold needed to decay strongly in DK and D^*K . The two states with $j_l = 3/2$, $D_{s1}(2536)$ and $D_{s2}(2575)$, instead, do not contribute significantly to the signal because they have a mass high enough that their dominant decay modes are the strong decays into D^*K and DK , respectively. Only the $D_{s1}(2536)$ has been observed to decay into a D_s meson. For the same reasons, also higher orbitally or radially excited states do not give D_s in the final state. After the full selection, the background due to the decay of excited state is only few percent of the full $D_s \mu$ sample. Also the normalization channels $B^0 \rightarrow D^- \mu \nu_\mu$ and $B^0 \rightarrow D^{*-} \mu \nu_\mu$ suffer of similar kind of background. This background results to be about 9% of the $D^- \mu$ sample.

††It is interesting to mention that m_{corr} can be generalized also to the case of a massive missing particle, assuming $B \rightarrow YX$ where Y is the visible system, and X a single particle with mass m_X . In this case, under the same assumptions behind the standard formula, one has

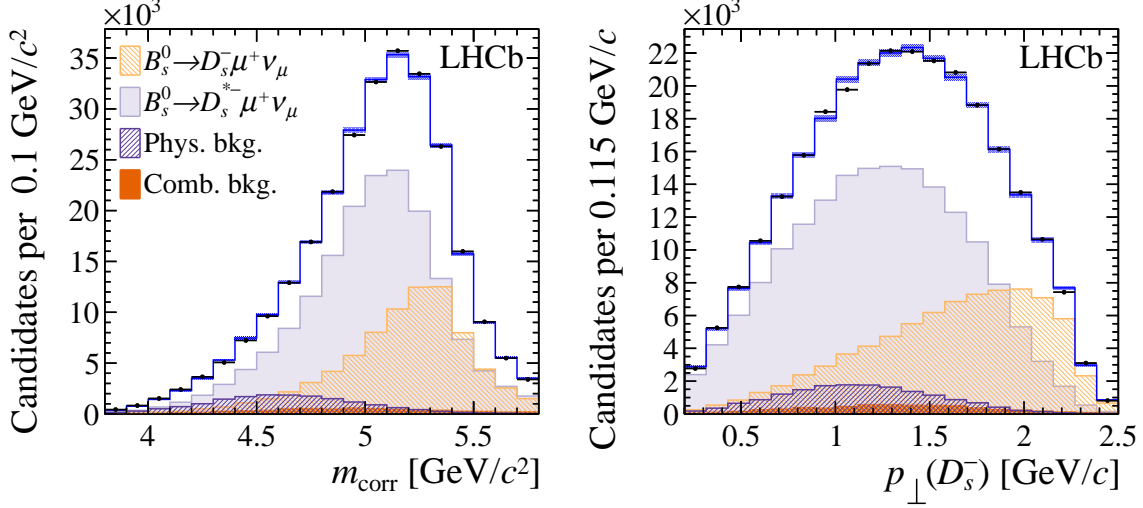


Figure 17. Distribution of m_{corr} (left) and $p_{\perp}(D_s^-)$ (right) for the inclusive sample of $D_s^- \mu^+$ signal candidates, with fit projections based on the CLN parameterization superimposed.

A fit to the $D_s^- \mu$ sample of the two dimensional distribution m_{corr} and $p_{\perp}(D_s)$ allows to identify $B_s^0 \rightarrow D_s^- \mu^+ \nu_{\mu}$ and $B_s^0 \rightarrow D_s^{*-} \mu^+ \nu_{\mu}$ signal yields, providing at the same time a measurements of the form factors parameters. The projections of the fit to the signal sample is reported in Figure 17. Analogously the yields of the normalisation channels are extracted from a fit to the $D^- \mu$ sample. For the $B_s \rightarrow D_s \mu \nu_{\mu}$ decay, $|V_{cb}|$ is connected with the measured ratio of signal yields, N_{sig} , and the normalization channel yields, N_{ref} , through the relation

$$\frac{N_{sig}}{N_{ref}} = \mathcal{K} \tau_s \int \frac{d\Gamma(B_s \rightarrow D_s \mu \nu_{\mu})}{dw} dw \quad (74)$$

where τ_s is the B_s lifetime, and the constant \mathcal{K} depends on the external inputs as

$$\mathcal{K} = \xi \frac{f_s \mathcal{B}(D_s^- \rightarrow K^+ K^- \pi^-)}{f_d \mathcal{B}(D^- \rightarrow K^+ K^- \pi^-)} \frac{1}{\mathcal{B}(B^0 \rightarrow D^- \mu \nu_{\mu})} \quad (75)$$

where ξ is the efficiency ratio between the signal and the normalization. In the analogous expression for the $B_s \rightarrow D_s^* \mu \nu_{\mu}$ decay, the integral of the decay width is done on the variables $(w, \cos \theta_{\ell}, \cos \theta_V, \chi)$, and there is an explicit dependence on the branching fraction of the $D^{*-} \rightarrow D^- \pi$ decay.

This analysis takes advantage of the recent results from lattice on the $B_s \rightarrow D_s^-$ and $B_s \rightarrow D_s^{*-}$ form factor calculations, summarized briefly in section 3.2.2. In particular for the $B_s \rightarrow D_s^{*-}$ only the calculations at zero recoil, $h_{A1}^{B_s}(1)$ is available, and the most recent result from Ref. [56] is used. For the $B_s \rightarrow D_s \mu \nu_{\mu}$ it has been exploited the very recent calculation of the $B_s \rightarrow D_s$ form factors performed in the full w -range [78].

$$m_{corr} = \sqrt{m_Y^2 + |p_{\perp}(Y)|^2} + \sqrt{m_X^2 + |p_{\perp}(Y)|^2}.$$

In this analysis both the CLN parameterization and a 5-parameter version of BGL have been used. In the analysis with the CLN parameterization, the form factor parameters $\rho^2(D_s^*)$, $R_1(1)$ and $R_2(1)$ are free to float in fit, while $\rho^2(D_s)$ and the normalizations $h_{A1}^{B_s}(1)$ and $\mathcal{G}^{B_s}(1)$ are constrained from the theory calculations. The results of the form factors are affected by large statistical uncertainty, but are consistent with the results from the B decays. The result for $|V_{cb}|$ is

$$|V_{cb}|_{CLN} = (41.4 \pm 0.6 \pm 0.9 \pm 1.2) \times 10^{-3},$$

where the first uncertainty is statistical, the second systematic and the third due to the limited knowledge of the external inputs, in particular the constant $f_s/f_d \times \mathcal{B}(D_s^- \rightarrow K^+ K^- \pi^+)$, which is known with an uncertainty of about 3%. It is worth to mention that the formulation of the CLN parameterization used is the same obtained for the B meson case. The constants that appear in the equations (58) could be slightly different for the B_s case, because the coefficients include the Blaschke factor, which depends on the masses of the initial and final mesons.

In the analysis with the BGL parameterization the fitted parameters are the coefficients of the series of the z expansions. For the $B_s \rightarrow D_s^* \mu \nu_\mu$ decays the expansion of the form factors $f(z)$, $\mathcal{F}_1(z)$ and $g(z)$ are truncated at the first order in z . For the $B_s \rightarrow D_s \mu \nu_\mu$ decays, the expansion of $f_+(z)$ is truncated at the second order in z , and the three coefficients constrained to the values obtained from Ref. [56]. The results for $|V_{cb}|$ is

$$|V_{cb}|_{BGL} = (42.3 \pm 0.8 \pm 0.9 \pm 1.29) \times 10^{-3},$$

which is consistent with the result based on CLN parameterization.

The results obtained are in agreement with the exclusive determinations of $|V_{cb}|$ with B^0 and B^+ , and also consistent with the inclusive determination. Although not competitive with the results obtained at the B -Factories, the novel approach used can be extended to the semileptonic B^0 decays in LHCb.

6.4. Direct measurement of $|V_{ub}|/|V_{cb}|$

The LHCb collaboration has measured the ratio of the branching fractions $\Lambda_b^0 \rightarrow p \mu^- \bar{\nu}_\mu$ and $\Lambda_b^0 \rightarrow \Lambda_c^+ \mu^- \bar{\nu}_\mu$ [136], from which they have determined the first direct measurement of the ratio $|V_{ub}|/|V_{cb}|$. The measured ratio of branching fractions is related to $|V_{ub}|/|V_{cb}|$ through the relation

$$\frac{|V_{ub}|}{|V_{cb}|} = \sqrt{R_{FF} \frac{\mathcal{B}(\Lambda_b^0 \rightarrow p \mu^- \bar{\nu}_\mu)}{\mathcal{B}(\Lambda_b^0 \rightarrow \Lambda_c^+ \mu^- \bar{\nu}_\mu)}} \quad (76)$$

where R_{FF} is the ratio of the relevant form factors, which have to be calculated using non perturbative approaches. In lattice QCD, unquenched results for the form factors away from the static limit have been performed in 2015 [135]. We discuss B -baryon form factors in section 3.5.

In the normalization channel $\Lambda_b^0 \rightarrow \Lambda_c^+ \mu^- \bar{\nu}_\mu$, the baryon Λ_c^+ is reconstructed in the $\Lambda_c^+ \rightarrow p K^- \pi^+$ decay mode. With the choice of this normalization channel,

many experimental uncertainties cancel, in particular the large uncertainty on the Λ_b^0 production rate and on the muon and proton identification efficiency. The remaining source of systematic uncertainty that has to be properly accounted for is mainly due to the reconstruction efficiency of the further K and π particles required to build the Λ_c^+ candidates.

The signal selection exploits the long lifetime of the Λ_b^0 baryon. The $p\mu^-$ and $\Lambda_c^+\mu^-$ vertexes are required to be displaced from the primary vertex and they are further required to be *isolated*, which means that there are no additional tracks that make a good vertex with the signal and normalization candidates. The isolation reduces most of the combinatorial background and feed-down from B -hadron decays with additional charged tracks. The remaining background comes from feed-down events with neutral or unreconstructed charged particles. For example, for the signal $\Lambda_b^0 \rightarrow p\mu^-\bar{\nu}_\mu$, it comes mainly from $\Lambda_b^0 \rightarrow \Lambda_c^+\mu^-\bar{\nu}_\mu$, where $\Lambda_c \rightarrow pX$ and $\Lambda_b^0 \rightarrow N^{*+}\mu^-\bar{\nu}_\mu$, with an excited baryon N^* decaying in proton and missing particles.

The available lattice QCD calculation [135] is more accurate in the high q^2 region, in particular the predicted ratio $1/R_{FF} = 1.471 \pm 0.095 \pm 0.109$, where the first uncertainty is statistical and the second systematic, is given in the regions $q^2 > 15 \text{ GeV}^2$ for $\Lambda_b^0 \rightarrow p\mu^-\bar{\nu}_\mu$ and $q^2 > 7 \text{ GeV}^2$ for $\Lambda_b^0 \rightarrow \Lambda_c^+\mu^-\bar{\nu}_\mu$. The measurement is performed in both regions, where also the signal extraction is cleaner. The q^2 reconstruction is described in section 4.3.1. The problem of having two equally probable solutions (see section 4.3.1) for each reconstructed Λ_b^0 momentum affects the resolution of q^2 . As a consequence, the measured partial fractions computed in the high q^2 range have to be corrected for the effect of the limited q^2 resolution. To avoid biases in the measurement, the ratio of branching fractions is extracted only for events where both the solutions are within the q^2 ranges considered. Even if this choice results in a loss of efficiency, it is beneficial for the control of the systematic uncertainties.

The measurement of the branching fraction of the normalization channel relies on the known absolute branching fraction $\mathcal{B}(\Lambda_c^+ \rightarrow pK^-\pi^+) = (6.28 \pm 0.32)\%$ [93], whose value is based on the average of the two most precise available measurements, performed by Belle [180] and BESIII [181]. It is worth to remark that these two measurements are only marginally consistent, and more effort should be pursued, using also BaBar and LHCb data.

Updating the measured ratio in [136] with the most recent value of $\mathcal{B}(\Lambda_c^+ \rightarrow pK^-\pi^+)$ [93], that we just mentioned, one obtains

$$\frac{|V_{ub}|}{|V_{cb}|} = 0.079 \pm 0.004 \pm 0.004 \quad (77)$$

where the first uncertainty is experimental and the second one is from the lattice QCD calculation. Even if this is not a direct measurement of $|V_{cb}|$, by taking $|V_{ub}|$ from external inputs it is possible to determine $|V_{cb}|$. For instance, using the exclusive determination of the $B \rightarrow \pi\ell\nu_\ell$ decay rate from HFLAV [126], one obtains $|V_{cb}| = (46.4 \pm 3.8) \times 10^{-3}$, which is compatible with the inclusive measurement, as reported in section 5.2. This measurement of $|V_{ub}|/|V_{cb}|$ relies only on a single lattice QCD calculation, but the

predicted q^2 shape for the normalization channel has been validated by a LHCb measurement of the q^2 spectrum of $\Lambda_b^0 \rightarrow \Lambda_c^+ \mu^- \bar{\nu}_\mu$ decays [182].

The $\Lambda_b^0 \rightarrow \Lambda_c^+ \mu^- \bar{\nu}_\mu$ decays, with a proper normalization channel, would allow a theoretically clean extraction of $|V_{cb}|$. Using semileptonic B meson decays as normalization, like $B^0 \rightarrow D^+ \mu^- \bar{\nu}$ decays, will have as limiting factor the uncertainty on the external parameters, analogously to the B_s^0 case described in section 6.3. In particular, it will be limited by the uncertainties on the production fraction ratio f_{Λ_b}/f_d and on the $B^0 \rightarrow D^+ \mu^- \bar{\nu}$ branching fraction.

The LHCb analysis, besides being the first one made at hadronic colliders, and the first one to use B -baryon decays, opened the possibility to extract $|V_{ub}|/|V_{cb}|$ from the ratio $\mathcal{B}(B_s^0 \rightarrow K^- \mu^+ \nu_\mu)/\mathcal{B}(B_s^0 \rightarrow D_s^- \mu^+ \nu_\mu)$, a measurement which is ongoing at LHCb.

6.5. The $|V_{cb}|$ puzzle

As we have seen, the inclusive and exclusive semileptonic searches rely on different theoretical tools and experimental techniques. The agreement among $|V_{cb}|$ values from inclusive and exclusive decays can be regarded as an interesting test of our capability to investigate weak interactions and QCD dynamics. From this prospective, a lot of attention has been devoted to a discrepancy which, since more than three decades, is observed between the values extracted from exclusive and inclusive decays. It is referred as the $|V_{cb}|$ puzzle.

In figure 18 we summarize exclusive and inclusive determinations of $|V_{cb}|$ and compare with the analogous determinations of $|V_{ub}|$. The CKM parameter $|V_{ub}|$ shares with $|V_{cb}|$ the discrepancy between inclusive and exclusive values, which is labelled, similarly, the $|V_{ub}|$ puzzle (for concise reviews see e.g. [183–186]).

The most precise estimates of $|V_{cb}|$ stem from the $B \rightarrow D^* \ell \nu_\ell$ channel with inputs from lattice, followed by determinations based on inclusive measurements. Their uncertainties all stay around 1.8%. In figure 18 the vertical bands represent the different determinations of $|V_{cb}|$. We have separated the bands relative to exclusive $|V_{cb}|$ determination with $B \rightarrow D^* \ell \nu_\ell$ and $B \rightarrow D \ell \nu_\ell$ decays. Both show a discrepancy with the the band relative to the inclusive determination. The bands relative to the exclusive $B \rightarrow D$ and $B \rightarrow D^*$ decays are the HFLAV averages done with the CLN parameterizations. Also considering the slightly larger uncertainty associated with the BGL fit to $B \rightarrow D^* \ell \nu_\ell$ decays described before, the discrepancy with the inclusive determinations remains significant. The tension amounts to about 3σ . The result using $B_s \rightarrow D_s^{(*)} \mu \nu_\mu$, still affected by large uncertainties, is compatible with both inclusive and exclusive determinations of $|V_{cb}|$.

It is also possible to determine $|V_{cb}|$ indirectly, using the CKM unitarity relations together with CP violation and flavour data, excluding direct information on decays. The indirect fits provided by the CKMfitter collaboration [5] and by the UTfit collaboration [6] are in agreement between them and seem to prefer the inclusive value for $|V_{cb}|$, as shown in figure 18.

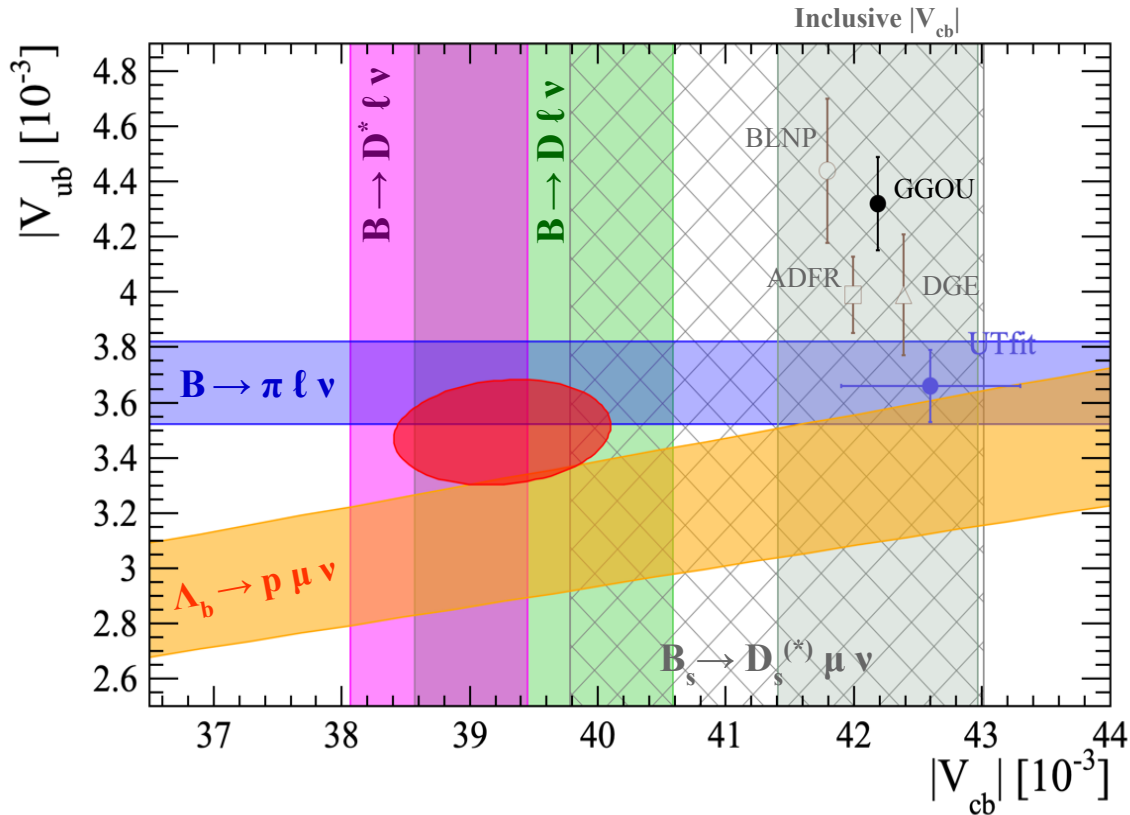


Figure 18. The combined $V_{ub} - V_{cb}$ average (red ellipses) obtained by HFLAV including the exclusive measurements of $|V_{ub}|$ from $B \rightarrow \pi \ell \nu$ (blue), $|V_{cb}|$ from $B \rightarrow D^* \ell \nu$ (magenta) and $B \rightarrow D \ell \nu$ (green) decays, and $|V_{ub}|/|V_{cb}|$ (orange) from $\Lambda_b \rightarrow p \mu \nu$ decay. The band filled with grid pattern corresponds to the LHCb result with $B_s \rightarrow D_s^{(*)} \mu \nu$ decays. The grey band refers to inclusive $|V_{cb}|$ in the kinetic scheme. The result on inclusive $|V_{ub}|$ with different calculations are the four points with vertical error bars. The shift along the x-axis of these four points is just arbitrary and has no meaning. The blue point is the result of the indirect predictions of $|V_{ub}|$ and $|V_{cb}|$ obtained by the UTfit collaboration [6] and based on the global fit to the unitarity triangle.

In figure 18 we also report the world average values of the CKM parameter $|V_{ub}|$ obtained by the HFLAV collaboration. The most precise values for $|V_{ub}|$ are also obtained from semileptonic decays. The CKM-suppressed decay $B \rightarrow \pi \ell \nu$ is the typical exclusive channel used to extract $|V_{ub}|$, being better controlled both experimentally and theoretically. We represent also the band constrained by the $|V_{ub}|/|V_{cb}|$ ratio measurement reported in equation (77). The LHCb measurement is consistent with the prediction from the indirect determination.

Most of the theoretical and experimental considerations presented in this review also apply to the $|V_{ub}|$ determination. The main differences between $|V_{cb}|$ and $|V_{ub}|$ determinations emerge in inclusive decays. Due to the large background to $B \rightarrow X_u \ell \nu$ decays represented by $B \rightarrow X_c \ell \nu$ decays, the phase space region is strongly limited by the experimental cuts needed to reduce the background. This requires to address

theoretical issues absent in the inclusive $|V_{cb}|$ determination, since the experimental cuts enhance the relevance of a region in the phase space, the so-called threshold region, where the applicability of HQE is compromised. In place of a widely accepted theoretical tool as the HQE, several models or schemes have been devised. They are all tailored to analyze data in the threshold region, but differ in their treatment of perturbative corrections and the parameterization of non-perturbative effects. In figure 18 we show the results for the four theoretical approaches included in the HFLAV averages [126]: ADFR (Aglietti, Di Lodovico, Ferrera, Ricciardi) [187–189], BLNP (Bosch, Lange, Neubert, Paz) [190–192], DGE (Dressed Gluon Exponentiation) [193] and GGOU (Gambino, Giordano, Ossola, Uraltsev) [194]. The results are based on the same experimental inputs (apart the one from ADFR which does not include the latest result from BaBar [195]), and are slightly above the exclusive $|V_{ub}|$ value, extracted from both $B \rightarrow \pi \ell \nu_\ell$ and $\Lambda_b \rightarrow p \mu \nu_\mu$ decays.

7. Future prospects

The pattern of quark and lepton masses and mixings remains one of the most debated and interesting open questions in particle physics, in spite of a plethora of new experimental results. The precise determination of the CKM matrix elements connects flavour physics with the Higgs sector, since they represent the couplings of the Higgs boson to fermions. Generations of dedicated experiments have provided us with more and more precise measurements and exposed a flavor pattern of an highly non-generic structure, begging for an underlying organizing principle, which is still unveiled. Experimental hints for deviations from SM predictions in flavour processes are one of our best hopes to direct research towards the right energy scale of new physics. As suggested by the 2020 EPPSU update [196], flavor physics should remain at the forefront of the European particle physics strategy. In this wide perspective, the search for very high precision in $|V_{cb}|$ determination is actively pursued on both experimental and theoretical sides.

In exclusive semileptonic B meson decays, the $|V_{cb}|$ determination from $B \rightarrow D^* \ell \nu_\ell$ decays has the largest theoretical uncertainty, amounting to about 1.4%, as can be seen by comparing the averages (72) and (73). By the same comparison, one observes that instead the experimental error is maximum, about 2%, for $|V_{cb}|$ values extracted from $B \rightarrow D \ell \nu_\ell$ decays. A theoretical research area with direct impact on future experimental programs is lattice gauge theory, the only systematically improvable method for nonperturbative calculations in QCD. Like in the case of the exclusive $|V_{cb}|$ determination from $B \rightarrow D \ell \nu_\ell$ decays, determinations from $B \rightarrow D^* \ell \nu_\ell$ decays are expected to improve significantly as soon as lattice calculations of the form factors at non-zero recoil will become fully available. The pivotal importance of precise information on the form factors is a clear outcome of the analyses on form factors parameterization in exclusive determinations, discussed in section 6.1.3. For example, it has been noted [89] that a possible steeper slope of the form factor $\mathcal{F}(w)$ at zero recoil could lift the value

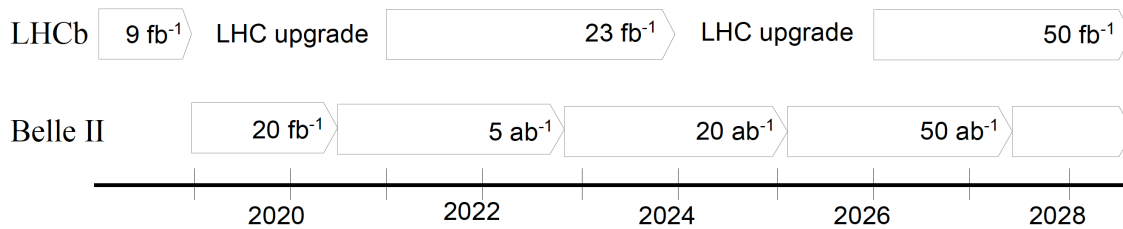


Figure 19. An overview of the expected Belle II and LHCb timelines along with their estimated integrated luminosities at various milestones.

of the exclusive $|V_{cb}|$ determination towards agreement with inclusive determinations.

While lattice unquenched results for the form factors of $B \rightarrow D^{(*)}$ semileptonic decays have been available since at least 10 years, lattice analyses for inclusive decays are now moving their first significant steps. On lattice it is not straightforward to extract inclusive observables, i.e. quantities that are summed over all multi-particle final states. Major challenges are that the lattice calculations are performed in a finite volume and naturally formulated in the Euclidean space, which complicates the analyses of correlation functions for the case of multi-particle states in the kinematic region accessible on the lattice. A large body of work has already gone into developing algorithms and theory to overcome these and similar limitations, with significant implications also on other branches of physics and mathematics (for details see e.g. [197]). A different suggestion, specific to inclusive semileptonic B decays, is to analytically continue the amplitude from the experimentally accessible physical kinematic region to a nonphysical region in which the lattice calculation can be performed [198].

The Belle II experiment at KEK started recently to take data from the renewed e^+e^- KEK-B accelerator (SuperKEKB), designed to reach an instantaneous luminosity 50 times higher than KEK-B. The final goal of Belle II is to collect 50 ab^{-1} by 2027. In figure 19 the expected timelines for both Belle II and LHCb are reported. The precise study of semileptonic B meson decays is a substantial part of the Belle II program [199]. However, the increase in luminosity is not enough by itself, because most of the measurements that we have presented above are limited by the systematics and not by the statistical uncertainties. For the exclusive $|V_{cb}|$, the most precise measurement comes from the Belle untagged analysis of $B \rightarrow D^* \ell \nu_\ell$ decays [168] (described in section 6.1.1), where the systematic uncertainty is 2.5 times the statistical one. The largest contributions to the systematics are due to the tracking and the particle identification, followed by the ones due to the external inputs, like the branching fractions of D mesons and f_{00} .

It is foreseen that the hadronic B tagged analysis will be the preferred approach to study semileptonic decays at Belle II. The tagged analyses of $B \rightarrow D^* \ell \nu_\ell$ are reaching the precision of the untagged measurements, but are at present affected by large uncertainties due to the calibration of the hadronic B tagging. The reduction of this

sources of systematics is paramount to exploit the huge statistics available at Belle II. With large statistics available the analyses approaches have to be revisited. For instance, the BaBar tagged measurement [132] described in section 6.1.2, which performed a truly four-dimensional fit, has reached precision comparable with the untagged Belle analysis [168], despite the fact that the signal yield was only 1/30 of the Belle signal yield.

The Belle II data taking is ongoing, and the first studies confirm the expected detector performances. Very recently, Belle II collaboration has released an untagged measurement of the branching fractions of the $B^0 \rightarrow D^{*-}\ell^+\nu_\ell$ decays using 8.7 fb^{-1} of data [200]. The result is consistent with the existing measurements. While the uncertainties are not competitive with the ones of the most recent results at B -Factories, this measurement validates the full chain of detector operation, calibration and analysis.

As mentioned in section 3.2.2, other interesting exclusive channels are the semileptonic $B_s \rightarrow D_s^{(*)}\ell\nu_\ell$ decays. The study of B_s decays at Belle II would require to run SuperKEKB at the energy corresponding to the $\Upsilon(5S)$ mass. At present there are no expected plans for Belle II to collect data at energy higher than the $\Upsilon(4S)$ mass. But the B_s^0 are copiously produced at LHC and recently LHCb has exploited these new calculations in the pioneering measurement of $|V_{cb}|$ using the semileptonic B_s decays [72] (see section 6.3). This measurement is at present limited by the precision of external parameters, but the developed technique can be applied to B meson decays, where their impact is reduced.

The LHCb experiment is undergoing a major upgrade of the detector, which was planned and designed in the 2011 [201] and should end in 2021, when LHC will restart the activity (see the timeline in figure 19). The upgrade will allow to collect data at higher instantaneous luminosity, so about five pp collisions per bunch crossing are foreseen. To cope with the higher occupancy in the detector, besides the improvements in the various subdetectors, a fully software L0 trigger will be employed (a configuration called *triggerless*). The software L0 trigger will add flexibility to the data taking, allowing to reduce the thresholds for muon and hadron trigger decisions and enlarge the physics capabilities. The analyses of semileptonic decays with tauons and electrons will benefit of the lower trigger thresholds in terms of signal efficiencies. With this upgraded detector, LHCb is planning to integrate a luminosity of 23 fb^{-1} by the 2024, and collect a total sample of 50 fb^{-1} by the 2028-2029, after LHC will have switched to higher luminosity.

A promising field of study are Λ_b baryons, which represent approximately 20% of all bottom hadrons produced at the LHC. The measurement of the ratio of $\Lambda_b^0 \rightarrow p\mu^-\bar{\nu}_\mu$ and $\Lambda_b^0 \rightarrow \Lambda_c^+\mu^-\bar{\nu}_\mu$ decay rates at LHCb, combined with a lattice QCD calculation of the $\Lambda_b \rightarrow p$ and $\Lambda_b \rightarrow \Lambda_c$ form factors [135], has allowed the first determination of $|V_{ub}|/|V_{cb}|$ at an hadron collider [136], as described in section 6.4. We have shown the band of results in figure 18. Right now, theory uncertainties are approximately 5%, comparable with the experimental uncertainty. As the latter is expected to reach about 3% at the integrated luminosity of 23 fb^{-1} foreseen by 2024 (see figure 19), further

theoretical progress is needed, which could come from lattice improvements to the form factors computation. With the huge data available in the next years, there are prospects to extend the measurement of $\Lambda_b \rightarrow p\mu\nu$ to a differential measurement in bins of q^2 . The baryon semileptonic decays are sensitive to both the vector and axial-vector currents in the weak effective Hamiltonian, and their high precision measurements can also represent a check of right-handed couplings beyond the SM.

Progress is also expected for B decays to excited D meson states. Form factors must be determined in all modes through precise differential measurements. The required accuracy could come from Belle II which has the potential to precisely isolate all four orbitally excited modes and characterize their sub-decay modes, constraining and measuring the branching ratios with higher accuracy [199]. LHCb has the capability to study with high precision the kinematics of the decays into narrow states. Furthermore LHCb can study in detail the production of excited states in semileptonic B_s^0 and Λ_b^0 decays.

Lattice studies are in progress with realistic charm mass, and results on $B \rightarrow D^{**}\ell\nu$ form factors are available, still at a preliminary stage, since 2013 [202]. For recent and more complete reviews on open charmed systems see e.g. [203, 204].

The semileptonic B decays we have considered are tree-level processes in the SM, which are generally assumed, in all analyses, unaffected by NP contributions. Because of their pivotal role in precise measurements of the CKM matrix elements, it is not without importance to ascertain the validity of this assumption, given also the tensions underlined above. There are many analyses addressing this issue (see e.g. [205–208]) and several models which do not seem to support evidence of NP in decays driven by $b \rightarrow c\ell\nu_\ell$ transitions, where ℓ is a light lepton. Particular attention deserves $R(D^{(*)})$, discussed in section 3.4, whose measured value differs from the SM prediction. A better understanding of this discrepancy could shed light on possible NP and as such it is a priority for Belle II and for the future planned LHCb upgrade.

Acknowledgments

It is a pleasure to thank Aoifa Barucha and Francesco Polci for their invitation to give GDR-InF lectures at the Institut Henri Poincaré (Paris, France), where part of this work was performed, and for providing a stimulating environment. G.R. acknowledges partial financial support from MIUR under Project No. 2015P5SBHT and from the INFN research initiative ENP.

8. Bibliography

- [1] Buras A J, De Fazio F and Girrbach J 2014 *Eur. Phys. J.* **C74** 2950 (*Preprint* 1404.3824)
- [2] Wolfenstein L 1983 *Phys. Rev. Lett.* **51** 1945
- [3] Buras A J, Lautenbacher M E and Ostermaier G 1994 *Phys. Rev.* **D50** 3433–3446 (*Preprint* hep-ph/9403384)
- [4] Jarlskog C 1985 *Phys. Rev. Lett.* **55** 1039

- [5] Charles J, Hocker A, Lackner H and Laplace S, Le Diberder F R, Malcles J, Ocariz J, Pivk M and L R (CKMfitter Group) updated results URL http://ckmfitter.in2p3.fr/www/html/ckm_main.html
- [6] Alpigiani C, Bevan A, Bona M, Ciuchini M, Derkach D, Franco E, Lubicz V, Martinelli G, Parodi F, Pierini M, Schiavi C, Silvestrini L, Sordini V, Stocchi A, Tarantino C and Vagnoni V (Utfit Group) updated results URL <http://www.utfit.org/Utfit/WebHome>
- [7] Shifman M A 2001 Quark hadron duality *At the frontier of particle physics. Handbook of QCD. Vol. 1-3* World Scientific (Singapore: World Scientific) pp 1447–1494 [3,1447(2000)] (*Preprint hep-ph/0009131*) URL <http://jhep.sissa.it/archive/prhep/preproceeding/hf8/013>
- [8] Bigi I I Y and Uraltsev N 2001 *Int. J. Mod. Phys. A* **16** 5201–5248 (*Preprint hep-ph/0106346*)
- [9] Manohar A V and Wise M B 2000 *Camb. Monogr. Part. Phys. Nucl. Phys. Cosmol.* **10** 1–191
- [10] Melnikov K 2008 *Phys. Lett.* **B666** 336–339 (*Preprint* 0803.0951)
- [11] Gambino P 2011 *JHEP* **09** 055 (*Preprint* 1107.3100)
- [12] Trott M 2004 *Phys. Rev.* **D70** 073003 (*Preprint hep-ph/0402120*)
- [13] Aquila V, Gambino P, Ridolfi G and Uraltsev N 2005 *Nucl. Phys.* **B719** 77–102 (*Preprint hep-ph/0503083*)
- [14] Pak A and Czarnecki A 2008 *Phys. Rev. Lett.* **100** 241807 (*Preprint* 0803.0960)
- [15] Pak A and Czarnecki A 2008 *Phys. Rev.* **D78** 114015 (*Preprint* 0808.3509)
- [16] Biswas S and Melnikov K 2010 *JHEP* **02** 089 (*Preprint* 0911.4142)
- [17] Benson D, Bigi I I, Mannel T and Uraltsev N 2003 *Nucl. Phys.* **B665** 367–401 (*Preprint hep-ph/0302262*)
- [18] Becher T, Boos H and Lunghi E 2007 *JHEP* **12** 062 (*Preprint* 0708.0855)
- [19] Alberti A, Ewerth T, Gambino P and Nandi S 2013 *Nucl. Phys.* **B870** 16–29 (*Preprint* 1212.5082)
- [20] Alberti A, Gambino P and Nandi S 2014 *JHEP* **01** 147 (*Preprint* 1311.7381)
- [21] Mannel T, Pivovarov A A and Rosenthal D 2015 *Phys. Lett.* **B741** 290–294 (*Preprint* 1405.5072)
- [22] Mannel T, Pivovarov A A and Rosenthal D 2015 *Phys. Rev.* **D92** 054025 (*Preprint* 1506.08167)
- [23] Gremm M and Kapustin A 1997 *Phys. Rev.* **D55** 6924–6932 (*Preprint hep-ph/9603448*)
- [24] Mannel T and Pivovarov A A 2019 (*Preprint* 1907.09187)
- [25] Bigi I I, Uraltsev N and Zwicky R 2007 *Eur. Phys. J.* **C50** 539–556 (*Preprint hep-ph/0511158*)
- [26] Breidenbach C, Feldmann T, Mannel T and Turczyk S 2008 *Phys. Rev.* **D78** 014022 (*Preprint* 0805.0971)
- [27] Bigi I, Mannel T, Turczyk S and Uraltsev N 2010 *JHEP* **04** 073 (*Preprint* 0911.3322)
- [28] Dassinger B M, Mannel T and Turczyk S 2007 *JHEP* **03** 087 (*Preprint hep-ph/0611168*)
- [29] Mannel T, Turczyk S and Uraltsev N 2010 *JHEP* **11** 109 (*Preprint* 1009.4622)
- [30] Heinonen J and Mannel T 2014 *Nucl. Phys.* **B889** 46–63 (*Preprint* 1407.4384)
- [31] Beneke M 1999 *Phys. Rept.* **317** 1–142 (*Preprint hep-ph/9807443*)
- [32] Bigi I I Y, Shifman M A, Uraltsev N G and Vainshtein A I 1995 *Phys. Rev.* **D52** 196–235 (*Preprint hep-ph/9405410*)
- [33] Bigi I I Y, Shifman M A, Uraltsev N and Vainshtein A I 1997 *Phys. Rev.* **D56** 4017–4030 [205(1996)] (*Preprint hep-ph/9704245*)
- [34] Bigi I I Y, Shifman M A and Uraltsev N 1997 *Ann. Rev. Nucl. Part. Sci.* **47** 591–661 (*Preprint hep-ph/9703290*)
- [35] Beneke M 1998 *Phys. Lett.* **B434** 115–125 (*Preprint hep-ph/9804241*)
- [36] Hoang A H, Ligeti Z and Manohar A V 1999 *Phys. Rev. Lett.* **82** 277–280 (*Preprint hep-ph/9809423*)
- [37] Hoang A H, Ligeti Z and Manohar A V 1999 *Phys. Rev.* **D59** 074017 (*Preprint hep-ph/9811239*)
- [38] Hoang A H and Teubner T 1999 *Phys. Rev.* **D60** 114027 (*Preprint hep-ph/9904468*)
- [39] Uraltsev N 2004 Heavy quark expansion in beauty: Recent successes and problems *Continuous advances in QCD. Proceedings, Conference, Minneapolis, USA, May 13-16, 2004* pp 100–114 (*Preprint hep-ph/0409125*)

- [40] Sirlin A 1982 *Nucl. Phys.* **B196** 83–92
- [41] Bailey J A *et al.* (Fermilab Lattice, MILC) 2014 *Phys. Rev.* **D89** 114504 (*Preprint* 1403.0635)
- [42] Ball P and Zwicky R 2001 *JHEP* **10** 019 (*Preprint* hep-ph/0110115)
- [43] Ball P and Zwicky R 2005 *Phys. Rev.* **D71** 014015 (*Preprint* hep-ph/0406232)
- [44] Becirevic D and Kaidalov A B 2000 *Phys. Lett.* **B478** 417–423 (*Preprint* hep-ph/9904490)
- [45] Meiman N 1963 *Sov. Phys. JETP* 830
- [46] Okubo S and Shih I F 1971 *Phys. Rev. D* **4** 2020–2029
- [47] Singh V and Raina A 1979 *Fortsch. Phys.* **27** 561
- [48] Bourrely C, Machet B and de Rafael E 1981 *Nucl. Phys.* **B189** 157–181
- [49] Caprini I, Lellouch L and Neubert M 1998 *Nucl. Phys.* **B530** 153–181 (*Preprint* hep-ph/9712417)
- [50] Boyd C G, Grinstein B and Lebed R F 1995 *Phys. Rev. Lett.* **74** 4603–4606 (*Preprint* hep-ph/9412324)
- [51] Bourrely C, Caprini I and Lellouch L 2009 *Phys. Rev.* **D79** 013008 [Erratum: *Phys. Rev.* D82,099902(2010)] (*Preprint* 0807.2722)
- [52] Isgur N and Wise M B 1989 *Phys. Lett.* **B232** 113–117
- [53] Isgur N and Wise M B 1990 *Phys. Lett.* **B237** 527–530
- [54] Caswell W E and Lepage G P 1986 *Phys. Lett.* **167B** 437–442
- [55] Harrison J, Davies C and Wingate M (HPQCD) 2018 *Phys. Rev.* **D97** 054502 (*Preprint* 1711.11013)
- [56] McLean E, Davies C T H, Lytle A T and Koponen J 2019 *Phys. Rev.* **D99** 114512 (*Preprint* 1904.02046)
- [57] Bailey J A, Bhattacharya T, Gupta R, Jang Y C, Lee W, Leem J, Park S and Yoon B (LANL-SWME) 2018 *EPJ Web Conf.* **175** 13012 (*Preprint* 1711.01786)
- [58] Bhattacharya T *et al.* (LANL/SWME) 2018 *PoS LATTICE2018* 283 (*Preprint* 1812.07675)
- [59] Bhattacharya T, Choi B J, Gupta R, Jang Y C, Jwa S, Lee S, Lee W, Leem J and Park S (LANL/SWME) 2019 *PoS LATTICE2019* 056 (*Preprint* 2003.09206)
- [60] Bailey J A, Jang Y C, Lee S, Lee W and Lee W (LANL-SWME) 2020 (*Preprint* 2001.05590)
- [61] de Divitiis G M, Petronzio R and Tantalo N 2009 *Nucl. Phys.* **B807** 373–395 (*Preprint* 0807.2944)
- [62] Vaquero Avilés-Casco A, DeTar C, Du D, El-Khadra A, Kronfeld A S, Laiho J and Van de Water R S 2018 *EPJ Web Conf.* **175** 13003 (*Preprint* 1710.09817)
- [63] Avilés-Casco A V, DeTar C, El-Khadra A X, Kronfeld A S, Laiho J and Van de Water R S (Fermilab Lattice, MILC) 2019 *PoS LATTICE2018* 282 (*Preprint* 1901.00216)
- [64] Avilés-Casco A V, DeTar C, El-Khadra A X, Kronfeld A S, Laiho J and Van de Water R S (Fermilab Lattice, MILC) 2019 The $B \rightarrow D^* \ell \nu$ Semileptonic Decay at Nonzero Recoil and Its Implications for $|V_{cb}|$ and $R(D^*)$ *37th International Symposium on Lattice Field Theory* (*Preprint* 1912.05886)
- [65] Kaneko T, Aoki Y, Colquhoun B, Fukaya H and Hashimoto S (JLQCD) 2018 *PoS LATTICE2018* 311 (*Preprint* 1811.00794)
- [66] Kaneko T, Aoki Y, Bailas G, Colquhoun B, Fukaya H, Hashimoto S and Koponen J (JLQCD) 2019 $B \rightarrow D^{(*)} \ell \nu$ form factors from lattice QCD with relativistic heavy quarks *37th International Symposium on Lattice Field Theory* (*Preprint* 1912.11770)
- [67] de Divitiis G M, Molinaro E, Petronzio R and Tantalo N 2007 *Phys. Lett.* **B655** 45–49 (*Preprint* 0707.0582)
- [68] Bailey J A *et al.* (MILC) 2015 *Phys. Rev.* **D92** 034506 (*Preprint* 1503.07237)
- [69] Na H, Bouchard C M, Lepage G P, Monahan C and Shigemitsu J (HPQCD) 2015 *Phys. Rev.* **D92** 054510 [Erratum: *Phys. Rev.* D93,no.11,119906(2016)] (*Preprint* 1505.03925)
- [70] Monahan C J, Na H, Bouchard C M, Lepage G P and Shigemitsu J 2017 *Phys. Rev.* **D95** 114506 (*Preprint* 1703.09728)
- [71] Atoui M, Morénas V, Bećirevic D and Sanfilippo F 2014 *Eur. Phys. J.* **C74** 2861 (*Preprint* 1310.5238)

- [72] Aaij R *et al.* (LHCb) 2020 *Phys. Rev. D* **101** 072004 (*Preprint* 2001.03225)
- [73] Bailey J A *et al.* 2012 *Phys. Rev.* **D85** 114502 [Erratum: *Phys. Rev.*D86,039904(2012)] (*Preprint* 1202.6346)
- [74] Bazavov A *et al.* (Fermilab Lattice, MILC) 2019 *Phys. Rev. D* **100** 034501 (*Preprint* 1901.02561)
- [75] Flynn J, Izubuchi T, Jüttner A, Kawanai T, Lehner C, Lizarazo E, Soni A, Tsang J T and Witzel O 2016 *PoS LATTICE2016* 296 (*Preprint* 1612.05112)
- [76] Flynn J M, Hill R C, Jüttner A, Soni A, Tsang J T and Witzel O 2019 *PoS LATTICE2018* 290 (*Preprint* 1903.02100)
- [77] Flynn J, Hill R, Jüttner A, Soni A, Tsang J T and Witzel O 2019 Semileptonic $B \rightarrow \pi l \nu$, $B \rightarrow D l \nu$, $B_s \rightarrow K l \nu$, and $B_s \rightarrow D_s l \nu$ decays *37th International Symposium on Lattice Field Theory* (*Preprint* 1912.09946)
- [78] McLean E, Davies C T H, Koponen J and Lytle A T 2019 (*Preprint* 1906.00701)
- [79] Gambino P, Mannel T and Uraltsev N 2010 *Phys. Rev.* **D81** 113002 (*Preprint* 1004.2859)
- [80] Gambino P, Mannel T and Uraltsev N 2012 *JHEP* **10** 169 (*Preprint* 1206.2296)
- [81] Gubernari N, Kokulu A and van Dyk D 2019 *JHEP* **01** 150 (*Preprint* 1811.00983)
- [82] Bordone M, Jung M and van Dyk D 2020 *Eur. Phys. J. C* **80** 74 (*Preprint* 1908.09398)
- [83] Abbas G, Ananthanarayan B, Caprini I, Sentitemsu Imsong I and Ramanan S 2010 *Eur. Phys. J.* **A45** 389–399 (*Preprint* 1004.4257)
- [84] Boyd C G, Grinstein B and Lebed R F 1997 *Phys. Rev.* **D56** 6895–6911 (*Preprint* hep-ph/9705252)
- [85] Boyd C G and Savage M J 1997 *Phys. Rev.* **D56** 303–311 (*Preprint* hep-ph/9702300)
- [86] Grinstein B and Lebed R F 2015 *Phys. Rev.* **D92** 116001 (*Preprint* 1509.04847)
- [87] Boyd C G, Grinstein B and Lebed R F 1996 *Nucl. Phys.* **B461** 493–511 (*Preprint* hep-ph/9508211)
- [88] Bigi D, Gambino P and Schacht S 2017 *JHEP* **11** 061 (*Preprint* 1707.09509)
- [89] Gambino P, Jung M and Schacht S 2019 *Phys. Lett.* **B795** 386–390 (*Preprint* 1905.08209)
- [90] Bigi D and Gambino P 2016 *Phys. Rev.* **D94** 094008 (*Preprint* 1606.08030)
- [91] Bigi D, Gambino P and Schacht S 2017 *Phys. Lett.* **B769** 441–445 (*Preprint* 1703.06124)
- [92] Grinstein B and Kobach A 2017 *Phys. Lett.* **B771** 359–364 (*Preprint* 1703.08170)
- [93] Tanabashi M *et al.* (Particle Data Group) 2018 *Phys. Rev.* **D98** 030001
- [94] Abe K *et al.* (Belle) 2004 *Phys. Rev.* **D69** 112002 (*Preprint* hep-ex/0307021)
- [95] Aubert B *et al.* (BaBar) 2009 *Phys. Rev.* **D79** 112004 (*Preprint* 0901.1291)
- [96] Aaij R *et al.* (LHCb) 2015 *Phys. Rev.* **D91** 092002 [Erratum: *Phys. Rev.*D93,no.11,119901(2016)] (*Preprint* 1503.02995)
- [97] Aaij R *et al.* (LHCb) 2015 *Phys. Rev.* **D92** 032002 (*Preprint* 1505.01710)
- [98] Aaij R *et al.* (LHCb) 2016 *Phys. Rev.* **D94** 072001 (*Preprint* 1608.01289)
- [99] Aubert B *et al.* (BaBar) 2008 *Phys. Rev. Lett.* **101** 261802 (*Preprint* 0808.0528)
- [100] Liventsev D *et al.* (Belle) 2008 *Phys. Rev.* **D77** 091503 (*Preprint* 0711.3252)
- [101] del Amo Sanchez P *et al.* (BaBar) 2010 *Phys. Rev.* **D82** 111101 (*Preprint* 1009.2076)
- [102] Aaij R *et al.* (LHCb) 2013 *JHEP* **09** 145 (*Preprint* 1307.4556)
- [103] Aubert B *et al.* (BaBar) 2008 *Phys. Rev. Lett.* **100** 151802 (*Preprint* 0712.3503)
- [104] Le Yaouanc A, Oliver L, Pene O and Raynal J C 1996 *Phys. Lett.* **B387** 582–592 (*Preprint* hep-ph/9607300)
- [105] Uraltsev N 2001 *Phys. Lett.* **B501** 86–91 [,195(2000)] (*Preprint* hep-ph/0011124)
- [106] Morenas V, Le Yaouanc A, Oliver L, Pene O and Raynal J C 1996 *Phys. Lett.* **B386** 315–327 (*Preprint* hep-ph/9605206)
- [107] Morenas V, Le Yaouanc A, Oliver L, Pene O and Raynal J C 1997 *Phys. Rev.* **D56** 5668–5680 (*Preprint* hep-ph/9706265)
- [108] Ebert D, Faustov R N and Galkin V O 1998 *Phys. Lett.* **B434** 365–372 (*Preprint* hep-ph/9805423)
- [109] Ebert D, Faustov R N and Galkin V O 2000 *Phys. Rev.* **D61** 014016 (*Preprint* hep-ph/9906415)

- [110] Segovia J, Albertus C, Entem D R, Fernandez F, Hernandez E and Perez-Garcia M A 2011 *Phys. Rev.* **D84** 094029 (*Preprint* 1107.4248)
- [111] Leibovich A K, Ligeti Z, Stewart I W and Wise M B 1998 *Phys. Rev.* **D57** 308–330 (*Preprint* hep-ph/9705467)
- [112] Bigi I I, Blossier B, Le Yaouanc A, Oliver L, Pene O, Raynal J C, Oyanguren A and Roudeau P 2007 *Eur. Phys. J.* **C52** 975–985 (*Preprint* 0708.1621)
- [113] Lees J P *et al.* (BaBar) 2016 *Phys. Rev. Lett.* **116** 041801 (*Preprint* 1507.08303)
- [114] Klein R, Mannel T, Shahriaran F and van Dyk D 2015 *Phys. Rev.* **D91** 094034 (*Preprint* 1503.00569)
- [115] Bernlochner F U, Ligeti Z and Turczyk S 2012 *Phys. Rev.* **D85** 094033 (*Preprint* 1202.1834)
- [116] Bečirević D, Le Yaouanc A, Oliver L and Raynal J C 2017 *Phys. Rev.* **D96** 036018 (*Preprint* 1705.05667)
- [117] Matyja A *et al.* (Belle) 2007 *Phys. Rev. Lett.* **99** 191807 (*Preprint* 0706.4429)
- [118] Lees J P *et al.* (BaBar) 2012 *Phys. Rev. Lett.* **109** 101802 (*Preprint* 1205.5442)
- [119] Lees J P *et al.* (BaBar) 2013 *Phys. Rev.* **D88** 072012 (*Preprint* 1303.0571)
- [120] Huschle M *et al.* (Belle) 2015 *Phys. Rev.* **D92** 072014 (*Preprint* 1507.03233)
- [121] Aaij R *et al.* (LHCb) 2015 *Phys. Rev. Lett.* **115** 111803 [Erratum: *Phys. Rev. Lett.* 115, no. 15, 159901 (2015)] (*Preprint* 1506.08614)
- [122] Sato Y *et al.* (Belle) 2016 *Phys. Rev.* **D94** 072007 (*Preprint* 1607.07923)
- [123] Caria G *et al.* (Belle) 2019 (*Preprint* 1910.05864)
- [124] Hirose S *et al.* (Belle) 2017 *Phys. Rev. Lett.* **118** 211801 (*Preprint* 1612.00529)
- [125] Aaij R *et al.* (LHCb) 2018 *Phys. Rev. Lett.* **120** 171802 (*Preprint* 1708.08856)
- [126] Amhis Y S *et al.* (HFLAV) 2019 updated results and plots available at <https://hflav.web.cern.ch/> (*Preprint* 1909.12524)
- [127] Bernlochner F U, Ligeti Z, Papucci M and Robinson D J 2017 *Phys. Rev.* **D95** 115008 [erratum: *Phys. Rev.* D97, no. 5, 059902 (2018)] (*Preprint* 1703.05330)
- [128] Jaiswal S, Nandi S and Patra S K 2017 *JHEP* **12** 060 (*Preprint* 1707.09977)
- [129] Fajfer S, Kamenik J F and Nisandzic I 2012 *Phys. Rev.* **D85** 094025 (*Preprint* 1203.2654)
- [130] Abdesselam A *et al.* (Belle) 2017 (*Preprint* 1702.01521)
- [131] Aoki S *et al.* (Flavour Lattice Averaging Group) 2019 (*Preprint* 1902.08191)
- [132] Lees J P *et al.* (BaBar) 2019 *Phys. Rev. Lett.* **123** 091801 (*Preprint* 1903.10002)
- [133] Feldmann T and Yip M W 2012 *Phys. Rev. D* **85** 014035 [Erratum: *Phys. Rev. D* 86, 079901 (2012)] (*Preprint* 1111.1844)
- [134] Falk A F and Neubert M 1993 *Phys. Rev. D* **47** 2982–2990 (*Preprint* hep-ph/9209269)
- [135] Detmold W, Lehner C and Meinel S 2015 *Phys. Rev.* **D92** 034503 (*Preprint* 1503.01421)
- [136] Aaij R *et al.* (LHCb) 2015 *Nature Phys.* **11** 743–747 (*Preprint* 1504.01568)
- [137] Bernlochner F U, Ligeti Z, Robinson D J and Sutcliffe W L 2019 *Phys. Rev. D* **99** 055008 (*Preprint* 1812.07593)
- [138] Bevan A J *et al.* (BaBar, Belle) 2014 *Eur. Phys. J.* **C74** 3026 (*Preprint* 1406.6311)
- [139] Nason P *et al.* 1999 Bottom production 1999 CERN Workshop on standard model physics (and more) at the LHC, CERN, Geneva, Switzerland, 25–26 May: *Proceedings* pp 231–304 (*Preprint* hep-ph/0003142)
- [140] Alves Jr A A *et al.* (LHCb) 2008 *JINST* **3** S08005
- [141] Aaij R *et al.* (LHCb) 2017 *Phys. Rev. Lett.* **118** 052002 [Erratum: *Phys. Rev. Lett.* 119, no. 16, 169901 (2017)] (*Preprint* 1612.05140)
- [142] Aaij R *et al.* (LHCb) 2019 *Phys. Rev.* **D100** 031102 (*Preprint* 1902.06794)
- [143] Aubert B *et al.* (BaBar) 2002 *Nucl. Instrum. Meth.* **A479** 1–116 (*Preprint* hep-ex/0105044)
- [144] Aubert B *et al.* (BaBar) 2013 *Nucl. Instrum. Meth.* **A729** 615–701 (*Preprint* 1305.3560)
- [145] Bondar A (Belle) 1998 *Nucl. Instrum. Meth.* **A408** 64–76
- [146] Allmendinger T *et al.* 2013 *Nucl. Instrum. Meth.* **A704** 44–59 (*Preprint* 1207.2849)
- [147] Aubert B *et al.* (BaBar) 2008 *Phys. Rev. Lett.* **100** 231803 (*Preprint* 0712.3493)

- [148] Feindt M, Keller F, Kreps M, Kuhr T, Neubauer S, Zander D and Zupanc A 2011 *Nucl. Instrum. Meth.* **A654** 432–440 (*Preprint* 1102.3876)
- [149] Aaij R *et al.* (LHCb) 2015 *Int. J. Mod. Phys.* **A30** 1530022 (*Preprint* 1412.6352)
- [150] Dambach S, Langenegger U and Starodumov A 2006 *Nucl. Instrum. Meth.* **A569** 824–828 (*Preprint* hep-ph/0607294)
- [151] Ciezarek G, Lupato A, Rotondo M and Vesterinen M 2017 *JHEP* **02** 021 (*Preprint* 1611.08522)
- [152] Stone S and Zhang L 2014 *Adv. High Energy Phys.* **2014** 931257 (*Preprint* 1402.4205)
- [153] Aaij R *et al.* (LHCb) 2019 *Phys. Rev.* **D99** 092009 (*Preprint* 1807.10722)
- [154] Aubert B *et al.* (BaBar) 2010 *Phys. Rev.* **D81** 032003 (*Preprint* 0908.0415)
- [155] Aubert B *et al.* (BaBar) 2004 *Phys. Rev.* **D69** 111104 (*Preprint* hep-ex/0403030)
- [156] Schwanda C *et al.* (Belle) 2007 *Phys. Rev.* **D75** 032005 (*Preprint* hep-ex/0611044)
- [157] Urquijo P *et al.* (Belle) 2007 *Phys. Rev.* **D75** 032001 (*Preprint* hep-ex/0610012)
- [158] Acosta D *et al.* (CDF) 2005 *Phys. Rev.* **D71** 051103 (*Preprint* hep-ex/0502003)
- [159] Csorna S E *et al.* (CLEO) 2004 *Phys. Rev.* **D70** 032002 (*Preprint* hep-ex/0403052)
- [160] Abdallah J *et al.* (DELPHI) 2006 *Eur. Phys. J.* **C45** 35–59 (*Preprint* hep-ex/0510024)
- [161] Hocker A and Kartvelishvili V 1996 *Nucl. Instrum. Meth.* **A372** 469–481 (*Preprint* hep-ph/9509307)
- [162] Gambino P and Schwanda C 2014 *Phys. Rev.* **D89** 014022 (*Preprint* 1307.4551)
- [163] Alberti A, Gambino P, Healey K J and Nandi S 2015 *Phys. Rev. Lett.* **114** 061802 (*Preprint* 1411.6560)
- [164] Chetyrkin K G, Kuhn J H, Maier A, Maierhofer P, Marquard P, Steinhauser M and Sturm C 2009 *Phys. Rev.* **D80** 074010 (*Preprint* 0907.2110)
- [165] Bauer C W, Ligeti Z, Luke M, Manohar A V and Trott M 2004 *Phys. Rev.* **D70** 094017 (*Preprint* hep-ph/0408002)
- [166] Gambino P, Healey K J and Turczyk S 2016 *Phys. Lett.* **B763** 60–65 (*Preprint* 1606.06174)
- [167] Fael M, Mannel T and Keri Vos K 2019 *JHEP* **02** 177 (*Preprint* 1812.07472)
- [168] Waheed E *et al.* (Belle) 2019 *Phys. Rev.* **D100** 052007 (*Preprint* 1809.03290)
- [169] Glattauer R *et al.* (Belle) 2016 *Phys. Rev.* **D93** 032006 (*Preprint* 1510.03657)
- [170] Duboscq J E *et al.* (CLEO) 1996 *Phys. Rev. Lett.* **76** 3898–3902
- [171] Aubert B *et al.* (BaBar) 2008 *Phys. Rev.* **D77** 032002 (*Preprint* 0705.4008)
- [172] Aubert B *et al.* (BaBar) 2006 *Phys. Rev.* **D74** 092004 (*Preprint* hep-ex/0602023)
- [173] Aubert B *et al.* (BaBar) 2009 *Phys. Rev.* **D79** 012002 (*Preprint* 0809.0828)
- [174] Bernlochner F U, Ligeti Z, Papucci M and Robinson D J 2017 *Phys. Rev.* **D96** 091503 (*Preprint* 1708.07134)
- [175] Bernlochner F U, Ligeti Z and Robinson D J 2019 *Phys. Rev.* **D100** 013005 (*Preprint* 1902.09553)
- [176] Bartelt J E *et al.* (CLEO) 1999 *Phys. Rev. Lett.* **82** 3746 (*Preprint* hep-ex/9811042)
- [177] Abe K *et al.* (Belle) 2002 *Phys. Lett.* **B526** 258–268 (*Preprint* hep-ex/0111082)
- [178] Aubert B *et al.* (BaBar) 2010 *Phys. Rev. Lett.* **104** 011802 (*Preprint* 0904.4063)
- [179] Barlow R J and Beeston C 1993 *Comput. Phys. Commun.* **77** 219–228
- [180] Zupanc A *et al.* (Belle) 2014 *Phys. Rev. Lett.* **113** 042002 (*Preprint* 1312.7826)
- [181] Ablikim M *et al.* (BESIII) 2016 *Phys. Rev. Lett.* **116** 052001 (*Preprint* 1511.08380)
- [182] Aaij R *et al.* (LHCb) 2017 *Phys. Rev.* **D96** 112005 (*Preprint* 1709.01920)
- [183] Ricciardi G 2017 *Mod. Phys. Lett.* **A32** 1730005 (*Preprint* 1610.04387)
- [184] Ricciardi G 2014 *Mod. Phys. Lett.* **A29** 1430019 (*Preprint* 1403.7750)
- [185] Ricciardi G 2013 *Mod. Phys. Lett.* **A28** 1330016 (*Preprint* 1305.2844)
- [186] Ricciardi G 2012 *Mod. Phys. Lett.* **A27** 1230037 (*Preprint* 1209.1407)
- [187] Aglietti U and Ricciardi G 2004 *Phys. Rev.* **D70** 114008 (*Preprint* hep-ph/0407225)
- [188] Aglietti U, Ferrera G and Ricciardi G 2007 *Nucl. Phys.* **B768** 85–115 (*Preprint* hep-ph/0608047)
- [189] Aglietti U, Di Lodovico F, Ferrera G and Ricciardi G 2009 *Eur. Phys. J.* **C59** 831–840 (*Preprint* 0711.0860)
- [190] Lange B O, Neubert M and Paz G 2005 *Phys. Rev.* **D72** 073006 (*Preprint* hep-ph/0504071)

- [191] Bosch S W, Lange B O, Neubert M and Paz G 2004 *Nucl. Phys.* **B699** 335–386 (*Preprint hep-ph/0402094*)
- [192] Bosch S W, Neubert M and Paz G 2004 *JHEP* **11** 073 (*Preprint hep-ph/0409115*)
- [193] Andersen J R and Gardi E 2006 *JHEP* **01** 097 (*Preprint hep-ph/0509360*)
- [194] Gambino P, Giordano P, Ossola G and Uraltsev N 2007 *JHEP* **10** 058 (*Preprint 0707.2493*)
- [195] Lees J P *et al.* (BaBar) 2017 *Phys. Rev.* **D95** 072001 (*Preprint 1611.05624*)
- [196] Ellis R K *et al.* 2019 (*Preprint 1910.11775*)
- [197] Lehner C *et al.* (USQCD) 2019 *Eur. Phys. J.* **A55** 195 (*Preprint 1904.09479*)
- [198] Hashimoto S 2017 *PTEP* **2017** 053B03 (*Preprint 1703.01881*)
- [199] Altmannshofer W *et al.* (Belle-II) 2018 (*Preprint 1808.10567*)
- [200] Abudinén F *et al.* (Belle-II) 2020 (*Preprint 2004.09066*)
- [201] 2012 Framework TDR for the LHCb Upgrade: Technical Design Report
- [202] Atoui M, Blossier B, Morénas V, Pène O and Petrov K 2015 *Eur. Phys. J.* **C75** 376 (*Preprint 1312.2914*)
- [203] Chen H X, Chen W, Liu X, Liu Y R and Zhu S L 2017 *Rept. Prog. Phys.* **80** 076201 (*Preprint 1609.08928*)
- [204] Le Yaouanc A and Pène O 2015 *Int. J. Mod. Phys.* **A30** 1543009 [,171(2014)] (*Preprint 1408.5104*)
- [205] Crivellin A and Pokorski S 2015 *Phys. Rev. Lett.* **114** 011802 (*Preprint 1407.1320*)
- [206] Colangelo P and De Fazio F 2017 *Phys. Rev.* **D95** 011701 (*Preprint 1611.07387*)
- [207] Jung M and Straub D M 2019 *JHEP* **01** 009 (*Preprint 1801.01112*)
- [208] Colangelo P and De Fazio F 2018 *JHEP* **06** 082 (*Preprint 1801.10468*)